ON THREE DIMENSIONAL DIGITAL TOPOLOGY AND ITS APPLICATION TO IMAGE PROCESSING

Punam Kumar Saha

Electronics and Communication Sciences Unit

Indian Statistical Institute

203 B T Road

Calcutta 700035

India

Thesis submitted to Indian Statistical Institute

for partial fulfillment of the requirements for

the degree of Doctor of Philosophy

July 20, 1995

(Revised December, 1996)

Dedicated to my parents

Babu Lakshmi Narayan Saha and Devi Nirmala Saha

Acknowledgement

I am one of the fortunate few who got the opportunity to work under the great professor to whom I owe a deep gratitude as my supervisor, guru and ideal **Prof. Dwijesh Dutta Majumder** who has taught me and guided me with patience and excused my short comings with magnanimity in course of this work. I shall have repaid the debt only if I live up to his high standards. I am also thankful to Prof. B. B. Chaudhuri for giving me the scope to work with him and for sparing me some of his valuable time and Dr. D. P. Mukherjee for his untiring help in completing the manuscript.

I am extremely thankful to all my colleagues at the Electronics and Communication Sciences Unit including Prof. J. Das, Prof. A. K. Dutta, Prof. N. R. Ganguli, Dr. K. S. Roy, Dr. B. Chanda, Dr. S. K Parui and Mr. B. Mukherjee.

I wish to acknowledge the encouragement I received from my brothers Dr. Uttam K. Saha, Dr. Goutam K. Saha, Mr. Rupam K. Saha, Dr. Bikram K. Saha and my sister-in-law Dr. Parul Saha and also to Dr. (Mrs.) Sabita Dutta Majumder for their encouragement in pursuing my research carrier. I also take opportunity to express my thankful appreciation for the discussion I could have with some of my friends such as Dr. Goutam Mukherjee, Dr. Mahua Dutta, Mr. Shantanu Chakraborty and Mr. Nanda Dulal Chatterjee.

Contents

List of Figures

List of Tables

Chapter 1

Introduction to Digital Topology

1.1 Introduction

Digital topology provides a sound mathematical basis for object classification, counting and labeling, border tracking, contour filling, thinning, segmentation and many other image processing applications. An important characteristic of topological properties is that they are invariant under translation, rotation, and more generally under any elastic deformation. The analysis of three dimensional (3D) digital images has generated increasing interest with the rapid growth of 3D image processing applications including computer vision. 3D digital images are common input/output media in the several application domains of image processing, pattern recognition and computer vision among which 3D medical imaging is of particular interest. In medical imaging, applications like Computed Tomography (CT), Magnetic Resonance Imaging (MRI), Positron Emission Tomography (PET), Ultrasound Echography (UE), Single Photon Emission Computed Tomography (SPECT), Digi-

tal Subtraction Angiography (DSA) are widely used in producing 3D digital images that carry many important information about organs interior to the human body. These images are routinely used by the doctors both for diagnosis of abnormalities in the structure and function of organs and also for therapeutic treatment planning. Lee and Rosenfeld [65] pointed out the fact that many organs are highly flexible and change shapes due to external forces or due to their own functions. For example, the heart always changes its shape with heart beats. However, these deformations generally follow elastic deformation rules. This phenomenon gives importance to topological features such as the numbers of components, tunnels, cavities etc. in the 3D digital images of interior organs. These are invariant under elastic deformation. These topological numbers, useful for organ identification, may also be used for diagnosis and therapeutic planning. For example, the usual number of passageways through the heart is used as a pathology. Udupa [136] discussed about the applications of digital topology in three-dimensional medical imaging.

This thesis is devoted to the study of topological properties in three dimensional digital space and their applications to image processing. Rosenfeld and Kak [105] and Chaudhuri and Dutta Majumder [22] among others discussed about the importance of geometrical and topological properties in digital image analysis and recognition. A well-developed theory of topological properties of 3D digital images may be found in [96]. A survey on digital topology was reported by Kong and Rosenfeld [51]. In general, digital topology deals with binary images (although some works [98,103] were reported on the topology of gray-tone images). In a binary digital image a point is either a black (object) point or a white (non-object) point. We mainly consider binary images and in the remaining part of the thesis 'image' will refer to 'binary image' unless stated otherwise.

The black points in an image may be grouped as a set of connected components. A component may contain tunnels and cavities. A cavity is a 3D analog of 2D 'hole' where white points generate a bounded component. A tunnel on the other hand, does not generate a component of white points. However, a component contains a

tunnel if it generates a solid handle or a hollow torus. An open-ended hollow cylinder also has a tunnel. In 2D there is no concept analogous to tunnel. It may be noted that the numbers of components, tunnels and cavities in an image correspond to its 0th, 1st, and 2nd Betti numbers [65] respectively. Alike Euler characteristic, these numbers are also topologically invariant. Both the Euler characteristic and these numbers can be used for global description of an object and also for object classification [33]. A point whose binary transformation does not change these topological invariants of an image is called a simple point [76,111,113,114,131]. Simple points have wide applications in homotopy preserving transformations including thinning. Thinning [32,69,70,76,79,111,114,117,122,123,128,130,131] is a useful preprocessing tool for image analysis and recognition since it produces a compact representation of an object while preserving its topology and shape. Such a compact representation is easier to trace and helps in recognizing an object. Practical applications of 3D thinning were discussed in [122,70]. 3D thinning is used for recognizing 'DNA' structures and human organs such as lungs, bronchi and for many such computer vision applications. It has another important application in image coding and data compression. For such cases, the algorithms must have the property that an object can be reproduced from its thinned version. Unfortunately, none of the thinning algorithms [32,69,70,76,79,111,114,117,122,123,128,130,131] in 3D, though the list is certainly not exhaustive, had adequately addressed this aspect.

Segmentation produces a structured representation of an object and plays an important role in feature selection and extraction that helps in object recognition and description. Topology also provides a sound mathematical tool for 3D object segmentation [73,115]. For this purpose point classification [115] (e.g. edge points and inner points of surfaces or curves, different types of junction points etc.) is first achieved by analyzing local topological parameters like the numbers of components, tunnels, cavities etc. Results of point classification are then applied for a meaningful segmentation [115] of 3D objects.

1.2 3D Digital Topology: Concepts and Definitions

Before we proceed further, we detail the fundamentals of 3D digital topology. Naturally, the basic issues have been discussed many times before in the digital topology literature. As a consequence, most of the results to be presented in this section are well-known, although not necessarily in the form they will be given here. General references are too numerous to list, however, a thorough and lucid discussion in this context is given in [53,54].

1.2.1 Digital Image Space and Voronoi Neighborhood

In digital topology, digital points are often referred as grid points [53]. A digital image space (referred as digital picture space in [51,53]) is defined by a triple $(\mathcal{V}, \alpha, \beta)$ where $\mathcal{V}$ is the set of grid points we often refer as image set and α, β are two binary relations between the points of $\mathcal{V}$. Two points $p, q \in \mathcal{V}$ are α-adjacent (β-adjacent) *if* $(p, q) \in \alpha$ *(respectively* $(p, q) \in \beta$*)*; α, β are also called adjacency relations. Two α-adjacent (β-adjacent) points are often referred as α-neighbors (β-neighbors). We call a closed line segment between two α-adjacent (β-adjacent) points as α-line (β-line) (referred as α-adjacency and β-adjacency in [53]). Adjacencies are mostly based on Voronoi neighborhood [2] of the grid points. Voronoi neighborhood of a grid point p is the set of all points in the Euclidean 3-space those are at least as close to p as any other grid point. In a Voronoi adjacency relation, two grid points are adjacent if their Voronoi neighborhood: 1) share a face, 2) share an edge, or 3) share a vertex. A Voronoi adjacency in which every grid point is adjacent to exactly n other grid points is also referred as n-adjacency relation.

In this thesis we mostly consider digital images in 3D cubic grid Z^3 (Z is the set of all integers), although we review important works in other three dimensional grids

also. Therefore, a need arises to respecify the adjacency relationships in the light of 3D cubic grid. A digital image in 3D cubic grid Z^3 is often represented in a 3D binary array where each array element is uniquely mapped to a point of 3D cubic grid. Each array element with a value of '1' or '0' represents that the corresponding grid point is black or white respectively. Three Voronoi adjacency relations exist in 3D cubic grid namely, 26-adjacency, 18-adjacency, and 6-adjacency relations. Let $p_1 = (i_1, j_1, k_1)$ and $p_2 = (i_2, j_2, k_2)$ be two points in Z^3. Then

1. p_1, p_2 are 26-adjacent if $\max(|i_1 - i_2|, |j_1 - j_2|, |k_1 - k_2|) = 1$,
2. p_1, p_2 are 18-adjacent if they are 26-adjacent and $|i_1 - i_2| + |j_1 - j_2| + |k_1 - k_2| \leq 2$,
3. p_1, p_2 are 6-adjacent if $|i_1 - i_2| + |j_1 - j_2| + |k_1 - k_2| = 1$.

An $(\alpha, \beta) \mid \alpha, \beta \in \{6, 18, 26\}$ digital image refers to a 3D digital image in (Z^3, α, β) while an $(\alpha, \beta) \mid \alpha, \beta \in \{4, 8\}$ digital image refers to a 2D digital image in (Z^2, α, β).

1.2.2 Three Dimensional Digital Grids

Three different digital grids are mostly considered in 3D image processing literatures depending upon the tessellation of 3-space. Following is the description of these digital grids and their possible adjacency relations:

1. **3D cubic grid:** The points with integer co-ordinates (i, j, k) are the grid points. This is the most popular digital grid in three dimension. The Voronoi neighborhood of each grid point in this case is a cube and the Voronoi adjacencies of grid points are 6-, 18-, and 26-adjacencies.
2. **3D face centered cubic grid:** In this case the points with integer co-ordinates (i, j, k) where $i + j + k$ is even, are the grid points and the Voronoi neighborhood of each grid point is a rhombic dodecahedron. Just two Voronoi

adjacency relations exist in this grid and they are 12-, and 18-adjacency relations.

3. **3D body centered cubic grid:** In this case the points with integer coordinates (i, j, k) where $i \equiv j \equiv k \pmod 2$, are the grid points and the Voronoi neighborhood of each grid point is a truncated octahedron. Only one Voronoi adjacency relation exists in this grid and it is a 14-adjacency relation.

1.2.3 Digital Image

In the remaining part of this thesis points will refer to digital grid points unless stated otherwise. A binary digital image (referred as binary digital picture in [51,53]) or simply a digital image P is defined by a quadruple $(\mathcal{V}, \alpha, \beta, \mathcal{B})$ where $\mathcal{V}$ is the image set, $\mathcal{B}$ is the set of black points in P, α-adjacency and β-adjacency relations are used for the points of $\mathcal{B}$ and $\mathcal{V} - \mathcal{B}$ respectively. Obviously, $\mathcal{V} - \mathcal{B}$ is the set of white points in P. An α-line between two black points is called a black-line while a β-line between two white points is called a white-line. For a digital image $P = (\mathcal{V}, \alpha, \beta, \mathcal{B})$ we define another digital image $\overline{P} = (\mathcal{V}, \beta, \alpha, \mathcal{V} - \mathcal{B})$ where $\overline{P}$ is called the inverse of P. A digital image $(\mathcal{V}, \alpha, \beta, \mathcal{B})$ is finite if $\mathcal{B}$ is finite. In this thesis we consider only finite digital images.

1.2.4 Regular and Strongly Normal Digital Image Space

Restrictions are imposed on the adjacency relations in a digital image space to avoid awkward and pathological situations [53]. A 3D digital image space $(\mathcal{V}, \alpha, \beta)$ is regular [53] if it satisfies the following two conditions:

1. no α-line or β-line passes through a point of $\mathcal{V}$ other than its end points, and
2. an α-line never meets a β-line with which it does not share an end point.

A regular 3D digital image space $(\mathcal{V}, \alpha, \beta)$ is strongly normal [53] if it satisfies all the following conditions:

1. $\mathcal{V} = Z^3$,
2. two 6-adjacent points of $\mathcal{V}$ are both α- and β-adjacent,
3. two α- or β-adjacent points are always 26-adjacent,
4. given any unit lattice square, either both diagonals are α-line or both diagonals are β-line or one diagonal is both α- and β-line, and
5. in every image on $(\mathcal{V}, \alpha, \beta)$ whenever a black component is either α-adjacent or β-adjacent to a white component, the black component is 6-adjacent to the white component.

1.2.5 Digital Fundamental Group

Here we define the digital fundamental group. A P-walk is a curve $\gamma : [0, 1] \rightarrow E^3$ (E^3 is the Euclidean 3-space) where $\gamma(0)$ and $\gamma(1)$ are black points and there exists a positive integer k such that all non-negative integers $i < k$ satisfy:

1. $\gamma(i/k)$ is a black point,
2. $\gamma(i/k)$ is equal or adjacent to $\gamma((i+1)/k)$, and
3. γ is linear in the closed interval $[i/k, (i+1)/k]$.

The length of the P-walk is k. Let γ_1 be a P-walk from p to q and let γ_2 be another P-walk from q to r. Let the lengths of γ_1 and γ_2 be m_1 and m_2 respectively. The product of γ_1 and γ_2 denoted as $\gamma_1.\gamma_2$, is defined as follows:

$$\gamma_1.\gamma_2(x) = \begin{cases} \gamma_1((m_1+m_2)x/m_1), & \text{if } 0 \leq x \leq m_1/(m_1+m_2), \\ \gamma_2((m_1+m_2)x/m_2 - m_1/m_2), & \text{if } m_1/(m_1+m_2) \leq x \leq 1. \end{cases}$$

A $\mathcal{P}$-walk γ is a $\mathcal{P}$-loop if $\gamma(0) = \gamma(1) = p$ and is said to be based at p. Two $\mathcal{P}$-loops with same base point are said to be equivalent if they are fixed base point homotopic in $E^3 - W$ where W is the union of all white-lines of $\mathcal{P}$. Let $[\lambda]_p$ denote the equivalence class consisting of all $\mathcal{P}$-loops that have the same base point as λ and are equivalent to λ. For two $\mathcal{P}$-loops λ_1 and λ_2 with the same base point, $[\lambda_1]_p.[\lambda_2]_p$ is defined to be the equivalence class $[\lambda_1.\lambda_2]_p$. We define the digital fundamental group as follows:

For a digital image $\mathcal{P}$ in a regular digital image space, the digital fundamental group with base point p denoted as $\pi(\mathcal{P}, p)$, is defined as the group of all equivalence classes $[\lambda]_p$ where λ is a $\mathcal{P}$-loop based at p, under the '.' (product) operation.

1.2.6 Continuous Analog of a Digital Image

The continuous analog of a 3D digital image $\mathcal{P}$ in a strongly normal digital image space, is a polyhedral set and is denoted as $C(\mathcal{P})$. Following methodology is required to define $C(\mathcal{P})$.

- Every unit lattice square is divided into two $(1, 1, \sqrt{2})$ triangles in one of the following three ways:

  1. When the four corners are all black or all white then the diagonal each of whose endpoints has co-ordinates that sum to an even integer, divides the unit lattice square.
  2. When the corners are not all black or all white but one of the diagonals is a black-line or a white-line then it is used to divide the square.
  3. When the corners are not all black or all white and neither diagonal is a black-line or a white-line then select the diagonal that joins a black point to a white point to divide the square.

- Let $T_2(P)$ be the set of all $(1, 1, \sqrt{2})$ triangles obtained by dividing all unit lattice squares as above. Every unit lattice cube is divided in one of the following two ways:

  1. A unit lattice cube K is special if there are three black-lines and three white-lines in K both of which form a $(\sqrt{2}, \sqrt{2}, \sqrt{2})$ equilateral triangles. Let e_1, e_2, e_3, e_4, e_5 and e_6 be the edges of these equilateral triangles. The seventh edge e_7 is the diameter of K, parallel to the vector $(1, 1, 1)$, if it is not perpendicular to the triangles. Otherwise e_7 is the diameter of K, parallel to the vector $(1, -1, 1)$. Thus, K is subdivided into six 3-simplexes each of whose edges is an edge of K or one of the e's.
  2. When K is not special i.e. ordinary then K is divided into twelve congruent 3-simplexes, each of which has a face in $T_2(P)$ and a vertex at the centroid of K.

- Let $T_3(P)$ be the set of 3-simplexes obtained by dividing all unit lattice cubes as above. The augmented black point set of P is the union of the set of black points of P with the set of centroids of every ordinary cube K satisfying at least one of the following two conditions:

  1. One of the four diameters of K is a black line.
  2. K contains a simple closed curve of black-lines not contained in a face of K and no diameter of K is a white-line.

- A triangle of $T_2(P)$ is a black triangle if all its vertices lie in the augmented set of black points. Similarly, a 3-simplex of $T_3(P)$ is a black 3-simplex if all its vertices lie in the augmented set of black points.

Based on the above procedure, the continuous analog is defined as follows:

For a 3D digital image P in a strongly normal digital image space, the continuous analog $C(P)$ is the union of the augmented set of black points, the set of black-lines, the set of black triangles and the set of black 3-simplexes of P.

Interested readers may refer to Kong, Roscoe and Rosenfeld [53] for more detailed discussion on digital fundamental group and continuous analog.

1.2.7 Paths and Curves in Digital Image

Let S be a non-empty subset of $\mathcal{V}$. A point $p \in \mathcal{V}$ is α-adjacent to S if p is α-adjacent to some point of S. Similarly, two non-empty subsets of $\mathcal{V}$ are α-adjacent if a point of one subset is α-adjacent to the other subset. An α-path between two grid points $p, q \in S$ is a sequence of distinct points $p = p_0, p_1, \cdots, p_n$ in S such that p_i is α-adjacent to p_{i+1} for $0 \leq i < n$. Let π be an α-path $p_0, p_1, \cdots, p_n$ and p be a point α-adjacent to p_n. We use π, p to denote the α-path $p_0, p_1, \cdots, p_n, p$. Also, $spt(\pi)$ is used to denote the set of points $\{p_0, p_1, \cdots, p_n\}$ unless stated otherwise. An α-curve is an α-path $p_0, p_1, \cdots, p_n$ such that $p_i \mid 1 \leq i < n$ is α-adjacent to exactly two other points of the α-path. An α-path $p_0, p_1, \cdots, p_n$ is an α-closed path if p_0 is α-adjacent to p_n. An α-closed curve is an α-closed path ς such that every point of ς is α-adjacent to exactly two other points of ς. An α-closed curve with more than three points is called a non-trivial α-closed curve. Let $\varsigma_0, \varsigma_1, \cdots, \varsigma_n$ denote $n+1$ non-trivial α-closed curves. We say that they are independent if for every ς_i there exists a sequence (though not necessarily unique) $\varsigma_{t_0}, \varsigma_{t_1} \cdots, \varsigma_{t_{n-1}}$ of other n non-trivial α-closed curves such that after their valid removal (taking one at a time according to the sequence) ς_i remains. Valid removal of ς_{t_j} at the j'th step means the removal of the set of points $spt(\varsigma_{t_j}) - ((\bigcup_{k=j+1}^{k=n-1} spt(\varsigma_{t_k})) \cup \varsigma_i)$ subject to the condition that it is non-empty. Let S be a non-empty finite subset of $\mathcal{V}$. A set A of independent non-trivial α-closed curves of S is a maximal set if any other non-trivial α-closed curve of S when included in A makes it's non-trivial α-closed curves dependent. It may be noted that S may have more that one maximal sets of independent non-trivial α-closed curves. Let A_1, A_2, $\cdots$, A_n be all possible maximal sets of independent non-trivial α-closed curves of S. Let a_i be the cardinality of A_i. Maximum possible independent non-trivial α-closed curves in S is $\max\{a_1, a_2, \cdots, a_n\}$.

1.2.8 Components, Tunnels, Cavities and Background

Let S be a non-empty subset of $\mathcal{V}$. Two points $p, q \in S$ are α-connected in S if there exists an α-path from p to q in S. An α-component of S is a maximal subset of S where each pair of points is α-connected. For a digital image $P = (\mathcal{V}, \alpha, \beta, B)$ an α-component of B is a black component while a β-component of $\mathcal{V} - B$ is a white component. In a finite digital image there is a unique unbounded white component [51] and it is called the background. Let X, Y be two subsets of $\mathcal{V}$ and let X be connected by its given adjacency relation[1]. We say that X surrounds Y if Y is a subset of a finite component (in $\overline{X}$ sense) of $\mathcal{V} - X$. A white component of P that is adjacent to and surrounded by a black component S is called a cavity in S. As pointed out by Kong and Rosenfeld [51] it is quite hard to define a tunnel although the number of tunnels has a precise definition. The number of tunnels in a polyhedral set is the rank of its first homology group [56]. According to Kong, Roscoe and Rosenfeld [53], if a polyhedron S' is derived from another polyhedron S after adding n 'solid handles' to S or removing the interior of a 'n-holed solid polyhedral torus' from the interior of S, then the number of tunnels in S' is equal to the number of tunnels in S plus n. Following [53], the number of tunnels in a 3D digital image may also be defined as follows: let $B_1, B_2, \cdots, B_n$ be the black components in a 3D digital image P and let $p_i \in B_i$ for $1 \leq i \leq n$. Then the number of tunnels in P is the sum of the ranks of abelianizations of the groups $\pi(P, p_i)$. A black point is a border point if it is adjacent (in the sense of white points) to a white component, otherwise it is an interior point. The border of a black component is the set of all border points in it. Similarly, the interior of a black component is the set of all interior points in it. Let X, Y be two non-empty subsets of $\mathcal{V}$ such that $X \subset Y$. We say that X is α-connected in Y if every two points $p, q \in X$ are α-connected in Y. The number of α-components of X in Y is defined similarly.

[1]Taking the example of the image P, for X containing only black points, adjacency relation is α. For X containing only white points, adjacency relation is β. For X containing both black and white points, adjacency relation of X is to be specified explicitly.

1.2.9 The Euler Characteristic

The Euler characteristic of a polyhedral set $S \subset E^3$, denoted as $\chi(S)$, is defined by the following axioms [51]:

1. $\chi(S) = 0$ if $S = \phi$,
2. $\chi(S) = 1$ if S is non-empty and convex,
3. for any two polyhedra X and Y, $\chi(X \cup Y) = \chi(X) + \chi(Y) - \chi(X \cap Y)$.

For any arbitrary triangulation of a set S, the value of $\chi(S)$ is equal to the following alternating sum [51]:

$$\begin{aligned}\chi(S) = \quad & \text{the number of points in } S - \text{the number of edges in } S \\ & + \text{the number of triangles in } S - \text{the number of tetrahedrons in } S.\end{aligned}$$

Also, the Euler characteristic of a set $S \subset E^3$ is equal to the number of connected components in S minus the number of tunnels in S plus the number of cavities in S [51]. For example, the Euler characteristic of a hollow cube is two since it has one component, one cavity and no tunnels; the Euler characteristic of the border of a rectangle is zero since it has one component, one tunnel and no cavities. For further development on the Euler characteristic interested readers may refer to [40,75].

An analogous definition of the Euler characteristic is introduced for a digital image P which is denoted as $\chi(P)$. Each digital image is associated with the polyhedral set $C(P)$ i.e. the continuous analog of P [53]. The Euler characteristic $\chi(P)$ of a digital picture is defined as $\chi(P) = \chi(C(P))$ [51].

1.2.10 Some Definitions in 3D Cubic Grid

All the definitions of this section are applicable in 3D cubic grid Z^3. Let p be a point in Z^3. $\mathcal{N}_\alpha(p)$ denotes the set of all α-neighbors of p including p itself. For example, $\mathcal{N}_{26}(p)$ denotes the set of 27 points in the $3 \times 3 \times 3$ neighborhood of a point p including p itself. Throughout the thesis $\mathcal{N}_{26}(p)$ is denoted as $\mathcal{N}(p)$. The set of points of $\mathcal{N}(p)$ excluding p is denoted as $\mathcal{N}^*(p)$. We classify the points of $\mathcal{N}^*(p)$ according to their adjacency relations with p as follows:

1. An *s-point* is 6-adjacent to p,
2. an *e-point* is 18-adjacent but not 6-adjacent to p, and
3. a *v-point* is 26-adjacent but not 18-adjacent to p.

Nomenclature of the points of $\mathcal{N}(p)$ is explained in Figure 1.1. In Figure 1.1, p_E, p_W, p_S, p_N, p_T, p_B denote the *east*, *west*, *south*, *north*, *top* and *bottom* points respectively. Similarly, p_{TE} denotes the *top-east point* and so on. Let p, q be two points in Z^3. $\mathcal{N}(p,q)$ is the set of points 26-adjacent to both p and q i.e. $\mathcal{N}(p,q) = \mathcal{N}(p) \cap \mathcal{N}(q)$.

Let $x = (k_0, k_1, k_2)$ be an s-point of $\mathcal{N}(p)$ where $p = (l_0, l_1, l_2)$ i.e. $|k_i - l_i| = 1$ for some i and $k_j = l_j$ for all $i \neq j$. We define $surface(x,p)$ as the set of points $(m_0, m_1, m_2) \in \mathcal{N}(p)$ such that $m_i = k_i$. It may be noted that a $surface(x,p)$ contains nine points and exactly one of them is an s-point of $\mathcal{N}(p)$. Let $x = (k_0, k_1, k_2)$ be an e-point of $\mathcal{N}(p)$ where $p = (l_0, l_1, l_2)$ i.e. $|k_i - l_i| = 1$ and $|k_j - l_j| = 1$ for some distinct i, j and $k_h = l_h$ for $h \neq i$, $h \neq j$. We define $edge(x,p)$ as the set of points $(m_0, m_1, m_2) \in \mathcal{N}(p)$ such that $m_i = k_i$ and $m_j = k_j$. It may be noted that an $edge(x,p)$ contains three points and exactly one of them is an e-point of $\mathcal{N}(p)$.

Two s-points $a, b \in \mathcal{N}(p)$ are called *opposite* if they are not 26-adjacent. Otherwise, they are called *non-opposite* s-points. Let a, b, c denote three non-opposite s-points of $\mathcal{N}(p)$. Then we define the following two functions:

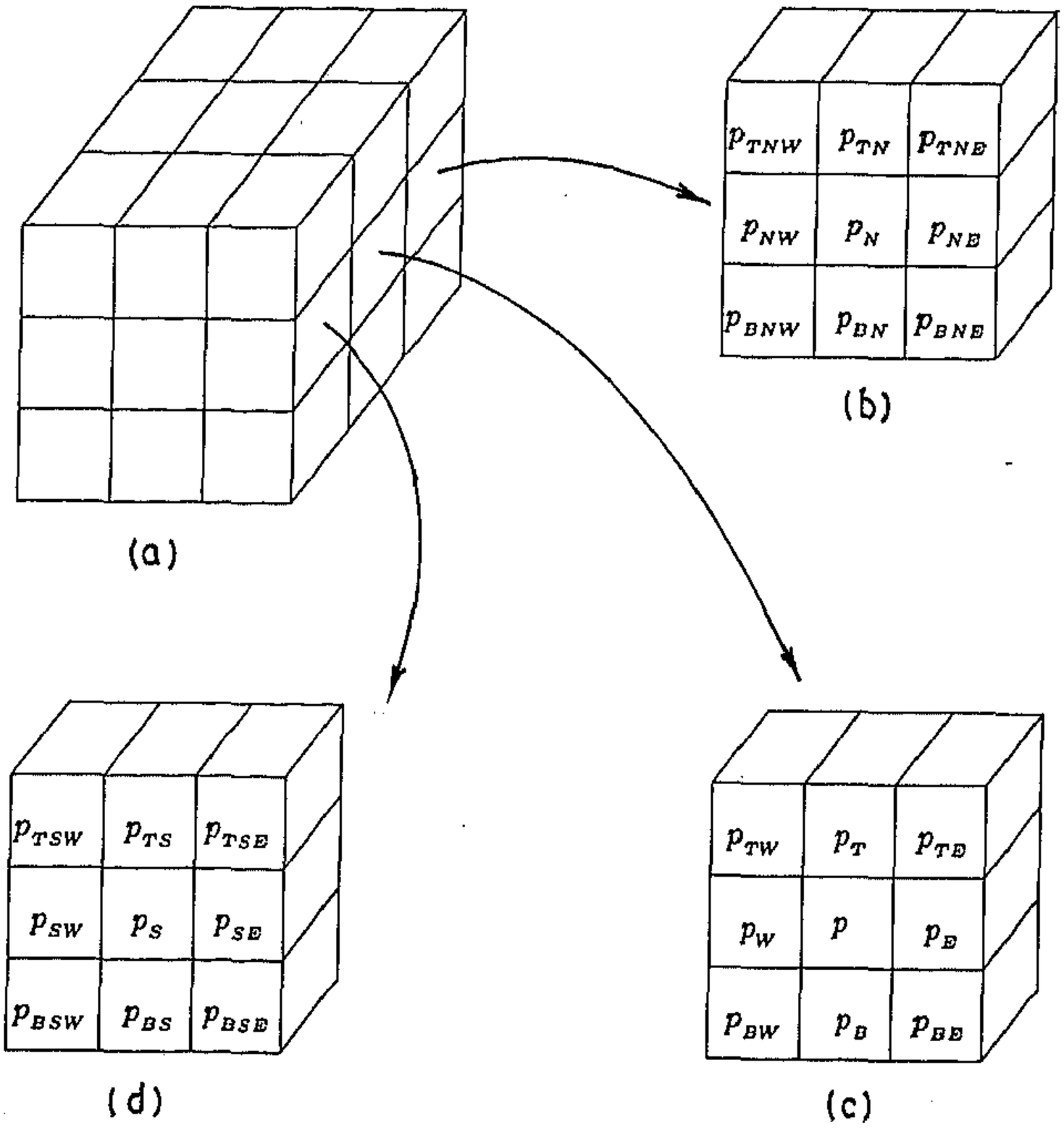

Figure 1.1: Nomenclature of the points in the $3 \times 3 \times 3$ neighborhood of a point p. Clock-wise from top-left corner — neighborhood representation, back vertical plane, middle vertical plane, and front vertical plane.

$e(a,b,p) = q \mid q \in \mathcal{N}^*(p)$ and 6-adjacent to a, b,
$v(a,b,c,p) = q \mid q \in \mathcal{N}^*(p)$ and 6-adjacent to $e(a,b,p), e(b,c,p), e(c,a,p)$.

For example, if a, b, c denote the points p_N, p_T, p_B in $\mathcal{N}(p)$ then according to the above definitions $e(a,b,p)$ and $v(a,b,c,p)$ will denote the points p_{TN} and p_{TNB} respectively. It may be noted that $e(a,b,p)$ is an e-point while $v(a,b,c,p)$ is a v-point of $\mathcal{N}(p)$. We define three more functions as follows:

$f_1(a,p) = q \mid q \notin \mathcal{N}(p)$ and 6-adjacent to a,
$f_2(a,b,p) = q \mid q \notin \mathcal{N}(p)$ and 6-adjacent to $f_1(a,p), e(a,b,p)$,
$f_3(a,b,p) = q \mid q \notin \mathcal{N}(p)$ and 6-adjacent to $f_2(a,b,p), f_2(b,a,p)$.

Let $(a,d),(b,e),(c,f)$ denote three distinct unordered pairs of opposite s-points of $\mathcal{N}(p)$. Let condition C_1 be '$x \in \{b,e,c,f\}$'; condition C_2 be '$x, y \in \{b,e,c,f\}$ and x, y are non-opposite'; condition C_3 be '$x \in \{b,e,c,f\}$ and $x \in \{p_B, p_S, p_W\}$'; condition C_4 be '$x, y \in \{b,e,c,f\}$; x, y are non-opposite and $x \in \{p_B, p_S, p_W\}$' and condition C_5 be '$x, y \in \{b,e,c,f\}$; x, y are non-opposite and $x, y \in \{p_B, p_S, p_W\}$'.

We define a middle plane and an extended middle plane of $\mathcal{N}(p)$ as follows:

$$M(a,d,p) = \{x \mid C_1\} \cup \{e(x,y,p) \mid C_2\},$$
$$\mathcal{E}M(a,d,p) = M(a,d,p) \cup \{f_1(x,p) \mid C_3\} \cup \{f_2(x,y,p) \mid C_4\} \cup \{f_3(x,y,p) \mid C_5\}.$$

We call $M(a,d,p)$ and $\mathcal{E}M(a,d,p)$ as middle plane and extended middle plane of $\mathcal{N}(p)$ respectively. It may be noted that $M(a,d,p)$ contains eight points while $\mathcal{E}M(a,d,p)$ contains fifteen points.

Let $\mathcal{P} = (Z^3, 26, 6, \mathcal{B})$ be the image under consideration. For every point $p \in Z^3$, we define two images as follows:

$$\dot{\mathcal{N}}(p) = (Z^3, 26, 6, (\mathcal{N}(p) \cap \mathcal{B}) \cup \{p\}),$$
$$\hat{\mathcal{N}}(p) = (Z^3, 26, 6, (\mathcal{N}(p) \cap \mathcal{B}) - \{p\}).$$

In other words, p is always white in $\hat{\mathcal{N}}(p)$ (i.e. p is deleted) while p is always black in $\dot{\mathcal{N}}(p)$ (i.e. p is added). For any other point of $\mathcal{N}(p)$, the color in $\hat{\mathcal{N}}(p)$ or $\dot{\mathcal{N}}(p)$ is the same as the color of corresponding point in $\mathcal{P}$. For any point of $Z^3 - \mathcal{N}(p)$, the color in $\hat{\mathcal{N}}(p)$ or $\dot{\mathcal{N}}(p)$ is always white. For a set of point $S \subset Z^3$ the 26-envelope $\mathcal{E}(S)$ of S is defined as follows:

$$\mathcal{E}(S) = \bigcup_{p \in S} \mathcal{N}(p) - S.$$

1.3 3D Digital Topology: Current Status

The research on digital topology started with the simple but important idea of using different adjacencies for black points and white points [25,107]. Both Gray [30] and Park and Rosenfeld [86] made extensive studies on digital geometry. Based on the notion of finitely presented Abelian group Mylopoulos and Pavlidis [82,83] made a theoretical study on the properties of quantized space and their higher dimensional generalizations. Tourlakis and Mylopoulos [129] also considered the topological aspects of higher dimensional digital space. Rosenfeld [96] introduced the basic concepts of digital topology for three dimensional array with mathematical rigor and soundness. He defined the concepts of connectedness, cavities, holes (tunnels), surroundedness, border, background, arcs, curves etc. and their topological properties. Kong and Rosenfeld [51] made a thorough survey on 2D and 3D digital topology which may be used as an introductory lesson for a researcher in this field. In fact it helped us a lot to do our work for this thesis.

1.3.1 Classical Topology in Image Processing

A few interesting publications [43,44,45,46,47,63,37] on the application of classical topology in digital image processing are found in the literatures of digital topology. Kovalevsky [63] and Herman [37] made a study in this respect. In his paper [63],

Kovalevsky proved that every finite T_0-space is an abstract cellular complex and based on that theorem he made a fundamental claim that "the topology of cellular complex is the only possible topology of finite sets". Herman [37] recognized the claim of Kovalevsky in a more generalized version. He replaced the finiteness condition which makes the results applicable to image analysis over infinite domain e.g. the infinite 3-space tessellation into equal sized cubes. Herman established his claim by showing that: 1) every finite T_0-space is a limited sparse T_0-space, 2) every limited sparse T_0-space is a limited partially ordered set, and finally, 3) every limited partially ordered set can be transformed to a (limited) cellular complex by complementing with a 'dim' (dimension) function. He also pointed out that the definition of 'dim' function attached with the definition of cellular complex "is quite different from what is 'natural' in image processing". Finally, he concluded that cellular complex is rich enough; however, a 'right' topology for image processing depends on a particular choice of the 'dim' function.

Khalimsky [43,44,45,46,47] introduced an approach of representing an image by locally finite T_0-space. He defined the topology of the set of integers with the basis as follows:

$$\{\{2k+1\} \mid k \in Z\} \cup \{\{2k-1, 2k, 2k+1\} \mid k \in Z\}.$$

The topology of Z^n is a product of n copies of this space. This space is often referred as Khalimsky n-space. In Khalimsky n-space, a point is a pure point if its coordinates are all even or all odd, and a mixed point otherwise. In three dimension the Khalimsky-adjacencies are the 26-adjacencies with at least one pure point together with all 6-adjacencies between two mixed points. Khalimsky-adjacency is a non Voronoi adjacency.

1.3.2 Digital Image Space and Adjacency Relation

In the definition of digital images two different adjacency relations are associated with each digital image space, one for black points and the other for white points. The novel idea of using different adjacency relations for black points and white points emerged at the early stage of digital topology and was first recommended by Duda, Hart and Munson [25]. Rosenfeld and Pfaltz [107] discussed this aspect and explained with example that if same adjacency relation is used for both black and white points then the discrete analog of the Jordan curve theorem does not hold. Later Kong, Roscoe and Rosenfeld [53] made a rigorous study to define proper restrictions on adjacency relations of black points and white points. Depending on these two adjacency relations they defined two classes of digital image space namely *regular digital image space* and *strongly normal digital image space*. Moreover, they discussed about many important topological properties (e.g. the continuous analog property, the discrete Jordan curve theorem etc.) of such digital image space.

1.3.3 Continuous Analog and Digital Fundamental Group

In a fascinating paper [53] Kong, Roscoe and Rosenfeld related the digital topology of strongly normal digital image space with the topology of the Euclidean space. They defined the concepts of digital fundamental group — an analog of fundamental group for digital images, and discrete digital fundamental group — a discrete version of digital fundamental group [53]. In the same paper [53] they defined 'continuous analog' $C(P)$, a polyhedral construction for the digital image P in a strongly normal digital image space. In this connection Kong et. al. [53] described 'continuous analog properties' and established that $C(P)$ holds these properties. They also proved that the digital fundamental group of a digital image P in a strongly normal digital image space is naturally isomorphic to the (classical) fundamental groups of $C(P)$. Moreover, they discussed many important properties of the Euclidean

space those have analogs for strongly normal digital image space. The concept of digital fundamental group and continuous analogs were also discussed in [59,61]. The concept of continuous analogs of digital image had previously been used by Kong and Roscoe [52,55], by Kong and Khalimsky [57] and by Kopperman, Meyer and Wilson [62].

1.3.4 The Jordan Theorem in Digital Topology

Rosenfeld [95,109] established the discrete analogs of the Jordan curve theorem for 2D digital images. In [95] he established for a (4,8) digital images that a simple closed curve not contained in a unit lattice square creates at least two white components and in [109] he strengthened the claim that it creates exactly two white components. In [102] Rosenfeld showed that the same result holds in (8,4) digital images also. Stout [125] presented interesting proofs of these theorems. Morgenthaler and Rosenfeld [77] established a three dimensional analog of the discrete Jordan curve theorem for (6,26) and (26,6) digital images and called it as the Jordan surface theorem. In a series of papers Reed and Rosenfeld [91,92] made a further study on three dimensional digital surfaces and the Jordan surface theorem. Using continuous analogs Kong and Roscoe [52] proved the Jordan surface theorem for (26,6), (6,26), (18,6), (6,18) and many other kinds of digital images. Khalimsky [47] presented the Jordan curve theorem for his digital images. Kopperman et. al. [62] established the Jordan surface theorem for Khalimsky's three dimensional digital images.

1.3.5 The Euler Characteristic and Other Topological Invariants

The Euler characteristic, components, tunnels and cavities are important topological invariants that have many applications in image classification and recognition among others. In a 3D image the numbers of components, tunnels and cavities denote its 0th, 1st and 2nd Betti numbers [65] respectively. In [96] *Rosenfeld defined* components, cavities, background and established their topological properties with mathematical rigor.

In 3D digital topology 'tunnel' [51,53,111,113,114,115,116] and 'hole' [76,95] refer to the same topological concept. Unlike components and cavities it is not possible to define a 'tunnel' although the number of tunnels has a precise definition [96,51]. The number of tunnels in a polyhedral set is the rank of its first homology group [56]. According to Morgenthaler, a component S contains no tunnel if each closed path in S is reducible i.e. equivalent to a degenerate closed path of single point. Kong, Roscoe and Rosenfeld [53] presented a physical sense about the number of tunnels in a polyhedral set. They [53] also gave a formal definition of the number of tunnels in 3D digital image. In a series of papers [111,113,114,115,116], we have presented a rigorous study on the existence of tunnel as well as the number of tunnels in $3 \times 3 \times 3$ neighborhood using (26,6) adjacency *relation. We have proposed the necessary* and the sufficient condition for the existence of tunnels in [111,113] and have also defined the number of tunnels [111,115] in $3 \times 3 \times 3$ neighborhood. In [114] we have established the claim of [111,113] about the existence of tunnels while in [116] we have established the claim of [111,115] about the number of tunnels. A detailed discussion on the number of tunnels in $3 \times 3 \times 3$ neighborhood may be found in Section 2.3.2.

Kong et. al. [53] gave a formal definition of the Euler characteristic of a digital image using continuous analog concept. Several publications on computation of the Euler characteristic of digital image could be found in the literature [14,15,26,139].

Dyer [26] proposed an interesting algorithm of computing the Euler characteristic of a 2D digital image from its quad-tree representation. In [14], a recursive algorithm was proposed for computing the Euler characteristic and other additive functionals of an n-dimensional digital image from its array representation. Bieri [15] modified their previous algorithm of computing the Euler characteristic and other additive functionals of an n-dimensional digital image from its n-tree representation. In [139] Voss proposed an interesting approach to computing the Euler characteristic of an object in n-dimensional homogeneous grid. In [115,116] we have described a parallel algorithm to compute the Euler characteristic of a 3D digital image from its array representation. While other algorithms work on the number of all i-dimensional elements for $0 \leq i \leq n$ in a polyhedral representation of a digital object, our algorithm is based on detecting the change in the numbers of black components, tunnels and cavities in the $3 \times 3 \times 3$ neighborhood of a point due to its deletion.

1.3.6 Topology Preservation in 3D Digital Space

A few definitions of what is meant by topology preservation or topological equivalence in 3D digital space, can be found in the literature [50,51,76,129,70]. Kong and Rosenfeld [51] made a survey on topology preservation in digital space. We intend to discuss topology preservation to some detail as we consider this to be a concept of vital importance in digital topology for many real-life image processing applications. Tourlakis and Mylopoulos [129] gave a sound definition of topological equivalence for finite (4,8) and (6,26) digital images and their higher dimensional analogs. According to them two finite digital images are topologically equivalent if and only if one can be transformed to the other by sequential binary transformations of simple points. This criterion of topology preservation claims a definition of simple point independent of the notion of topology preservation. Kong and Rosenfeld [51] mentioned the following criterion of topology preservation on the basis of Morgenthaler's [76] discussion.

Criterion 1.1 *Let $P_1 = (Z^3, \alpha, \beta, B)$ be a 3D digital image. Let $P_2 = (Z^3, \alpha, \beta, B - D)$ be the image obtained by deleting the set of points D from B. This deletion preserves topology if and only if all the following conditions are satisfied:*

1. *Each black component of P_1 contains exactly one black component of P_2.*

2. *Each white component of P_2 contains exactly one white component of P_1.*

3. *Each closed path of B can be digitally deformed in B to a closed path of $B - D$.*

4. *If one closed path ς_1 in $B - D$ can be digitally deformed in B to another closed path ς_2 in $B - D$ then ς_1 can be digitally deformed to ς_2 in $B - D$.*

The definition of the phrase 'can be digitally deformed' by Morgenthaler [76] is only appropriate for (6,26) digital images and there is no base point that remains fixed [51]. In the above criterion Conditions 1 and 2 preserve one to one correspondence between black components and white components respectively in P_1 and P_2. On the other hand, Conditions 3 and 4 together preserve one to one correspondence of solid handles and torus (in connection with tunnels) in P_1 and P_2.

Kong [54] proposed the following criterion of topology preservation in 3D digital space based on the concept of digital fundamental group.

Criterion 1.2 *Let $P_1 = (Z^3, \alpha, \beta, B)$ be a 3D digital image. Let $P_2 = (Z^3, \alpha, \beta, B - D)$ be the image obtained by deleting the set of points D from B. This deletion preserves topology if and only if all the following conditions are satisfied:*

1. *Each black component of P_1 contains exactly one black component of P_2.*

2. *Each white component of P_2 contains exactly one white component of P_1.*

3. *For each point $p \in \mathcal{B} - D$, the inclusion map $i : \mathcal{B} - D \to \mathcal{B}$ induces a group isomorphism $i_* : \pi(P_2, p) \to \pi(P_1, p)$.*

4. *For each point $q \in Z^3 - \mathcal{B}$, the inclusion map $j : Z^3 - \mathcal{B} \to Z^3 - (\mathcal{B} - D)$ induces a group isomorphism $j_* : \pi(\overline{P_1}, q) \to \pi(\overline{P_2}, q)$.*

As mentioned by Kong and Rosenfeld [51] Criterion 1.2 is more stringent than Criterion 1.1. Conditions 1 and 2 of both the criteria are exactly the same. Conditions 1 and 3 of Criterion 1.2 together imply Conditions 3 and 4 of Criterion 1.1. Also, it is possible to find an example where all the four conditions of Criterion 1.1 are satisfied while Condition 4 of Criterion 1.2 is not satisfied.

Kong [50] proposed another definition of topology preservation as follows: let P_2 be obtained from a 3D digital image P_1 after deleting a set of black points. This conversion from P_1 to P_2 preserves topology if and only if $C(P_2)$ can be obtained by collapsing [41] of $C(P_1)$.

Ma [70] presented a sufficient condition for topology preservation in connection with 3D parallel thinning. We state his sufficient condition for topology preservation in (26,6) digital images.

Criterion 1.3 *A parallel reduction operator D is topology preserving in a* (26,6) *digital image P if both the following conditions are satisfied by D:*

1. *Each set of black points of P that is deleted by D and is contained in a unit lattice square is a simple set.*

2. *D never deletes a black component of P that is contained in a unit lattice cube.*

A set of black points S is a simple set in P if S can be arranged in a sequence $p_1, p_2, \cdots, p_n$ such that each p_i is a simple point in P after deleting the points $p_1, \cdots, p_{i-1}$.

Ma [70] also established similar conditions of topology preservation for (6,26), (18,6) and (6,18) digital images.

1.3.7 3D Simple Point

Simple point has applications [70] in many homotopy preserving operations of image processing e.g. shrinking, thinning etc. While the concept of 2D simple point was realized by simple conditions in early seventies [95,83], the concept of 3D simple point has been realized by straightforward conditions very recently when we have presented the characterization of 3D simple point [111,113,114] based on connectedness of the points in $3 \times 3 \times 3$ neighborhood. Basic difficulty in defining 3D simple point is the concept of 'tunnel' in 3D that does not exist in 2D. In [111,113,114] we have established that the existence of tunnels in the $3 \times 3 \times 3$ neighborhood of a point p can be defined by connectedness of points in $\mathcal{N}(p)$. Some characterizations of 3D simple point exist in literature [129,76,131]. Tourlakis and Mylopoulos [129] gave a characterization of simple point applicable in any number of dimensions. They used the term 'deletable point' instead of simple point. Morgenthaler [76] used the notion of tunnels while Tsao and Fu [131] used the notion of the Euler characteristic to characterize 3D simple points. The elegance of our characterization [111,113,114] of 3D simple point lies in the fact that it neither uses the notion of tunnel nor the Euler characteristic. An efficient algorithm to detect 3D simple point using the notions of 'dead-surface', 'dead-edge', 'effective point', 'isolated point' and 'geometric class' has been proposed in [111,113]. The algorithm has been further modified in [114]. A detailed discussion on the theoretical aspects of 3D simple point may be found in Section 2.2 and Section 2.4. The computational aspects of 3D simple point are elaborately described in Section 3.4.

1.3.8 Object Thinning, Labeling and Border Tracking

Although 3D thinning has a lot of interest in 3D image processing [122,70], only a few publications [32,69,70,76,79,111,113,114,117,122,123,128,130,131] are found in 3D thinning. Based on preservation of the Euler characteristic, Lobregt et. al. [69] proposed an algorithm for detecting simple points applied in 3D thinning. Unfortunately, their algorithm fails in some situations as pointed out in [113]. Morgenthaler [76] described a parallel thinning algorithm based on his notion of 'end' point. His notion of 'end' point is different from the notion of end point of curves or edge point of surfaces. Based on path connectivity, Srihari et. al. [122] described a sequential boundary removal algorithm for 3D thinning. They also discussed about the practical applications of 3D thinning. Tsao and Fu [130] proposed a parallel 3D thinning algorithm based on the notion of surface connectivity. In the same paper [130] they pointed out that in 3D parallel thinning situations may occur where each of two points preserves topology when deleted separately while topology preservation is violated when the same two points are deleted in parallel. They gave solution to this problem by imposing an additional topology preservation check in 3×3 middle planes of deletable points. Hafford and Preston [32] extended the concept of sub-fields [28] in 3D and developed a parallel thinning algorithm for tetradecahedral tessellation. Mukherjee et. al. [79] extended the 2D thinning algorithm SPTA [84] to develop a 3D thinning algorithm. In [71] Ma suggested sufficient conditions of 3D parallel reduction operator that preserves topology for (26,6), (18,6), (6,26) and (6,18) 3D digital images. In [70], he established the topological soundness of his early results on parallel reduction operator [71] using the notion of minimal non-simple set. He also discussed many interesting properties of minimal non-simple set. In [117] we have presented a parallel thinning algorithm for 3D objects and studied its topology and shape preserving properties. Behavior of the thinning algorithm around different types of corners have been studied in the same paper. The notions of shape points and open points have been introduced which lead to good quality skeletons as verified by experimental results. Robustness

of the thinning algorithm under pseudo random contour noise and rotation has been studied and the results have been presented in [117].

Border tracking algorithms have applications [136] in medical image processing such as detection and display of isolated internal organs from 3D CT data. Artzy, Frieder and Herman [10] proposed an efficient algorithm of border tracking in three dimensional (18,6) digital images. Herman and Webster [35] established the topological correctness of the algorithm. Udupa, Srihari and Herman [134] gave a border tracking algorithm that can be applied to any dimensions. Gorden and Udupa [29] presented an efficient border tracking algorithm for three dimensional digital images. In [135] Udupa and Ajjanagadde discussed the application of object labeling algorithms [93,86,120,133,1] to three dimensional medical image display. In the same paper [135] they presented an algorithm for tracking all connected surfaces and for generating information about the connected objects in a three dimensional digital image.

1.3.9 Topology Based Segmentation

Local topological parameters may be used to produce a meaningful segmentation of 3D objects [73,115] from their surface skeletal representations. Segmentation produces a more compact and highly structured representation of an object which is useful in recognition and analysis. Malandain et. al. [73] presented a topology based segmentation of digital surface. They used the classification of points in the Euclidean 3-space and directly applied to digital space that leads to undesired situations some of which were discussed by them [73]. Their approach of point classification used the numbers of adjacent object components (called as C^* in [73]) and adjacent background components (called as $\overline{C}$ in [73]) of a point in its $3 \times 3 \times 3$ neighborhood. The concept of using 18-neighborhood in computing $\overline{C}$ was first proposed by Saha et. al. [111]. In [115] we have developed a segmentation approach of 3D objects from their surface skeleton. Our point classification method has been

based on the change in the numbers of black components, tunnels and cavities in the $3 \times 3 \times 3$ neighborhood of a point under its binary transformation. The classification method [115] has the property that it produces exactly one curve of junction points when two or more surfaces join and produces exactly one junction point when one or more curves join a surface or two or more curves join themselves. This property was violated by the classification method of [73]. The results of point classification method have been applied for a meaningful segmentation [115] of 3D digital objects. The segmentation method has also been supported by experimental results [115].

1.4 Scope and Layout of the Thesis

In **Chapter 1** after presenting basic concepts and useful definitions of 3D digital topology the current status has been surveyed. We have discussed different existing definitions of topology preservation in 3D digital space, 3D simple points and their applications to object thinning and segmentation.

In **Chapter 2**, at first, we make an in-depth study on 3D simple point. We establish a theorem that defines the number of tunnels in $3 \times 3 \times 3$ neighborhood in terms of the connectedness of points which was a 'bottle-neck' in characterizing 3D simple points. In this connection the notion of minimal separator is introduced. An efficient characterization of (26,6) simple point is developed. The theorem defining the number of tunnels leads to an effective measure of local topological changes under binary transformation of a point.

In **Chapter 3**, we investigate the computational aspects of 3D simple point and the measure of local topological changes in the context of image processing. Efficient algorithms are developed to detect (26,6) simple points and to compute local topological parameters (these parameters also characterize a measure of local topological changes under binary transformation of a point) using the concepts of 'dead-surface', 'effective points', 'geometric class' and some other interesting properties of

$3 \times 3 \times 3$ neighborhood. A parallel algorithm is also developed for computing the Euler characteristic of a 3D digital object.

In **Chapter 4**, we develop a new shape preserving parallel thinning algorithm for 3D digital images. Along with topological aspects we discuss about non-topological aspects of the 3D thinning algorithm. We study the quality of skeletons around different types of corners and make an extensive study on the behavior of the algorithm under pseudo random contour noise and rotation using shape distance measure. The parallel thinning algorithm is also supported by experimental results.

In **Chapter 5**, we describe a topology based 3D object segmentation approach from its surface skeletal representation. At first we classify the points to detect the junction points in a digital surface. For this purpose we use local topological parameters of every point. After detecting the junction points, the information is applied to develop a new segmentation method. Finally the results of segmentation of different 3D objects are presented and discussed.

In **Chapter 6**, we present the conclusion of the work and suggest some directions for future research.

Chapter 2

3D Digital Topology Under Binary Transformation

2.1 Introduction

Most of the binary image processing techniques (e.g. shrinking, thinning, erosion, dilation, closing, etc.) *need sequential or parallel transformation of points* under some predetermined constraints. One such useful constraint is the topology preservation mostly used in shrinking, thinning and other homotopy preserving transforms. In this chapter we consider the issues concerned with topology preservation in 3D digital space. Topology preservation mainly deals with the question — whether the binary transformation of a point (or a set of points) preserves the topology of an image or not. However, it is also interesting to answer the question — if the binary transformation of a point (or a set of points) at all changes the image topology then is it possible to have a measure of the change? If 'yes' then

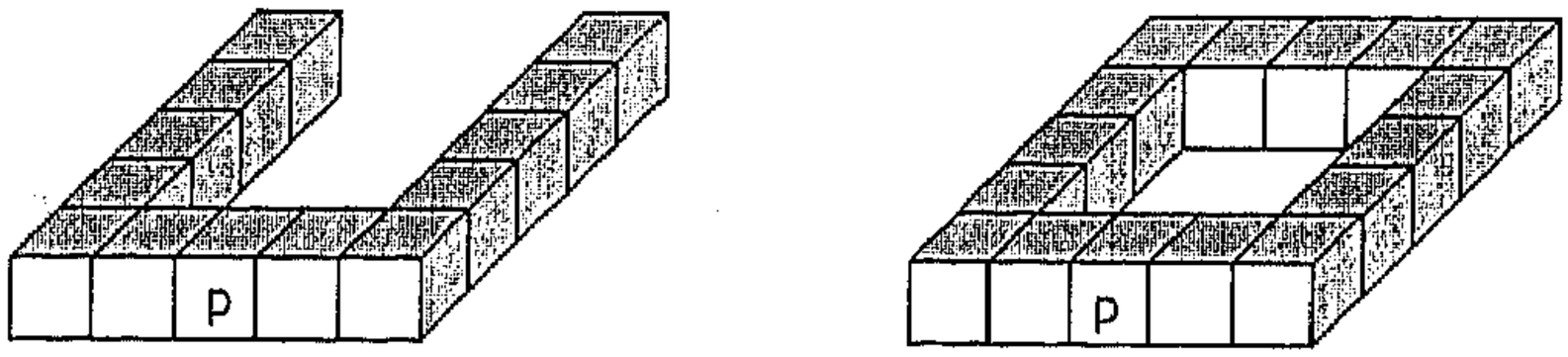

(a) (b)

Figure 2.1: (a) Deletion of p splits one black component into two. (b) Deletion of p removes a tunnel. The $3 \times 3 \times 3$ neighborhood configurations of p are same in both (a) and (b).

how to measure and what is the measure? This measure gives us an idea about the loss of topological information in relevant operations. This information may be used in classification of points, junction detection, meaningful segmentation of digital surface representations and in other relevant applications.

In this thesis, we restrict ourselves to the binary transformation of single point. A point whose binary transformation does not change the image topology is referred as simple point [76,130,129,51]. One major hurdle in characterizing 3D simple point is the concept of 'tunnels'. In Section 2.3.2, we establish a theorem [111,113,114,115,116] that defines the number of tunnels in $3 \times 3 \times 3$ neighborhood. Based on this theorem, an efficient characterization [111,113,114] of (26,6) simple point is developed in Section 2.4. A measure of the topological changes under binary transformation of a point has a lot of interest which is another contribution of this chapter. For example, the deletion of a point may remove a black component or split a black component into two or more black components. Further, the deletion of a point may remove or create tunnels. Similarly, the transformation may remove or create cavities. We measure the topological changes in an image under binary transformation of a point in terms of these numbers. As mentioned in [65], using any local window analysis it is not possible to measure this change in the entire image. For example, see Figure 2.1. In Figure 2.1(a), the deletion of

the point p splits one black component into two while in Figure 2.1(b) the deletion of p removes a tunnel from the image. It may be noted from Figure 2.1(a) and (b) that the $3 \times 3 \times 3$ neighborhood configurations of p are same in both the cases. Therefore, we confine ourselves to the computation of the topological changes in the $3 \times 3 \times 3$ neighborhood only. This measure of local topological changes is presented in Section 2.5.

2.2 3D Simple Point

2.2.1 Discussion

In an image $P = (Z^3, \alpha, \beta, B)$, a point $p \in B$ is a simple point if and only if its removal from B preserves the topology of P. As considered by many authors [69,51,76,130], topology preservation in the $3 \times 3 \times 3$ neighborhood under binary transformation is the necessary and sufficient condition for simple point. In other words, a point is a simple point if and only if its deletion does not change the numbers of black components, tunnels and cavities in its $3 \times 3 \times 3$ neighborhood. It may be noted that various definitions of topology preservation in 3D digital space, presented in Section 1.3.6, are not equivalent to each other. However, the different definitions of topology preservation uniquely characterizes simple points [51]. In other words, the different definitions of topology preservation are equivalent for sequential deletion of one black point.

For the convenience of the reader, we demonstrate the idea of simple points in $(26,6)$ connectivity. Let $P_1 = (Z^3, 26, 6, B)$ be an image and let $P_2 = (Z^3, 26, 6, B - \{p\})$ be obtained from P_1 after the removal of $p \in B$ from B. The following topological

changes may occur in P_2 under the above transformation [111]:

1. one black component of P_1 is removed in P_2 (at most one black component may be removed due to deletion of single point),
2. one black component of P_1 splits into two or more black components in P_2,
3. one or more tunnels of P_1 are removed in P_2,
4. one or more tunnels are created in P_2,
5. one or more cavities of P_1 are removed in P_2,
6. one cavity is created in P_2 (at most one new cavity may be created due to deletion of single point).

It may be noted that (1) occurs if and only if p is not 26-adjacent to any black point. In other words p has no black 26-neighbor. Either (2) or (3) occurs if and only if the deletion of p creates two or more black components in its $3 \times 3 \times 3$ neighborhood. Either (4) or (5) occurs if and only if the deletion of p creates one or more tunnels in its $3 \times 3 \times 3$ neighborhood. Finally, (6) occurs *if and only if the deletion of* p creates a cavity in its $3 \times 3 \times 3$ neighborhood.

We present a few examples to illustrate simple points in (26,6) connectivity. In Figure 2.2, deletion of the point p creates two black components in its $3 \times 3 \times 3$ neighborhood. In Figure 2.3, deletion of p creates a tunnel in its $3 \times 3 \times 3$ neighborhood. In Figure 2.4, deletion of p creates a cavity in $\mathcal{N}(p)$ while in Figure 2.5, the deletion of p removes a black component from its $3 \times 3 \times 3$ neighborhood. Thus, p is not a (26,6) simple point in each of Figures 2.2– 2.5. On the other hand, in Figure 2.6, deletion of p leads to exactly one black component without tunnels and cavities in its $3 \times 3 \times 3$ neighborhood. Thus, in Figure 2.6, p is an example of (26,6) simple point.

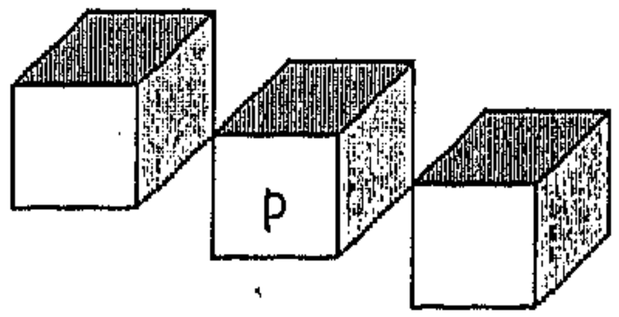

Figure 2.2: An example of (26,6) non-simple point. Deletion of the point p creates two black components in its $3 \times 3 \times 3$ neighborhood.

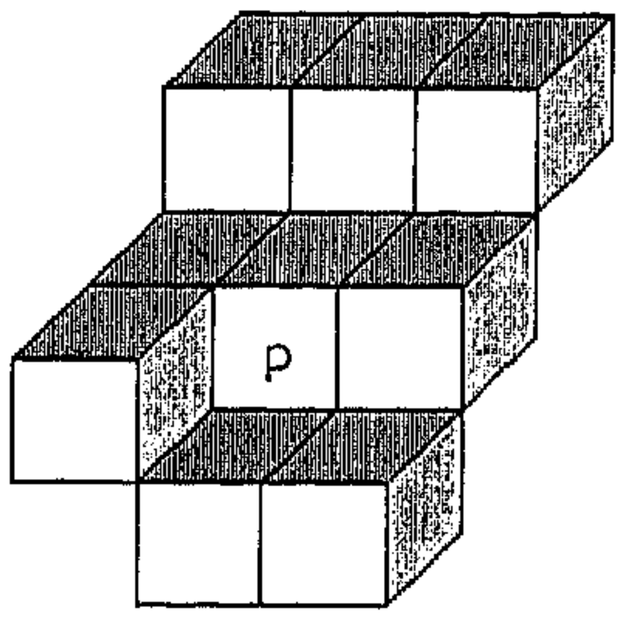

Figure 2.3: An example of (26,6) non-simple point. Deletion of the point p creates a tunnel in its $3 \times 3 \times 3$ neighborhood.

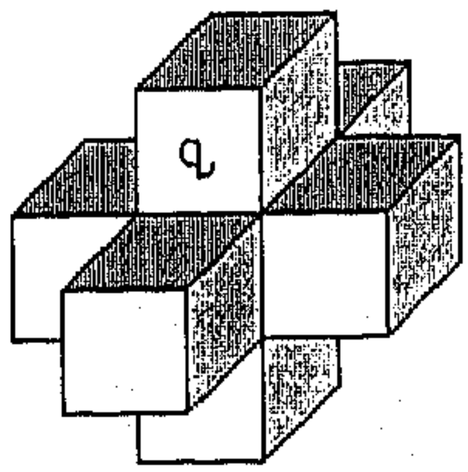

Figure 2.4: An example of (26,6) non-simple point. p is the hidden point just below the point q. Deletion of the point p creates a cavity in its $3 \times 3 \times 3$ neighborhood.

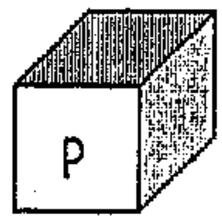

Figure 2.5: An example of (26,6) non-simple point. Deletion of the point p removes a black component from its $3 \times 3 \times 3$ neighborhood.

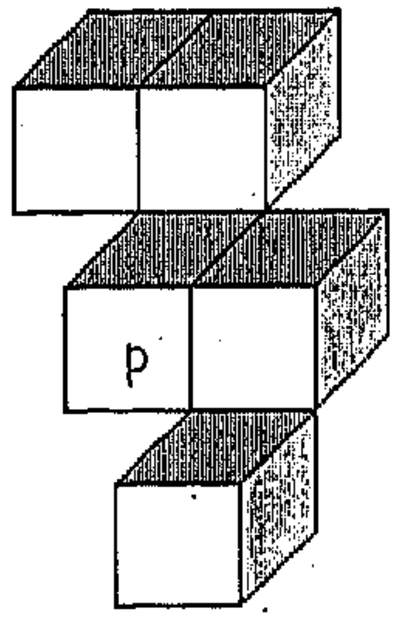

Figure 2.6: An example of (26,6) simple point. Deletion of the point p leads to exactly one black component without tunnels and cavities in its $3 \times 3 \times 3$ neighborhood.

2.2.2 Previous works

Morgenthaler [76] proposed a characterization of 3D simple point as follows:

Characterization 2.1 *Let $P = (Z^3, \alpha, \beta, B)$ be a 3D digital image. A point $p \in B$ is a simple point if and only if the following four conditions are satisfied:*

1. *The number of components of $B \cap N(p)$ is equal to that of $B \cap N^*(p)$.*

2. *The number of components of $((Z^3 - B) \cap N(p)) \cup \{p\}$ is equal to that of $(Z^3 - B) \cap N^*(p)$.*

3. *The number of tunnels in $B \cap N(p)$ is equal to that in $B \cap N^*(p)$.*

4. *The number of tunnels in $((Z^3 - B) \cap N(p)) \cup \{p\}$ is equal to that in $(Z^3 - B) \cap N^*(p)$.*

Kong and Rosenfeld [51] presented a simpler characterization of simple point (as mentioned by them this characterization is essentially due to Tsao and Fu [130]) using the Euler characteristic.

Characterization 2.2 *A black point p is a simple point in a 3D digital image $P = (Z^3, \alpha, \beta, B)$, where $(\alpha, \beta) = (26, 6)$ or $(6, 26)$, if and only if the following three conditions are satisfied:*

1. *Exactly one component of $N^*(p) \cap B$ is adjacent to p.*

2. *Exactly one component of $N(p) - B$ is adjacent to p.*

3. $\chi(Z^3, \alpha, \beta, B \cap N(p)) = \chi(Z^3, \alpha, \beta, B \cap N^*(p))$, *where* $\chi(\cdot)$ *is the Euler characteristic.*

In [130], Tsao and Fu made the following observation on 3D simple point: let $P = (Z^3, \alpha, \beta, B)$, where $(\alpha, \beta) = (26,6)$ or (6,26), be a 3D digital image. Let $p = (x_0, y_0, z_0)$ be a black point of P. Let P_x, P_y, P_z be three co-ordinate planes $x = x_0$, $y = y_0$, and $z = z_0$ respectively. Then one can find a 2D digital image P_x in P_x as $P_x = (Z^2, \alpha', \beta', B_x)$, where $B_x = \{(y,z) \in Z^2 \mid (x_0, y, z) \in B\}$ and $(\alpha', \beta') = (8,4)$ if $(\alpha, \beta) = (26,6)$ and $(\alpha', \beta') = (4,8)$ if $(\alpha, \beta) = (6,26)$. Similarly, one can define other two 2D digital images P_y and P_z in P_y and P_z respectively. Tsao and Fu [130] observed that if p is a simple point in at least two of P_x, P_y, P_z then p is a simple point in P. A simple point p in P_x means that the point (y_0, z_0) is a simple point in P_x, and similarly for P_y and P_z. Tsao and Fu proposed the result for (26,6) and (6,26) connectivity. Kong and Rosenfeld [51] mentioned that this result is true for (6,18) and (18,6) connectivity relations also. However, the above condition is sufficient but not necessary for p to be a simple point, and so it is not a characterization of simple points.

Characterizations 2.1 and 2.2 of 3D simple points are not attractive from computational point of view since they use the concepts of tunnels (Characterization 2.1) and the Euler characteristic (Characterization 2.2). Towards developing a computaionally attractive solution, in Section 2.3.2 we establish a new definition of the number of tunnels in $3 \times 3 \times 3$ neighborhood [111,113,114]. This uses only the connectivity of points of $3 \times 3 \times 3$ neighborhood. This results in a new characterization of (26,6) simple point [111,113,114] in Section 2.4 that neither needs the concept of tunnels nor the Euler characteristic.

2.2.3 Formal Definition

To reach the new characterization of 3D simple point we start with Characterization 2.2 as a definition of simple points. However, it is observed that this characterization is also valid for $p \in Z^3 - B$. Therefore, we start with the following definition of (26, 6) simple point which differs from Characterization 2.2 in the only respect that here the definition is valid irrespective of whether p is black or white.

Definition 2.1 *Let $P = (Z^3, 26, 6, B)$ be a 3D digital image. A point $p \in Z^3$ is a simple point in P if and only if the following four conditions are satisfied:*

1. *Exactly one 26-component of $N^*(p) \cap B$ is 26-adjacent to p.*

2. *Exactly one 6-component of $N(p) - B$ is 6-adjacent to p.*

3. $\chi(\dot{N}(p)) = \chi(\hat{N}(p))$.

It may be noted that the Definition 2.1 of simple points is independent of the notion of tunnels (as $\chi(\cdot)$ may be defined without the notion of tunnels). Therefore, we can define the number of tunnels using the notion of simple points.

2.3 3D Simple Point: Prerequisite

As a prerequisite to the characterization of (26,6) simple points detailed in Section 2.4 we need to define the followings:

(a) the number of black components, tunnels and cavities in $\dot{N}(p)$,

(b) the number of black components, tunnels and cavities in $\hat{N}(p)$.

Note that the key contribution of this section is to define the topological parameters of (a) and (b) using only the connectivity of points of $3 \times 3 \times 3$ neighborhood. The topological parameters of (a) are defined by Proposition 2.1. For (b), the number of black components of $\hat{\mathcal{N}}(p)$ needs no further clarification while the numbers of cavities and tunnels are defined in Equation 2.1 and Theorem 2.1 respectively. However, the proof of Theorem 2.1 demands a new look of the connectivity relationship through minimal separator which is detailed in Section 2.3.1. Henceforth, we consider Z^3 as the image set and (26,6) connectivity relation unless stated otherwise.

Definition 2.2 *Shrinking is a process of sequential transformation of black simple points (see Definition 2.1) to white in an image as long as the image contains any black simple point. Let $P = (Z^3, 26, 6, B)$ be a 3D digital image. Let $P' = (Z^3, 26, 6, B')$ be a shrunk version of P. Then $B' \subset B$ and B' contains no simple point.*

Definition 2.3 *Let $x = (x_1, x_2, x_3)$ and $y = (y_1, y_2, y_3)$ be two points in Z^3. Four sets on x, y are defined as follows: $rt(x,y) = \{(z_1, z_2, z_3) \mid (z_1, z_2, z_3) \in Z^3$ and $\max(x_i, y_i) \geq z_i \geq \min(x_i, y_i)$, for $1 \leq i \leq 3\}$; $rti(x,y) = \{(z_1, z_2, z_3) \mid (z_1, z_2, z_3) \in Z^3$ and $\max(x_i, y_i) > z_i > \min(x_i, y_i)$, for $1 \leq i \leq 3\}$; $rts(x,y) = rt(x,y) - rti(x,y)$; $rts^*(x,y) = \{p \mid p \in rts(x,y)$ and p is 6-adjacent to $rti(x,y)\}$.*

Proposition 2.1 *The numbers of black components, tunnels and cavities in $\dot{\mathcal{N}}(p)$ are always 1, 0, 0 respectively.*

Proof. Let (a,d), (b,e), (c,f) be three distinct unordered pairs of opposite s-points of $\mathcal{N}(p)$. In $\dot{\mathcal{N}}(p)$, a v-point $v(a,b,c,p)$ is 26-adjacent to the black points $\{p,\ a,\ b,\ c,\ e(a,b,p),\ e(b,c,p),\ e(c,a,p)\} \cap B$. For all possible combinations of B, $v(a,b,c,p)$ is a simple point in $\dot{\mathcal{N}}(p)$ (see Definition 2.1). Thus, we can remove all black v-points during the shrinking process of $\dot{\mathcal{N}}(p)$. After removing all black

v-points from $\dot{\mathcal{N}}(p)$, an e-point $e(a,b,p)$ is 26-adjacent to the black points $\{p,\ a,\ b,\ c,\ f,\ e(a,c,p),\ e(b,c,p),\ e(a,f,p),\ e(b,f,p)\} \cap \mathcal{B}$. For all possible combinations of $\mathcal{B}$, $e(a,b,p)$ is also a simple point in $\dot{\mathcal{N}}(p)$ (see Definition 2.1). After removing all black v-points and e-points from $\dot{\mathcal{N}}(p)$, an s-point a is 26-adjacent to the black points $\{p,\ b,\ c,\ e,\ f\} \cap \mathcal{B}$. Again, a is a simple point in $\dot{\mathcal{N}}(p)$ for all possible combination of $\mathcal{B}$ (see Definition 2.1). Thus, all black s-points may be removed during the shrinking process of $\dot{\mathcal{N}}(p)$ and the black points of $\dot{\mathcal{N}}(p)$ may be shrunk to p which is single black component without cavities. Further, $\chi(Z^3, 26, 6, \{p\})$ equals to one and thus, the number of tunnels in $(Z^3, 26, 6, \{p\})$ is zero[1]. Hence, the number of black components, tunnels, and cavities in $\dot{\mathcal{N}}(p)$ are 1, 0, 0 respectively. □

In $\hat{\mathcal{N}}(p)$, the unbounded white component contains the set of points $Z^3 - \mathcal{N}(p)$. It may be noted that p is the only white point in $\hat{\mathcal{N}}(p)$ which is not 6-adjacent to $Z^3 - \mathcal{N}(p)$. Therefore, the set of white points of $\hat{\mathcal{N}}(p)$ is not 6-connected i.e. $\{p\}$ is a white component of $\hat{\mathcal{N}}(p)$, if and only if all the 6-neighbors of p are black. Hence, the number of cavities in $\hat{\mathcal{N}}(p)$ is stated as follows:

$$\text{number of cavities in } \hat{\mathcal{N}}(p) = \begin{cases} 1 & \text{if all 6-neighbors of } p \text{ are black,} \\ 0 & \text{otherwise.} \end{cases} \tag{2.1}$$

2.3.1 Minimal Separator

In this section we develop a new approach of defining connectivity of a set of points through the concept of minimal separators. Also, we find out the exhaustive set of minimal separators (with respect to 26-connectivity) of $\mathcal{N}(p)$. This formulation is useful to establish some propositions which are the building blocks of Theorem 2.1.

Definition 2.4 *Let S be an α-connected non-empty subset of Z^3 where $\alpha \in \{6, 18, 26\}$. A minimal α-separator of S is defined as a minimal subset $\mathcal{F}$ of S such*

[1]the Euler characteristic is the number of components minus the number of tunnels plus the number of cavities

that $\mathcal{F} - S$ is not α-connected. The minimality is achieved in the sense that for any proper subset X of $\mathcal{F}$, $S - X$ is α-connected.

Using the above definition of minimal α-separators, the α-connectivity of a set of points may be stated as follows:

Proposition 2.2 *Let S be the set $rt(x,y)$ for some $x, y \in Z^3$ and let X be a subset of S. Under this assumption, X is not α-connected if and only if there exists a minimal α-separator of S, say $\mathcal{F}$, such that $\mathcal{F} \subset S - X$ and at least two α-components of $S - \mathcal{F}$ intersect with X.*

Proof. Let us consider the "*If part*" and the "*Only if part*" of this proposition separately as follows:

If part

Let us assume that there exists a minimal α-separator $\mathcal{F}$ such that $\mathcal{F} \subset S - X$, and two α-components of $S - \mathcal{F}$, say A_1 and A_2 intersect with X. From the definition of minimal α-separators it follows that a point of $A_1 \cap X$ is never α-connected to a point of $A_2 \cap X$ in $S - \mathcal{F}$. Now, $\mathcal{F} \subset S - X$ and $X \subset S$ imply $X \subset S - \mathcal{F}$. Thus, a point of $A_1 \cap X$ is never α-connected in X to a point of $A_2 \cap X$. Hence the "*If part*" is established.

Only if part

Let us assume that X is not α-connected. Let two α-components of X be X_1 and X_2. Let us define two sets as follows: $E = (\bigcup_{p \in X_1} \mathcal{N}_\alpha(p)) \cap S$ and $E' = E - X_1$. Now, X_1 is an α-component of X implies that $E' \cap X = \phi$ *i.e.* $E' \subset S - X$. Again X_1 is an α-component of $S - E'$ and $X_2 \subset S - (E' \cup X_1)$. Thus, $S - E'$ is not α-connected. Obviously, X_1 and X_2 belong to different α-components of $S - E'$. From E' we can find a minimal α-separator $\mathcal{F} \subset E'$ *i.e.* $\mathcal{F} \subset S - X$, such that one α-component of $S - \mathcal{F}$ contains X_1 while another α-component contains X_2. One of

the methods of finding $\mathcal{F}$ from E' is as follows: remove a point from E' which is not α-adjacent to the component of $S - E'$ containing X_2. This process is repeated as long as E' contains any removable point. It goes without saying that this process is bound to terminate within a finite number of steps for the simple reason that the whole set-up is dealt with finite number of points. Finally, E' is assigned to $\mathcal{F}$. Hence the "*Only if part*" is established.

□

Although we impose a restriction on S in Proposition 2.2, it remains valid for any α-connected S. We impose this restriction for two reasons: (a) the proof is valid under this restriction (the approach of getting $\mathcal{F}$ in "Only if part"), (b) we are interested about the subsets of $\mathcal{N}(p)$ which fulfills the restriction. However, it would be of interest to find a generalized version of this proof.

Proposition 2.3 *Let $\mathcal{F}$ be a minimal α-separator of a non-empty α-connected set $S \subset Z^3$ such that $X_1, X_2, \cdots, X_n$ are α-components of $S - \mathcal{F}$, then each point of $\mathcal{F}$ is α-adjacent to all X_is for $i = 1, 2, \cdots, n$.*

Proof. Let us consider that there exists a point $p \in \mathcal{F}$ such that it is not α-adjacent to an α-component of $S - \mathcal{F}$, say X_1. Since X_1 is an α-component of $S - \mathcal{F}$, X_1 is not α-adjacent to any point of $S - (\mathcal{F} \cup X_1)$. Again, X_1 is not α-adjacent to p. It implies that X_1 is not α-adjacent to any point of $S - ((\mathcal{F} - \{p\}) \cup X_1)$. Thus, X_1 is an α-component of $S - (\mathcal{F} - \{p\})$. Hence, $S - (\mathcal{F} - \{p\})$ is not α-connected. This contradicts the definition of minimal α-separators.

□

It may be noted that $\mathcal{N}(p)$ is the set $rt(x, y)$ where $x = (i_p + 1, j_p + 1, k_p + 1)$ and $y = (i_p - 1, j_p - 1, k_p - 1)$ assuming that $p = (i_p, j_p, k_p)$. Therefore, Proposition 2.2 is true for any set lying within $\mathcal{N}(p)$. In the remaining part of this section, we find out the set of all possible minimal 26-separators of $\mathcal{N}(p)$. In this section, $\mathcal{F}(p)$ represents a minimal 26-separator of $\mathcal{N}(p)$ unless stated otherwise.

Proposition 2.4 *$\mathcal{F}(p)$ contains p.*

Proof. This proposition is proved by contradiction. Let us assume that $p \notin \mathcal{F}(p)$. Then $p \in \mathcal{N}(p) - \mathcal{F}(p)$. Further, every point of $\mathcal{N}(p)$ is 26-adjacent to p. Thus, each $q, r \in \mathcal{N}(p) - \mathcal{F}(p)$ are 26-connected by the 26-path q, p, r. Hence, $\mathcal{N}(p) - \mathcal{F}(p)$ is 26-connected. Contradiction!!

□

Proposition 2.5 *$\mathcal{F}(p)$ does not contain any v-point.*

proof. This proposition is proved by contradiction. Let us assume that a v-point $x \in \mathcal{F}(p)$. Hence $(\mathcal{N}(p) - \mathcal{F}(p)) \cup \{x\}$ is 26-connected by the definition of $\mathcal{F}(p)$. Let us consider two points $q, r \in \mathcal{N}(p) - \mathcal{F}(p)$ which are not 26-connected in $\mathcal{N}(p) - \mathcal{F}(p)$. As q and r are 26-connected in $(\mathcal{N}(p) - \mathcal{F}(p)) \cup \{x\}$, there must be a 26-path $q = p_0, p_1, \cdots, p_i, x, p_{i+1}, \cdots, p_n = r$ in $(\mathcal{N}(p) - \mathcal{F}(p)) \cup \{x\}$. Since, x is a v-point, every two points of $\mathcal{N}(p, x)$ are 26-adjacent to each other. Thus, p_i and p_{i+1} are 26-adjacent to each other. Therefore, there exists a 26-path $q = p_0, p_1, \cdots, p_i, p_{i+1}, \cdots, p_n = r$ from q to r in $\mathcal{N}(p) - \mathcal{F}(p)$. This contradicts the assumption that q and r are not 26-connected in $\mathcal{N}(p) - \mathcal{F}(p)$.

□

Proposition 2.6 *$\mathcal{N}(p) - \mathcal{F}(p)$ contains exactly two 26-components.*

proof. Let us assume that $\mathcal{N}(p) - \mathcal{F}(p)$ contains more than two 26-components, say, $X_1, X_2, \cdots, X_n$. According to Proposition 2.5, $\mathcal{F}(p)$ contains no v-point. Let S be the set of all s-points of $\mathcal{N}(p)$. Then $\mathcal{N}(p) - S$ is always 26-connected. Thus, $\mathcal{N}(p) - S'$ is 26-connected for all $S' \subset S$. Therefore, $\mathcal{F}(p)$ must contain some e-point. Let a, b, c be three mutually non-opposite s-points of $\mathcal{N}(p)$ and let f be the s-point opposite to c. Without loss of generality, let us assume that $e(a, b, p) \in \mathcal{F}(p)$.

By definition, $\mathcal{N}(p, e(a,b,p))$ is the set of all points of $\mathcal{N}(p)$ which are 26-adjacent to $e(a,b,p)$. $\mathcal{N}(p, e(a,b,p))$ is equal to $\{p,\ a,\ b,\ e(a,b,p),\ c,\ e(a,c,p),\ e(b,c,p),\ v(a,b,c,p),\ f,\ e(a,f,p),\ e(b,f,p),\ v(a,b,f,p)\}$. According to Proposition 2.4, p belongs to $\mathcal{F}(p)$ and $e(a,b,p)$ belongs to $\mathcal{F}(p)$ by assumption. Also, a, b must belong to $\mathcal{F}(p)$. Otherwise, $(\mathcal{N}(p) - \mathcal{F}(p)) \cap \mathcal{N}(a, e(a,b,p))$ is 26-connected (as all points of $\mathcal{N}(p, e(a,b,p))$ are 26-adjacent to both a and b) and $e(a,b,p) \in \mathcal{F}(p)$ is 26-adjacent to exactly one 26-component of $\mathcal{N}(p) - \mathcal{F}(p)$. Hence, $\mathcal{N}(p) - \mathcal{F}(p)$ is 26-connected according Proposition 2.3. Contradiction!! Therefore, $a, b \in \mathcal{F}(p)$. Rest of the points of $\mathcal{N}(p, e(a,b,p))$ can be divided into two subsets $\{c,\ e(a,c,p),\ e(b,c,p),\ v(a,b,c,p)\}$ and $\{f,\ e(a,f,p),\ e(b,f,p),\ v(a,b,f,p)\}$ such that every two points belonging to that same subset are 26-adjacent. Hence $e(a,b,p)$ is 26-adjacent to at most two 26-components of $\mathcal{N}(p) - \mathcal{F}(p)$. Thus, $\mathcal{N}(p) - \mathcal{F}(p)$ contains at most two 26-components. By the definition of $\mathcal{F}(p)$, $\mathcal{N}(p) - \mathcal{F}(p)$ contains at least two 26-components. Hence, $\mathcal{N}(p) - \mathcal{F}(p)$ contains exactly two 26-components.

□

Proposition 2.7 *Let x be an s-point of $\mathcal{N}(p)$. If $\mathcal{F}(p)$ intersects $surface(x,p)$ then $surface(x,p) - \mathcal{F}(p)$ is not 26-connected.*

Proof. Let us consider that $\mathcal{F}(p)$ intersects $surface(x,p)$ and $surface(x,p) - \mathcal{F}(p)$ is 26-connected. Let y be a point in $surface(x,p) \cap \mathcal{F}(p)$ and let v_1, v_2, v_3, and v_4 be four v-points belonging to $surface(x,p)$. It may be noted from $\mathcal{N}(p)$ that for any point $q \in surface(x,p)$, $\mathcal{N}(p,q) \subset \bigcup_{i=1}^{4} \mathcal{N}(p, v_i)$. Facts that $v_1, v_2, v_3, v_4 \in \mathcal{N}(p) - \mathcal{F}(p)$ (see Proposition 2.7) and they are 26-connected in $surface(x,p) - \mathcal{F}(p)$ imply that $\bigcup_{i=1}^{4} \mathcal{N}(p, v_i) - \mathcal{F}(p)$ is 26-connected and is a subset of the same 26-component of $\mathcal{N}(p) - \mathcal{F}(p)$. Therefore, $\mathcal{N}(p,y) - \mathcal{F}(p)$ is a subset of one 26-component of $\mathcal{N}(p) - \mathcal{F}(p)$. Hence, y is adjacent to exactly one 26-component of $\mathcal{N}(p) - \mathcal{F}(p)$ and $\mathcal{N}(p) - \mathcal{F}(p)$ is 26-connected according to Proposition 2.3. Contradiction!! □

Proposition 2.8 *Let x be an s-point of $\mathcal{N}(p)$. Then either $surface(x,p) \cap \mathcal{F}(p)$ is empty or it contains x and exactly two e-points.*

Proof. Let us consider that $surface(x,p) \cap \mathcal{F}(p) \neq \phi$. Then $surface(x,p) - \mathcal{F}(p)$ is not 26-connected according to Proposition 2.7. Each point of $surface(x,p)$ is 26-adjacent to x and hence $x \in \mathcal{F}(p)$. According to Proposition 2.5, the v-points of $surface(x,p)$ do not belong to $\mathcal{F}(p)$. Thus, $surface(x,p) \cap \mathcal{F}(p)$ must contain at least two e-points (as $surface(x,p) - \mathcal{F}(p)$ is not 26-connected). We shall show that $surface(x,p) \cap \mathcal{F}(p)$ contains x and exactly two e-points. If this is not true, let us assume that three e-points $e(a,x,p)$, $e(b,x,p)$ and $e(d,x,p)$ belong to $surface(x,p) \cap \mathcal{F}(p)$ where a, d are opposite s-points and a, b, x are mutually non-opposite s-points of $\mathcal{N}(p)$. Let e be the s-point opposite to b. Under this situation, one of the following cases must occur:

(a) $v(a,e,x,p)$ and $v(a,b,x,p)$ belong to the same 26-component of $\mathcal{N}(p) - \mathcal{F}(p)$,

(b) $v(a,b,x,p)$ and $v(b,d,x,p)$ belong to the same 26-component of $\mathcal{N}(p) - \mathcal{F}(p)$,

(c) $v(b,d,x,p)$ and $v(d,e,x,p)$ belong to the same 26-component of $\mathcal{N}(p) - \mathcal{F}(p)$,

or

(d) $v(b,d,x,p)$ and $v(a,e,x,p)$ belong to one 26-component of $\mathcal{N}(p) - \mathcal{F}(p)$ while $v(a,b,x,p)$ and $v(d,e,x,p)$ belong to the other 26-component of $\mathcal{N}(p) - \mathcal{F}(p)$.

For each of the Cases (a)–(c), the e-point being 6-adjacent to both the v-points (mentioned in corresponding case) is 26-adjacent to exactly one 26-component of $\mathcal{N}(p) - \mathcal{F}(p)$. Hence, the contradiction following Propositions 2.3 and 2.6. Now, we consider the situation when none of the Cases (a), (b), (c) occurs whereas Case (d) occurs. It follows that $e(e,x,p) \in \mathcal{F}(p)$ as $v(a,e,x,p)$ and $v(d,e,x,p)$ belong to distinct 26-components of $\mathcal{N}(p) - \mathcal{F}(p)$. As $v(a,e,x,p)$ and $v(a,b,x,p)$ are not 26-connected in $\mathcal{N}(p) - \mathcal{F}(p)$, $\mathcal{N}(p, v(a,e,x,p)) \cap \mathcal{N}(p, v(a,b,x,p))$ must be a subset of $\mathcal{F}(p)$. Hence, the points $a \in \mathcal{F}(p)$. Again, $v(a,b,x,p)$ and $v(b,d,x,p)$ are not 26-connected in $\mathcal{N}(p) - \mathcal{F}(p)$ implies that $b \in \mathcal{F}(p)$. Similarly, $d \in \mathcal{F}(p)$ as $v(b,d,x,p)$ and $v(d,e,x,p)$ are not 26-connected in $\mathcal{N}(p) - \mathcal{F}(p)$ and $e \in \mathcal{F}(p)$ as $v(d,e,x,p)$ and $v(a,e,x,p)$ are not 26-connected in $\mathcal{N}(p) - \mathcal{F}(p)$. Again, $v(a,e,x,p)$ and $v(b,d,x,p)$

are 26-connected in $\mathcal{N}(p) - \mathcal{F}(p)$. Hence, neither $\mathcal{N}(p, v(a, e, x, p)) \cap (\mathcal{N}(p) - \mathcal{F}(p)) = \phi$ nor $\mathcal{N}(p, v(b, d, x, p)) \cap (\mathcal{N}(p) - \mathcal{F}(p)) = \phi$. Thus, the points $e(a, e, p)$ and $e(b, d, p)$ belong to $\mathcal{N}(p) - \mathcal{F}(p)$. Similarly, the points $e(a, b, p)$ and $e(d, e, p)$ belong to $\mathcal{N}(p) - \mathcal{F}(p)$ as $v(a, b, x, p)$ and $v(d, e, x, p)$ are 26-connected in $\mathcal{N}(p) - \mathcal{F}(p)$. Moreover, in $\mathcal{N}(p) - \mathcal{F}(p)$, the following pairs of points are not 26-connected to each other: (1) $e(a, e, p)$ and $e(a, b, p)$, (2) $e(a, b, p)$ and $e(b, d, p)$, (3) $e(b, d, p)$ and $e(d, e, p)$, and (4) $e(d, e, p)$ and $e(a, e, p)$. Thus, the points y, $e(a, y, p)$, $e(b, y, p)$, $e(d, y, p)$ and $e(e, y, p)$ belong to $\mathcal{F}(p)$ where y *is the s-point of* $\mathcal{N}(p)$ opposite to x. We can find a set $X = \{p, x, e(a, x, p), a, e(a, y, p), y, e(d, y, p), d, e(d, x, p)\}$ which is a proper subset of $\mathcal{F}(p)$ and $\mathcal{N}(p) - X$ is not 26-connected. Hence, the contradiction that $\mathcal{F}(p)$ is a minimal 26-separator of $\mathcal{N}(p)$.

□

Proposition 2.9 *$\mathcal{F}(p)$ contains a 6-closed path π of s-points and e-points.*

proof. As $\mathcal{F}(p) - \{p\}$ is non-empty, $\mathcal{F}(p)$ meets a surface of $\mathcal{N}(p)$. Let $\mathcal{F}(p)$ meets $surface(x_1, p)$ such that $\{x_1, e_{1,2}\} \subset \mathcal{F}(p) \cap surface(x_1, p)$, where $e_{1,2}$ is an e-point of $surface(x_1, p)$. Thus, we can find a 6-path $\pi_1 = x_1, e_{1,2}$ of s-points and e-points in $\mathcal{F}(p)$. The e-point $e_{1,2}$ belongs to another surface of $\mathcal{N}(p)$, say $surface(x_2, p)$. According to Proposition 2.8, $surface(x_2, p) \cap \mathcal{F}(p)$ contains x_2, $e_{1,2}$ and another e-point, say, $e_{2,3}$. Thus, we can extend π_1 to another 6-path $\pi_2 = \pi_1, x_2, e_{2,3}$ of four s-points and e-points in $\mathcal{F}(p)$. Let us assume that there exists a 6-path $\pi_{i-1} = x_1, e_{1,2}, \cdots, x_{i-1}, e_{i-1,i}$ of $2 * (i - 1)$ number of s-points and e-points in $\mathcal{F}(p)$. We would like to show that either $e_{i-1,i}$ is 6-adjacent to a point of π_{i-1} other than x_{i-1} or π_{i-1} is extensible to another 6-path $\pi_i = \pi_{i-1}, x_i, e_{i,i+1}$ in $\mathcal{F}(p)$.

Let us assume that $e_{i-1,i}$ is not 6-adjacent to any point of π_{i-1} other than x_{i-1}. Each e-point of $\mathcal{N}(p)$ is 6-adjacent to exactly two s-points. Therefore, $e_{i-1,i}$ is 6-adjacent to an s-point x_i other than x_{i-1}. By assumption, x_i does not belong to $spt(\pi_{i-1})$. According to Proposition 2.8, $\mathcal{F}(p) \cap surface(x_i, p)$ contains the points $e_{i-1,i}, x_i$ and another e-point, say $e_{i,i+1}$. Note that in $\mathcal{N}(p)$, one e-point has exactly

two 6-adjacent s-points and no two e-points are 6-adjacent. Hence $e_{i,i+1}$ does not belong to $spt(\pi_{i-1})$ as $x_i \notin spt(\pi_{i-1})$. Thus, $\pi_i = \pi_{i-1}, x_i, e_{i,i+1}$ is a 6-path in $\mathcal{F}(p)$. Hence, a 6-path π_{i-1} is always extensible in $\mathcal{F}(p)$ unless $e_{i-1,i}$ is 6-adjacent to a point of π_{i-1} other than x_{i-1}. Moreover, the number of s-points and e-points is finite in $\mathcal{N}(p)$. Thus, there exists a 6-path, say π_k where $e_{k,k+1}$ is 6-adjacent to a point of π_k other than x_k. Hence, we may conclude that we would get a 6-closed path π in the limiting case of including all s-points and e-points or earlier.

□

Proposition 2.10 *Let π be a 6-closed path of s-points and e-points of $\mathcal{N}(p)$. Then $\mathcal{F}(p) = \{p\} \cup spt(\pi)$.*

Proof. According to Proposition 2.4 and Proposition 2.9, $\{p\} \cup spt(\pi)$ is a subset of $\mathcal{F}(p)$. We shall prove this proposition by showing that $\mathcal{F}(p)$ is a subset of $\{p\} \cup spt(\pi)$. We do this by finding the exhaustive set of 6-closed paths of $\mathcal{N}(p)$. In $\mathcal{N}(p)$, there are only sixty three possible 6-closed paths of s-points and e-points. Moreover, they can be grouped into six geometric classes (two 6-closed paths belong to the same geometric class if and only if one can be changed to the other by rotation in integral multiples of 90° about different axes with p as origin). Six 6-closed paths of s-points and e-points one from each geometric class are shown in Figure 2.7. Numbers of possible 6-closed of s-points and e-points corresponding to Figure 2.7(a)–(f) are 8, 12, 3, 24, 4, and 12 respectively. It may be noted that for each cases $\mathcal{N}(p) - (\{p\} \cup spt(\pi))$ is not 26-connected. Thus, $\mathcal{F}(p)$ is a subset of $\{p\} \cup spt(\pi)$. Hence, $\mathcal{F}(p) = \{p\} \cup spt(\pi)$.

□

2.3.2 Number of Tunnels in $\hat{\mathcal{N}}(p)$

In this section we establish a theorem that defines the number of tunnels in $\hat{\mathcal{N}}(p)$. To prove the theorem we start with a definition (Definitions 2.5 and 2.6 given

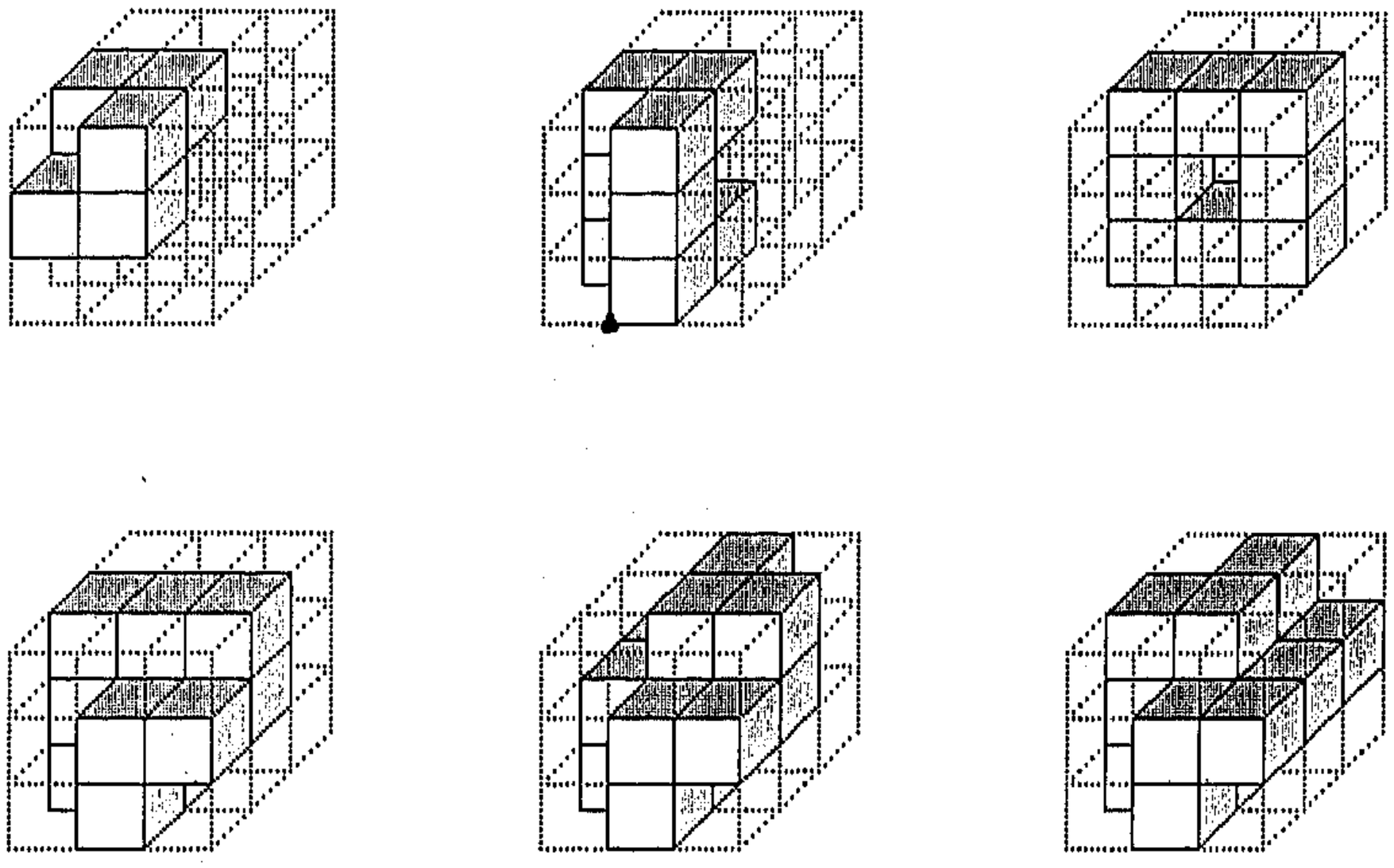

Figure 2.7: All possible geometric classes of 6-closed paths of *s*-points and *e*-points.

below) of the number of tunnels in a restricted class of digital images. An intuitive discussion is given in favor of the definitions as follows:

Following Kong et. al. [53], a 3D digital image $P = (Z^3, 26, 6, B)$ contains no hollow torus implies that the number of tunnels in the image equals to the number of solid handles. Let us consider an image $P = (Z^3, 26, 6, B)$ where $B \subset rts(x, y)$ for some $x, y \in Z^3$ (in other words all black points lie on the border of a rectangular parallelepiped). Since the set of black points of P is a subset of the border of the rectangular parallelepiped $rts(x, y)$, it cannot contain a hollow torus. Otherwise, at least one point of $rti(x, y)$ must be black. Thus, the number of tunnels in P is equal to the number of solid handles in B. Again each solid handle of B leads to an independent non-trivial 26-closed curve of black points in a shrunk version of the image. Moreover, P can contain at most one cavity that occurs only when all of the points of $rts^*(x, y)$ are black. In that case all black points of P are 26-connected and also P cannot contain any solid handle i.e. P cannot contain any tunnel. In a shrunk version of P, each simply connected black component (i.e. a black component containing neither a cavity nor a tunnel) leads to a black point having no black 26-neighbor. Based on this discussion we put forward a formal definition of the number of tunnels to prove Theorem 2.1.

Definition 2.5 *Let $P = (Z^3, 26, 6, B)$ be a 3D digital image where $B \subset rts(x, y)$ and $rts^*(x, y) \subset B$ for some $x, y \in Z^3$. Under this assumption, the number of tunnels in P is zero.*

Definition 2.6 *Let $P = (Z^3, 26, 6, B)$ be a 3D digital image where $B \subset rts(x, y)$ and $rts^*(x, y) - B \neq \phi$ for some $x, y \in Z^3$ and let $P' = (Z^3, 26, 6, B')$ be a shrunk version of P. Under this assumption, the number of tunnels in P is equal to the number of independent non-trivial 26-closed curves in B'.*

Proposition 2.11 *The number of tunnels in $\hat{N}(p)$ is zero when all the s-points are black (i.e. $\hat{N}(p)$ contains a cavity), otherwise the number of tunnels in $\hat{N}(p)$ is*

equal to the number of independent non-trivial 26-closed curves in X. Here, X is the set of black points in a shrunk version of $\hat{\mathcal{N}}(p)$.

Proof. In $\hat{\mathcal{N}}(p)$, the set of black points $\mathcal{N}^*(p) \cap \mathcal{B} \subset rts((i+1, j+1, k+1), (i-1, j-1, k-1))$ where $p = (i, j, k)$. Again, the set of s-points of $\mathcal{N}(p)$ is the set $rts^*((i+1, j+1, k+1), (i-1, j-1, k-1))$. Hence, this proposition is a straightforward consequence of Definitions 2.5 and 2.6. □

Henceforth, the following notations are used in this chapter subsequently:

$\mathcal{B}(p)$: $\mathcal{N}^*(p) \cap \mathcal{B}$ i.e. the set of black points of $\hat{\mathcal{N}}(p)$.
$\mathcal{W}(p)$: $\mathcal{N}^*(p) - \mathcal{B}(p)$ i.e. the set of white points in $\mathcal{N}^*(p)$.
$W_s(p)$: the set of white s-points of $\hat{\mathcal{N}}(p)$ i.e. the set white 6-neighbors of p.
$W_e(p)$: the set of white e-points of $\hat{\mathcal{N}}(p)$.
$W_{se}(p)$: $W_s(p) \cup W_e(p)$ i.e. the set of white 18-neighbors of p.
$\hat{\mathcal{N}}'(p)$: a shrunk version of $\hat{\mathcal{N}}(p)$.
$\mathcal{B}'(p)$: the set of black points of $\hat{\mathcal{N}}'(p)$.
$W'_s(p)$: the set of white s-points of $\hat{\mathcal{N}}'(p)$.
$W'_e(p)$: the set of white e-points of $\hat{\mathcal{N}}'(p)$.
$W'_{se}(p)$: $W'_s(p) \cup W'_e(p)$.

Proposition 2.12 *In $\hat{\mathcal{N}}(p)$, if two opposite s-points are white and other four s-points are black then the number of tunnels in $\hat{\mathcal{N}}(p)$ is exactly one.*

Proof. Let (a, d), (b, e), and (c, f) denote three distinct unordered pairs of opposite s-points of $\mathcal{N}(p)$ and let a, d be white while b, e, c, f be black in $\hat{\mathcal{N}}(p)$. In that case all e-points and v-points are simple points of $\hat{\mathcal{N}}(p)$ (see Definition 2.1). Thus, a shrunk version of $\hat{\mathcal{N}}(p)$ contains the set of black points $\{b, e, c, f\}$. Again, b, c, e, f is one and only one independent non-trivial 26-closed curve of black points in the shrunk version of $\hat{\mathcal{N}}(p)$. Therefore, according to Proposition 2.11, $\hat{\mathcal{N}}(p)$

contains exactly one tunnel.

□

Proposition 2.13 *Let $\mathcal{P}' = (Z^3, 26, 6, \mathcal{B}')$ be a shrunk version of some 3D digital image such that: (1) $\mathcal{B}' \subset rts(x, y)$ for some $x, y \in Z^3$, (2) $\mathcal{B}'$ contains no cavity, and (3) maximum possible independent non-trivial 26-closed curves in $\mathcal{B}'$ is n. Let p be a point in $\mathcal{B}'$ such that: (1) $\mathcal{N}^*(p) \cap \mathcal{B}'$ contains exactly two 26-components, (2) $\mathcal{N}^*(p) \cap \mathcal{B}'$ contains no tunnels, and (3) the number of 26-components in $\mathcal{B}'$ is same as that of $\mathcal{B}' - \{p\}$. Under this assumption, maximum possible independent non-trivial 26-closed curves in $\mathcal{B}' - \{p\}$ is exactly $n - 1$. In other word, removal of p from $\mathcal{B}'$ removes exactly one independent non-trivial 26-closed curve from $\mathcal{B}'$.*

Proof. The difference in the Euler characteristics of $\mathcal{B}'$ and $\mathcal{B}' - \{p\}$ is equal to that of $\mathcal{N}(p) \cap \mathcal{B}'$ and $\mathcal{N}^*(p) \cap \mathcal{B}'$. The difference in the Euler characteristics of $\mathcal{B}'$ and $\mathcal{B}' - \{p\}$ equals to the difference in the number of 26-components in $\mathcal{B}'$ and $\mathcal{B}' - \{p\}$ minus the difference in the number of tunnels plus the difference in the number of cavities. By assumption, the number of 26-components of $\mathcal{B}'$ and that of $\mathcal{B}' - \{p\}$ are same. Also, the number of cavities in $\mathcal{B}'$ is zero. The number of cavities in $\mathcal{B}' - \{p\}$ may be at most one and it occurs only when the removal of p creates a cavity in its $3 \times 3 \times 3$ neighborhood. In that case all the 6-neighbors of p must belong to $\mathcal{B}'$ (see Equation 2.1) and $\mathcal{N}^*(p) \cap \mathcal{B}'$ must be 26-connected. But it contradicts the assumption that $\mathcal{N}^*(p) \cap \mathcal{B}'$ contains two 26-components. Hence, $\mathcal{B}' - \{p\}$ does not contain any cavity. Since, $\mathcal{B}'$ contains maximum n independent non-trivial 26-closed curves, the number of tunnels in $\mathcal{B}'$ is n (see Definition 2.6) Therefore, the difference in the Euler characteristics of $\mathcal{B}'$ and $\mathcal{B}' - \{p\}$ is n minus the number of tunnels in $\mathcal{B}' - \{p\}$ i.e. n minus the maximum number of independent non-trivial 26-closed curves in $\mathcal{B}' - \{p\}$. The Euler characteristics of $\mathcal{N}(p) \cap \mathcal{B}'$ is one (see Proposition 2.1). By assumption, the numbers of 26-components and tunnels in $\mathcal{N}^*(p) \cap \mathcal{B}'$ are two and zero respectively. Following the same logic as in the case of cavities in $\mathcal{B}' - \{p\}$, the number of cavities in $\mathcal{N}^*(p) \cap \mathcal{B}'$ is zero. Thus, the Euler

characteristic of $\mathcal{N}^*(p) \cap \mathcal{B}'$ is two. Therefore, n minus the maximum number of independent non-trivial 26-closed curves in $\mathcal{B}' - \{p\}$ is equal to minus one. Hence, the maximum number of independent non-trivial 26-closed curves in $\mathcal{B}' - \{p\}$ is n minus one. □

Proposition 2.14 *Let x, y be two s-points in $W_s(p)$ such that they are not 6-connected in $W_{se}(p)$. Under this assumption, x, y are not 6-connected in $W'_{se}(p)$.*

Proof. Before we begin the proof let us develop some necessary background. Let $(a, d), (b, e), (c, f)$ denote three distinct unordered pairs of opposite s-points of $\mathcal{N}(p)$. As mentioned earlier shrinking is a process of sequential deletion of black simple points. Let $\mathcal{B}_i(p)$ and $W^i_{se}(p)$ denote the set of black points and the set of white s-points and e-points respectively, after the completion of ith step of the shrinking process on $\hat{\mathcal{N}}(p)$ (at each step one black simple point is deleted). Let p' be a 26-neighbor of p. We define a 3D digital image as follows:

$$\hat{\mathcal{N}}_i(p, p') = (Z^3, 26, 6, \mathcal{B}_{i-1}(p) \cap \mathcal{N}^*(p')).$$

Thus, $\hat{\mathcal{N}}_i(p, p')$ is a digital image with the set of black point as $\mathcal{B}_{i-1}(p) \cap \mathcal{N}^*(p')$. The point p' is removable at ith step of shrinking if and only if p' is a simple point in $\mathcal{B}_{i-1}(p)$. By definition of shrinking we have

- $\mathcal{B}_i(p) \subset \mathcal{B}_{i-1}(p)$, and $\mathcal{B}_{i-1}(p) - \mathcal{B}_i(p) = \{p'\}$, where p' is deleted at ith step.
- If p' is a v-point then $W^{i-1}_{se}(p) = W^i_{se}(p)$, otherwise, $W^{i-1}_{se}(p) \subset W^i_{se}(p)$, and $W^i_{se}(p) - W^{i-1}_{se}(p) = \{p'\}$.

Coming back to the proof, we prove this proposition by the method of contradiction. Let us assume that the proposition is not true i.e. x, y are 6-connected in $W'_{se}(p)$. Since, they are not 6-connected in $W_{se}(p)$ but are 6-connected in $W'_{se}(p)$, there must be some i such that x, y are not 6-connected in $W^{i-1}_{se}(p)$ but are 6-connected in $W^i_{se}(p)$. If this is true then $\mathcal{B}_{i-1}(p) - \mathcal{B}_i(p)$ must be an e-point or an s-point.

At first, let us consider the case that $B_{i-1}(p) - B_i(p)$ is an e-point, say $e(a,b,p)$. Since, x, y are not 6-connected in $W_{se}^{i-1}(p)$ but are 6-connected in $W_{se}^{i}(p)$ i.e. $W_{se}^{i-1}(p) \cup \{e(a,b,p)\}$, each 6-path between x, y in $W_{se}^{i}(p)$ contains $e(a,b,p)$. Again a 6-path of $W_{se}^{i}(p)$ between x, y through $e(a,b,p)$ must contain the points a, b (no e-point of $\mathcal{N}(p)$ is 6-adjacent to $e(a,b,p)$ and a, b are only s-points which are 6-adjacent to $e(a,b,p)$) i.e. $a, b \notin B_{i-1}(p)$. Since the 6-path between x, y in $W_{se}^{i}(p)$ contains $a, e(a,b,p), b$, without loss of generality we can assume that x is 6-connected to a and b is 6-connected to y in $W_{se}^{i-1}(p)$. According to our assumption, x is not 6-connected to y in $W_{se}^{i-1}(p)$. This implies that a is not 6-connected to b in $W_{se}^{i-1}(p)$. Thus, both the sets $\{e(a,c,p),\ c,\ e(b,c,p)\}$ and $\{e(a,f,p),\ f,\ e(b,f,p)\}$ intersect with $B_{i-1}(p)$. Otherwise, $a,\ e(a,c,p),\ c,\ e(b,c,p),\ b$ or $a,\ e(a,f,p),\ f,\ e(b,f,p),\ b$ will lead to a 6-path in $W_{se}^{i-1}(p)$. The set of black points of $\hat{N}_i(p, e(a,b,p))$ is a subset of $\{v(a,b,c,p),\ e(a,c,p),\ c,\ e(b,c,p),\ v(a,b,f,p),\ e(a,f,p),\ f,\ e(b,f,p)\}$. This may be derived as follows:

$$B_{i-1}(p) \subset \mathcal{N}^*(p),$$

$$\mathcal{N}^*(p) \cap \mathcal{N}^*(e(a,b,p)) = \{a, b, v(a,b,c,p), e(a,c,p), c, e(b,c,p), v(a,b,f,p), e(a,f,p), f, e(b,f,p)\},$$

and

$$a, b \notin B_{i-1}(p)$$

imply that

$$B_{i-1}(p) \cap \mathcal{N}^*(e(a,b,p)) \subset \mathcal{N}^*(p) \cap \mathcal{N}^*(e(a,b,p)) - \{a,b\},$$

or

$$B_{i-1}(p) \cap \mathcal{N}^*(e(a,b,p)) \subset \{v(a,b,c,p), e(a,c,p), c, e(b,c,p), v(a,b,f,p), e(a,f,p), f, e(b,f,p)\}.$$

From the set of black points of $\hat{N}_i(p, e(a,b,p))$ one can find two non-empty subsets $(B_{i-1}(p) \cap \mathcal{N}^*(e(a,b,p))) \cap \{e(a,c,p),\ c,\ e(b,c,p)\}$ and $(B_{i-1}(p) \cap \mathcal{N}^*(e(a,b,p))) \cap \{e(a,f,p),\ f,\ e(b,f,p)\}$ such that *no two points* taking one from each subset are 26-connected in $\{v(a,b,c,p), e(a,c,p), c, e(b,c,p), v(a,b,f,p), e(a,f,p), f, e(b,f,p)\}$ and hence they are not 26-connected in a smaller (or equal) set $B_{i-1}(p) \cap \mathcal{N}^*(e(a,b,p))$.

Thus, the black points of $\hat{\mathcal{N}}_i(p, e(a,b,p))$ are not 26-connected and hence $e(a,b,p)$ is not a simple point in $\mathcal{B}_{i-1}(p)$ (see Definition 2.1). Contradiction!!

Let us consider the situation that $\mathcal{B}_{i-1}(p) - \mathcal{B}_i(p)$ is an s-point say a $(a \neq x; a \neq y)$. Thus, every 6-path of $W^i_{se}(p)$ between x, y contains a. Again, a 6-path of $W^i_{se}(p)$ from x to y through a must contain one of the following two types of sequences.

Sequence1: b, $e(a,b,p)$, a, $e(a,c,p)$, c (b, c are non-opposite).
Sequence2: b, $e(a,b,p)$, a, $e(a,e,p)$, e (b, e are opposite).

Following similar approach as in the case of e-point it can be shown that $\mathcal{B}_{i-1}(p) \cap \mathcal{N}^*(a)$ is not 26-connected for both the sequences. In other words a is never a simple point in $\mathcal{B}_{i-1}(p)$ (according to Definition 2.1). This leads to the same contradiction as earlier. Hence, x, y are not 6-connected in $W'_{se}(p)$. □

The following corollary is a straightforward consequence of the above proposition.

Corollary 2.1 *The number of 6-components of $W_s(p)$ in $W_{se}(p)$ is less than equal to that of $W'_s(p)$ in $W'_{se}(p)$.*

Proposition 2.15 *The number of 6-components of $W'_s(p)$ in $W'_{se}(p)$ is less than equal to that of $W_s(p)$ in $W_{se}(p)$.*

Proof. Following the notations detailed in the proof of Proposition 2.14 if this proposition is not true then at ith step of shrinking of $\hat{\mathcal{N}}(p)$ an s-point is deleted which is not 6-connected to any point of $W^i_s(p)$ $(W^i_s(p) = W_s(p) \cap \mathcal{B}_i(p))$ in $W^i_{se}(p)$. Let a be the point which is deleted at ith step. By assumption, a is not 6-connected to a point of $W^i_s(p)$ in $W^i_{se}(p)$. Thus, at least one point of the sets $\{b, e(a,b,p)\}$, $\{e, e(a,e,p)\}$, $\{c, e(a,c,p)\}$, $\{f, e(a,f,p)\}$ must belong to $\mathcal{B}_{i-1}(p)$. For all these possibilities $\chi(\hat{\mathcal{N}}_{i-1}(p,a))$ is zero. According to Proposition 2.1, $\chi(Z^3, 26, 6, \mathcal{B}_{i-1} \cap \mathcal{N}(a))$ is always one as $a \in \mathcal{B}_{i-1}(p)$. Hence a is not a simple point in $\mathcal{B}_{i-1}(p)$ according to Definition 2.1. Contradiction!! □

The following corollary is a straightforward consequence of Propositions 2.15 and Corollary 2.1.

Corollary 2.2 *The number of 6-components of $W_s(p)$ in $W_{sc}(p)$ is exactly the same as that of $W_s'(p)$ in $W_{sc}'(p)$.*

Proposition 2.16 *No non-trivial 26-closed curve of $B'(p)$ contains a v-point.*

Proof. If this proposition is not true, let us consider a non-trivial 26-closed curve $\cdots, x, v, y, z \cdots$ in $B'(p)$ (a non-trivial 26-closed curve contains at least four points) where v is a v-point. From $N(p)$ it may be noted that for any v-point q, every two points of $N(p,q)$ are 26-adjacent. Thus, $x, y \in N(p,v)$ and are 26-adjacent. Hence the contradiction that $\cdots, x, v, y, z, \cdots$ is a non-trivial 26-closed curve (y is 26-adjacent to three points of the 26-closed curve). □

Proposition 2.17 *$\hat{N}(p)$ contains no tunnel when $W_s(p)$ is 6-connected in $W_{sc}(p)$.*

Proof. According to Proposition 2.11, $\hat{N}(p)$ contains no tunnels when $W_s(p)$ is empty. To prove this proposition we shall show that $B'(p)$ contains no non-trivial 26-closed curve when $W_s(p)$ is non-empty and 6-connected in $W_{sc}(p)$. According to Proposition 2.16, non-trivial 26-closed curves of $B'(p)$ do not contain v-points.

First, we consider the cases when non-trivial 26-closed curves of $B'(p)$ contain only s-points. Then $B'(p)$ contains at least four s-points. Let (a,d), (b,e), (c,f) be three distinct unordered pairs of opposite s-points of $N(p)$. When $B'(p)$ contains exactly four s-points, the s-points of $B'(p)$ are either of the form $\{a, d, b, c\}$ or $\{a, d, b, e\}$. In the first case we cannot find a non-trivial 26-closed curve in $B'(p)$ as b is 26-adjacent to all the three points a, d, c. In the second case where $B'(p)$ contains $\{a, d, b, e\}$, the s-points $c, f, \in W_s'(p)$ are not 6-connected in $W_{sc}'(p)$ as $a, d, b, e \notin W_{sc}'(p)$. According

to Corollary 2.2, $W_s'(p)$ is not 6-connected in $W_{se}'(p)$ implies that $W_s(p)$ is not 6-connected in $W_{se}(p)$. Let us consider the case where $\mathcal{B}'(p)$ contains five s-points, say $\{a, b, c, d, e\}$. The point a is a simple point (see Definition 2.1). Hence the contradiction that $\mathcal{B}'(p)$ is a shrunk version (consequently, $\mathcal{B}'(p)$ contains no simple point). When $\mathcal{B}'(p)$ contains six s-points, $W_s(p)$ is empty. Hence the proposition is proved when the non-trivial 26-closed curves of $\mathcal{B}'(p)$ contain no e-point.

We shall show that the proposition is true when a non-trivial 26-closed curve of $\mathcal{B}'(p)$ contains an e-point. Let us assume that the proposition is not true i.e. $W_s(p)$ is 6-connected in $W_{se}(p)$ and $\mathcal{B}'(p)$ contains a non-trivial 26-closed curve. Let ς be a non-trivial 26-closed curve in $\mathcal{B}'(p)$. Let $e(a, b, p)$ be an e-point in ς. According to Corollary 2.2, $W_s(p)$ is 6-connected in $W_{se}(p)$ implies that $W_s'(p)$ is 6-connected in $W_{se}'(p)$. As $e(a, b, p)$ belong to $\mathcal{B}'(p)$ both a and b belong to $W_{se}'(p)$. Otherwise, $e(a, b, p)$ is a simple point in $\mathcal{B}'(p)$ (see Definition 2.1). The point $e(a, b, p)$ lies in the non-trivial 26-closed curve ς. So, $e(a, b, p)$ must be 26-adjacent to two points of ς which are not 26-adjacent to each other. Therefore, both the sets $\{e(a, c, p),\ c,\ e(b, c, p)\}$ and $\{e(a, f, p),\ f,\ e(b, f, p)\}$ intersect ς (note that ς does not contain v-points). By assumption, a, b are 26-connected in $W_{se}'(p)$. Let π be a 6-path from a to b in $W_{se}'(p)$. Thus, $e(a, b, p), \pi$ is a 6-closed path of s-points and e-points and $\mathcal{F} = \{p,\ e(a, b, p)\} \cup spt(\pi)$ is a minimal 26-separator of $\mathcal{N}(p)$. The cases, $\mathcal{F} \subset \mathcal{N}(p) - (\mathcal{B}'(p) - \{e(a, b, p)\})$ and $spt(\varsigma) \subset \mathcal{B}'(p)$ imply that $\mathcal{F} \subset \mathcal{N}(p) - (spt(\varsigma) - \{e(a, b, p\})$. Also, one 26-component of $\mathcal{N}(p) - \mathcal{F}$ contains $\{e(a, c, p),\ c,\ e(b, c, p)\} \cap spt(\varsigma)$ while the other 26-component of $\mathcal{N}(p) - \mathcal{F}$ contains $\{e(a, f, p),\ f,\ e(b, f, p)\} \cap spt(\varsigma)$. Thus, $spt(\varsigma) - \{e(a, b, p)\}$ is not 26-connected. Hence, the contradiction that ς is 26-closed curve (removal of one point from a 26-closed curve cannot disconnect the 26-closed curve into two or more 26-components). □

Proposition 2.18 *Let $a, b \in W_s(p)$ be two non-opposite s-points of $\mathcal{N}(p)$ such that a, b are not 6-connected in $W_{se}(p)$. Under this assumption, the number of 26-components of $\mathcal{B}'(p)$ is same as that of $\mathcal{B}'(p) - \{e(a, b, p)\}$.*

Proof. According to Proposition 2.14, $a, b \in W_s(p)$ are not 6-connected in $W_{se}(p)$ implies that a, b are not 6-connected in $W'_{se}(p)$. Therefore, $e(a,b,p) \in B'(p)$ and both the set $\{e(a,c,p),\ c,\ e(a,f,p)\}$ and $\{e(b,c,p),\ c,\ e(b,f,p)\}$ intersect $B'(p)$. Thus, $e(a,b,p)$ is not an isolated point of $B'(p)$. Therefore, the number of 26-components of $B'(p) - \{e(a,b,p)\}$ is not less than that of $B'(p)$. Let us assume that the number of 26-components of $B'(p) - \{e(a,b,p)\}$ is more than that of $B'(p)$. In that case there must be two point $x, y \in B'(p) - \{e(a,b,p)\}$ such that they are 26-connected in $B'(p)$ but they are not so in $B'(p) - \{e(a,b,p)\}$. Following Proposition 2.2, there must be a minimal 26-separator $\mathcal{F}$ of $\mathcal{N}(p)$ such that $\mathcal{F} \subset \mathcal{N}(p) - (B'(p) - \{e(a,b,p)\})$ and x, y belong to two distinct 26-components of $\mathcal{N}(p) - \mathcal{F}$. As x, y are 26-connected in $B'(p)$, $\mathcal{F}$ must contain $e(a,b,p)$. Again, a minimal 26-separator containing $e(a,b,p)$ contains both a and b. Thus, $\mathcal{F} = \{p,\ e(a,b,p)\} \cup spt(\pi)$ where π is a 6-path of s-points and e-points from a to b not containing $e(a,b,p)$. Further, $\mathcal{F} = \{p,\ e(a,b,p)\} \cup spt(\pi) \subset \mathcal{N}(p) - (B'(p) - \{e(a,b,p)\})$, π contains only s-points and e-points and does not contain $e(a,b,p)$ together imply that $spt(\pi) \subset W'_{se}(p)$. Hence, the contradiction that a, b are not 6-connected in $W'_{se}(p)$. □

Proposition 2.19 *Let $a, b \in W_s(p)$ be two non-opposite s-points of $\mathcal{N}(p)$ and they are not 6-connected in $W_{se}(p)$. Under this assumption, $\mathcal{N}^*(e(a,b,p)) \cap B'(p)$ contains no tunnel.*

Proof. It may be noted that $f_2(a,b,p)$ is a 6-neighbor of $e(a,b,p)$ and it does not belong to $\mathcal{N}^*(e(a,b,p)) \cap B'(p)$. Let X be the set of all s-points and e-points of $\mathcal{N}(e(a,b,p))$ belonging to $\mathcal{N}^*(e(a,b,p)) - B'(p)$. It may be noted that all s-points of $\mathcal{N}(e(a,b,p))$ belonging to $\mathcal{N}^*(p) - B'(p)$ are 6-connected to $f_2(a,b,p)$ in X. Also, all points of $\mathcal{N}(e(a,b,p))$ belonging to $\mathcal{N}^*(e(a,b,p)) - \mathcal{N}^*(p)$ (note that $B'(p) \subset \mathcal{N}^*(p)$) are 6-connected to $f_2(a,b,p)$ in X. Thus, the set of s-points of $\mathcal{N}(e(a,b,p))$ belonging to $\mathcal{N}^*(e(a,b,p)) - B'(p)$ is 6-connected in X. Hence, $\mathcal{N}^*(e(a,b,p)) \cap B'(p)$ contains no tunnel according to Proposition 2.17. □

Proposition 2.20 *Let $x, y \in W_s(p)$ be two non-opposite s-points of $\mathcal{N}(p)$ and*

they are not 6-connected in $W_{se}(p)$. Under this assumption, removal of $e(x,y,p)$ from $B'(p)$ removes exactly one tunnel from $\hat{\mathcal{N}}(p)$.

Proof. Following Proposition 2.11 we establish this proposition by showing that removal of $e(x,y,p)$ from $B'(p)$ removes exactly one independent non-trivial 26-closed curve from $B'(p)$. Let (u,v), (w,x), (y,z) be three distinct unordered pairs of opposite s-points of $\mathcal{N}(p)$ (by assumption, x, y are non-opposite s-points of $\mathcal{N}(p)$). According to Proposition 2.14 x, y are not 6-connected in $W'_{se}(p)$. Considering this, we draw the following three inferences:

1. $e(x,y,p) \in B'(p)$ otherwise x, $e(x,y,p)$, y leads to a 6-path in $W'_{se}(p)$,
2. $\{e(u,x,p), u, e(u,y,p)\} \cap B'(p) \neq \phi$ otherwise x, $e(u,x,p)$, u, $e(u,y,p)$, y leads to a 6-path in $W'_{se}(p)$,
3. $\{e(v,x,p), v, e(v,y,p)\} \cap B'(p) \neq \phi$ otherwise x, $e(v,x,p)$, v, $e(v,y,p)$, y leads to a 6-path in $W'_{se}(p)$.

It may be shown that $B'(p) \cap \mathcal{N}^*(e(x,y,p)) \subset \{v(u,x,y,p),\ e(u,x,p),\ u,\ e(u,y,p),\ v(v,x,y,p),\ e(v,x,p),\ v,\ e(v,y,p)\}$. Every two points of $\{v(u,x,y,p),\ e(u,x,p),\ u,\ e(u,y,p)\}$ are 26-adjacent to each other and the same is true for $\{v(v,x,y,p),\ e(v,x,p),\ v,\ e(v,y,p)\}$. Again, $B'(p) \cap \{v(u,x,y,p),\ e(u,x,p),\ u,\ e(u,y,p)\}$ and $B'(p) \cap \{v(v,x,y,p),\ e(v,x,p),\ v,\ e(v,y,p)\}$ are two non-empty subsets of $B'(p) \cap \mathcal{N}^*(e(x,y,p))$ such that no two points taking one from each subset are 26-connected in $\{v(u,x,y,p),\ e(u,x,p),\ u,\ e(u,y,p),\ v(v,x,y,p),\ e(v,x,p),\ v,\ e(v,y,p)\}$ and hence they are not 26-connected in a smaller set $B'(p) \cap \mathcal{N}^*(e(x,y,p))$. So, $B'(p) \cap \mathcal{N}^*(e(x,y,p))$ contains exactly two 26-components, namely, $B'(p) \cap \{v(u,x,y,p),\ e(u,x,p),\ u,\ e(u,y,p)\}$ and $B'(p) \cap \{v(v,x,y,p),\ e(v,x,p),\ v,\ e(v,y,p)\}$. $B'(p)$ contains no cavity because x is a 6-neighbor of p and $x \notin B'(p)$. As follows from Propositions 2.18 and 2.19, the number of 26-components of $B'(p)$ is same as that of $B'(p) - \{e(a,b,p)\}$ and also, $\mathcal{N}^*(e(a,b,p)) \cap B'(p)$ contains no tunnel. Therefore,

according to Proposition 2.13, removal of $e(x,y,p)$ from $\mathcal{B}'(p)$ removes exactly one independent non-trivial 26-closed curve from $\mathcal{B}'(p)$.

□

The number of tunnels in $\hat{\mathcal{N}}(p)$ is defined in the following theorem which is one of the major contribution of this chapter.

Theorem 2.1 *The number of tunnels in $\hat{\mathcal{N}}(p)$ is one less than the number of 6-components of $W_s(p)$ in $W_{sc}(p)$ when $W_s(p)$ is non-empty. Otherwise, the number of tunnels in $\hat{\mathcal{N}}(p)$ is zero.*

proof. The 'otherwise' part of the theorem when $W_s(p)$ is empty (i.e. all s-points are black) immediately follows from Proposition 2.11. To prove the theorem for $W_s(p) \neq \phi$, we use the method of induction. Let n denote the number of 6-components of $W_s(p)$ in $W_{sc}(p)$. It follows from Proposition 2.17 that for $n = 1$, $\hat{\mathcal{N}}(p)$ contains no tunnel. We shall show that for $n = 2$, $\hat{\mathcal{N}}(p)$ contains exactly one tunnel and for $n > 2$, removal of one tunnel from $\hat{\mathcal{N}}(p)$ leaves exactly $n-1$ number of 6-components of $W_s(p)$ in $W_{sc}(p)$.

For $n = 2$, one of the following cases may occur:

Case 1: $W_s(p)$ contains exactly two opposite s-points which are not 6-connected in $W_{sc}(p)$,

Case 2: $W_s(p)$ contains at least two non-opposite s-points which are not 6-connected in $W_{sc}(p)$.

By Proposition 2.12, $\hat{\mathcal{N}}(p)$ contains exactly one tunnel for Case 1. For Case 2, let us consider two non-opposite s-points a and b which are not 6-connected in $W_{sc}(p)$. Since a, b are not 6-connected in $W_{sc}(p)$ the e-point $e(a,b,p)$ is black i.e. $e(a,b,p) \in \mathcal{B}(p)$. Following Proposition 2.14, $e(a,b,p) \in \mathcal{B}'(p)$. According to Proposition 2.20, the removal of $e(a,b,p)$ from $\mathcal{B}'(p)$ removes exactly one tunnel from $\hat{\mathcal{N}}(p)$. Again,

after the removal of $e(a,b,p)$ from $B'(p)$, $W'_s(p)$ becomes 6-connected in $W'_{se}(p) \cup \{e(a,b,p)\}$. Thus, $\hat{\mathcal{N}}(p)$ contains exactly one tunnel.

To prove the induction part, let n (> 2) 6-components of $W'_s(p)$ in $W'_{se}(p)$ be $W_1, W_2, \cdots, W_n$. Let us consider that the theorem is true for $n-1$. Following Proposition 2.20, we need to establish the following two statements to prove the theorem:

1. There exists an e-point $e(a,b,p) \in B'(p)$ such that the s-points $a \in W_i$ and $b \in W_j$ for some $i \neq j$, and
2. the number of 6-components of $W'_s(p)$ in $W'_{se}(p) \cup \{e(a,b,p)\}$ is $n-1$.

Since $n > 2$, let us consider three s-points $a \in W_1$, $b \in W_2$, $c \in W_3$. Then at least two s-points among a, b, c are mutually non-opposite. Let us consider that a, b are mutually non-opposite. Moreover, a, b belonging to different 6-components of $W'_s(p)$ in $W_{se}(p)$, they are not 6-connected in $W'_{se}(p)$. Thus, the e-point $e(a,b,p) \notin W'_{se}(p)$ i.e. $e(a,b,p) \in B'(p)$. Also, none of the points of $W'_{se}(p)$ except a, b is 6-adjacent to $e(a,b,p)$. Thus, $W_1 \cup W_2, W_3, \cdots, W_n$ are the 6-components of $W'_s(p)$ in $W'_{se}(p) \cup \{e(a,b,p)\}$. Hence, the number of 6-components of $W'_s(p)$ in $W'_{se}(p) \cup \{e(a,b,p)\}$ is exactly $n-1$.

□

Corollary 2.3 *The number of tunnels in $\hat{\mathcal{N}}(p)$ is independent of the color of v-points.*

Corollary 2.3 is a straightforward consequence of Theorem 2.1.

2.4 A New Characterization of Simple Point

In this section we establish a new characterization of (26,6) simple point. The Definition 2.1 is considered as the definition of (26,6) simple point.

Proposition 2.21 *Let $P = (Z^3, 26, 6, B)$ be a 3D digital image. A point $p \in Z^3$ is a simple point in P if and only if the following three conditions are satisfied:*

1. *$\hat{\mathcal{N}}(p)$ contains exactly one black point,*
2. *$\hat{\mathcal{N}}(p)$ contains no cavity,*
3. *$\hat{\mathcal{N}}(p)$ contains no tunnel.*

Proof. To prove that Definition 2.1 and this proposition are equivalent we have to show that Conditions 1–3 of this proposition both side imply Conditions 1–3 of Definition 2.1 ('*A* both side implies *B*' means '*A* implies *B* and also *B* implies *A*'). Condition 1 of this proposition and Condition 1 of Definition 2.1 are identical. Condition 2 of Definition 2.1 implies that p has at least one white 6-neighbor. Consequently, $\hat{\mathcal{N}}(p)$ *contains no cavity (see Equation 2.1)*. Thus, Condition 2 of Definition 2.1 implies Condition 2 of this proposition. According to Proposition 2.1, $\chi(\dot{\mathcal{N}}(p))$ is one. When Conditions 1 and 2 of Definition 2.1 are satisfied we have $\chi(\hat{\mathcal{N}}(p)) = 1 -$ the number of tunnels in $\hat{\mathcal{N}}(p)$. Thus, Conditions 1–3 of Definition 2.1 imply Condition 3 of this proposition and consequently, imply Conditions 1–3 of this proposition.

We have to show that the inverse is also true. Following Equation 2.1 and Theorem 2.1, Conditions 2 and 3 of this proposition imply that p has at least one white 6-neighbor and the set of white 6-neighbor is 6-connected in the set of white 18-neighbors of p. So, the set of white 6-neighbors of p is obviously 6-connected in

the set of white 26-neighbors of p. In other words, p is 6-adjacent to exactly one white component of $\mathcal{N}^*(p) - \mathcal{B}(p)$. Thus, Conditions 2 and 3 of this proposition imply Condition 2 of Definition 2.1. Further, Conditions 1–3 of this proposition imply that $\chi(\hat{\mathcal{N}}(p))$ is equal to $\chi(\dot{\mathcal{N}}(p))$ which is one. Hence, Conditions 1–3 of this proposition imply Conditions 1–3 of Definition 2.1. □

The major results in characterizing (26,6) simple points [111,113,114] are compiled as follows:

Characterization 2.3 *Let $\mathcal{P} = (Z^3, 26, 6, \mathcal{B})$ be a 3D digital image. A point $p \in Z^3$ is simple point in $\mathcal{P}$ if and only if the following four conditions are satisfied:*

1. *p has at least one white 6-neighbor,*

2. *p has at least one black 26-neighbor,*

3. *$\mathcal{N}^*(p) \cap \mathcal{B}$ is 26-connected, and*

4. *the set of white 6-neighbors of p is 6-connected in the set of white 18-neighbors of p.*

The above characterization of (26,6) simple is a straightforward consequence of Proposition 2.21, Theorem 2.1 and Equation 2.1. It may be noted that the concept of simple point defined by Characterization 2.3 is valid for both deletion and addition.

2.5 A Measure of Topological Changes

Recalling the issues of establishing topological changes due to the binary transformation as detailed in introduction, in this section, we describe such a measure

of topological changes in the $3 \times 3 \times 3$ neighborhood. For a point p under binary transformation, this measure generates a change vector which has three elements. The first element defines the change in the number of black components in $\mathcal{N}(p)$; the second element defines the change in the number of tunnels in $\mathcal{N}(p)$ while the third element defines the change in the number of cavities in $\mathcal{N}(p)$. The numbers of black components, tunnels and cavities in $\dot{\mathcal{N}}(p)$ are defined in Proposition 2.1. The number of cavities in $\hat{\mathcal{N}}(p)$ is defined by Equation 2.1 while the number of tunnels in $\hat{\mathcal{N}}(p)$ is defined by Theorem 2.1. Following corollaries are straightforward consequences of previous discussions.

Corollary 2.4 *Let $P = (Z^3, 26, 6, B)$ be a 3D digital image. Topological changes in the $3 \times 3 \times 3$ neighborhood of a point $p \in B$ due to the removal of p from B are stated as follows:*

1. *change in the number of black components = the number of 26-components of $\mathcal{N}^*(p) \cap B - 1$,*

2. *change in the number of tunnels = the number of 6-components of $W_s(p)$ in $W_{se}(p) - 1$, when $W_s(p)$ is non-empty and '0' otherwise, and*

3. *change in the number of cavities = '1' when all the 6-neighbors of p are black and '0' otherwise.*

Corollary 2.5 *Let $P = (Z^3, 26, 6, B)$ be a 3D digital image. Topological changes in the $3 \times 3 \times 3$ neighborhood of a point $p \in Z^3 - B$ due to the addition of p to B are stated as follows:*

1. *change in the number of black components = 1− the number of 26-components of $\mathcal{N}^*(p) \cap B$,*

2. *change in the number of tunnels = 1− the number of 6-components of $W_s(p)$ in $W_{sc}(p)$, when $W_s(p)$ is non-empty and '0' otherwise, and*

3. *change in the number of cavities = '−1' when all the 6-neighbors of p are black and '0' otherwise.*

2.6 Conclusion

In this chapter, we have established a theorem that defines the number of tunnels in $3 \times 3 \times 3$ neighborhood. Using this theorem we have developed an efficient characterization of (26,6) simple points. This characterization is valid both in case of addition as well as deletion of simple points. The theorem defining the number of tunnels in $3 \times 3 \times 3$ neighborhood leads to an effective measure of topological changes in the $3 \times 3 \times 3$ neighborhood of a point under binary transformation. Overall, this chapter gives us a quantitative sense about the topology preservation under binary transformation.

Chapter 3

3D Topological Operations: A Computational Approach

3.1 Introduction

A straightforward and efficient characterization of (26,6) simple point as well as an effective measure of local topological changes under binary transformation have been developed in Chapter 2. In this chapter we study computational aspects of three topological operations based on the results developed in Chapter 2. This chapter may be considered in three modules. The first module is a discussion on a previous work due to Lobregt et. al. [69] on detection of 3D simple point that is presented in Section 3.2. The second module is the new theoretical approach proposed by us and subsequently used in the topological operations established in Section 3.3. In that connection the concept of geometric class of $3 \times 3 \times 3$ neighborhood is described in Section 3.3.1. In the third module we describe the algorithms for three useful topological operations in Sections 3.4 to 3.6. At first we develop an algorithm for detection of (26,6) simple points in Section 3.4. After which we

describe the algorithm in Section 3.5 that computes local topological parameters (these parameters also define local topological changes under binary transformation). The algorithm, described in Section 3.6, computes the Euler characteristic of a 3D digital image in a parallel manner.

3.2 Previous Works on 3D Simple Point Detection

Several works could be found in literature [76,111,113,114,129,17,131] on theoretical aspects of 3D simple point. On the other hand, just a few publications were reported on its computational aspect before we have made an extensive study [111,113,114] on the same. Lobregt et. al. [69] made a meaningful effort to solve the problems of 3D simple point from computational point of view. Their algorithm of 3D simple point detection is based on the notion of the Euler characteristic preservation. We shall make a brief description of their approach.

Let S_i^* be a netted surface that encloses an object or a cavity. Let n_i, e_i and f_i denote the numbers of vertices, edges and faces in S_i^* respectively. Then

$$n_i - e_i + f_i = 2 - 2h_i \tag{3.1}$$

where h_i denotes the number of tunnels in S_i^*. The connectivity number N is defined for a 3D image as follows:

$$N = \sum_i (2 - 2h_i) \tag{3.2}$$

According to their definition, a point is a 3D simple point if and only if its deletion preserves the connectivity number in its $3 \times 3 \times 3$ neighborhood. To test the preservation of connectivity number, the $3 \times 3 \times 3$ neighborhood of a point p is divided into eight partially overlapping $2 \times 2 \times 2$ cubes (centered around each vertex or nodal point j of p) and for each of which the contribution N_j to N is computed separately.

. There are $2^8 = 256$ possible configurations in a $2 \times 2 \times 2$ cube. For a configuration value c, $N_6^{(c)}$ (here, 6-connectivity is used for object points and 26-connectivity for non-object points) is computed as follows:

1) When all object points of the $2 \times 2 \times 2$ cube are 6-connected then contribution $N_6^{(c)}$ to N is

$$N_6^{(c)} = n^{(c)} - \frac{e^{(c)}}{2} + \frac{f^{(c)}}{4} \tag{3.3}$$

where, $n^{(c)}$ is the number of nodal points of S_i^* at the center of the $2 \times 2 \times 2$ cube, $e^{(c)}$ is the number of edges of S_i^* which join the center of the $2 \times 2 \times 2$ cube and $f^{(c)}$ is the number of faces of S_i^* which touch the center of the $2 \times 2 \times 2$ cube. It may be noted that $n^{(c)}$ is either zero or one and when $n^{(c)} = 0$ then $e^{(c)} = f^{(c)} = 0$.

2) When the object points of the $2 \times 2 \times 2$ cube are not 6-connected then contribution $N_6^{(c)}$ to N is

$$N_6^{(c)} = kn^{(c)} - \frac{e^{(c)} + e_s^{(c)}}{2} + \frac{f^{(c)}}{4} \tag{3.4}$$

where, $n^{(c)}$, $e^{(c)}$ and $f^{(c)}$ bear the same meaning as above. The number of edges shared by two object components of the $2 \times 2 \times 2$ cube is $e_s^{(c)}$ and k is the number of object components.

When 26-connectivity is used for object points and 6-connectivity for non-object points, $N_{26}^{(c)}$ is equal to $N_6^{(\bar{c})}$; here $\bar{c}$ is the complementary configuration of c. For example, if $c = 11011100$ then $\bar{c} = 00100011$. Thus, $N_{26}^{(220)} = N_6^{(35)}$; also, $N_{26}^{(35)} = N_6^{(220)}$.

As discussed above, the algorithm of 3D simple point detection due to Lobregt et. al. [69] is based on preservation of the Euler characteristic in the $3 \times 3 \times 3$ neighborhood of a point. Unfortunately, the Euler characteristic preservation is a necessary condition for topology preservation but not a sufficient condition for the same. The Euler characteristic of an object equals to the number of components

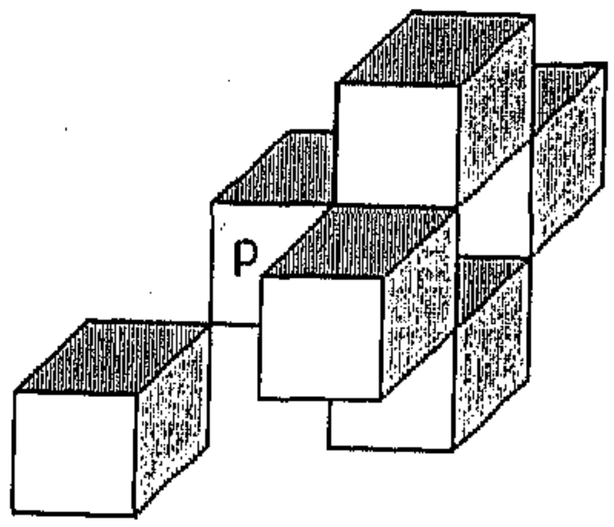

Figure 3.1: An example where Lobregt et. al.'s algorithm fails to detect that p is not a simple point.

minus the number of tunnels plus the number of cavities in it. As a result, if the deletion of a point in an image splits one black component to two and creates one tunnel in the transformed image then the Euler characteristic of the first image will be exactly the same as that of the second. However, these two images are not topologically equivalent. Such a situation may occur in $3 \times 3 \times 3$ neighborhood. Consider an object in the $3 \times 3 \times 3$ neighborhood of a point p as shown in Figure 3.1. In Figure 3.1, 26-connectivity is used for object points and 6-connectivity for non-object points. Although p is not a simple point (deletion of p creates a tunnel and splits one object component into two) deletion of p preserves the Euler characteristic. The algorithm by Lobregt et. al. [69] makes a mistake by certifying p as a (26,6) simple point.

3.3 The New Theoretical Approach

As described in Chapter 2 both the characterization of (26,6) simple point and the measure of topological changes in $3 \times 3 \times 3$ neighborhood under binary transformation invoke with the difference between $\dot{N}(p)$ and $\hat{N}(p)$ in terms of the numbers of

black components, tunnels and cavities. In Chapter 2 it has also been shown that the numbers of black components, tunnels and cavities in $\dot{\mathcal{N}}(p)$ are always '1', '0' and '0' respectively. Thus, the work essentially boils down to the computation of the numbers of black components, tunnels and cavities in $\hat{\mathcal{N}}(p)$. We establish an interesting theory that results in an efficient computation of these numbers in $\hat{\mathcal{N}}(p)$. This theory is applied to develop efficient algorithms for simple point detection, computation of local topological parameters and the Euler characteristic computation. Let $\xi(p)$, $\eta(p)$, and $\delta(p)$ denote the numbers of black components, tunnels, and cavities in $\hat{\mathcal{N}}(p)$ respectively. They are referred as topological parameters of p. As described in Section 2.5, $\xi(p)$, $\eta(p)$, and $\delta(p)$ also define local topological changes under binary transformation of a point. We use following two important and useful properties of $\mathcal{N}(p)$ to develop above mentioned three algorithms.

Property 3.1 *Let x be an s-point of $\mathcal{N}(p)$ and y be a point of $surface(x,p)$. Then for any point $q \in \mathcal{N}(p)$, q is 26-adjacent to y implies that q is 26-adjacent to x.*

Property 3.2 *Let x be an e-point of $\mathcal{N}(p)$ and y be a point of $edge(x,p)$. Then for any point $q \in \mathcal{N}(p)$, q is 26-adjacent to y implies that q is 26-adjacent to x.*

Proposition 3.1 *If an s-point x is black in $\hat{\mathcal{N}}(p)$ then $\xi(p)$ is independent of the color of other points of $surface(x,p)$.*

Proof: Let S denote the set of black points of $\hat{\mathcal{N}}(p)$ and let $y \neq x$ be a point on $surface(x,p)$. To establish the proposition we shall show that the number of 26-components of $S - \{y\}$ and that of $S \cup \{y\}$ are the same. If this is not true then one of the following two cases must occur.

Case 1: None of the points of $S - \{y\}$ is 26-adjacent to y. In other words, the number of 26-components of $S \cup \{y\}$ is greater than that of $S - \{y\}$.

Case 2: Two or more 26-components of $S - \{y\}$ are 26-adjacent to y. In other words, the number of 26-components of $S - \{y\}$ is greater than that of $S \cup \{y\}$.

By assumption x is black i.e. $x \in S - \{y\}$ and $y \in surface(x, p)$ i.e. y is 26-adjacent to x. Hence, Case 1 could not occur. About Case 2, let us assume that two points $q, r \in S - \{y\}$ belong to two different 26-components of $S - \{y\}$ and they are also 26-adjacent to y. Since, q, r are 26-adjacent to y they are also 26-adjacent to x (see Property 3.1). Thus, q, r are 26-connected in $S - \{y\}$ by the 26-path q, x, r. Hence the contradiction that q, r belong to two different 26-components of $S - \{y\}$. Thus, neither Case 1 nor Case 2 may occur and hence the number of 26-components of $S - \{y\}$ is the same as that of $S \cup \{y\}$.

□

Proposition 3.2 *If an s-point x is black in $\hat{\mathcal{N}}(p)$ then the number of tunnels in $\hat{\mathcal{N}}(p)$ is independent of the color of other points of $surface(x, p)$.*

Proof. According to Corollary 2.3, the number of tunnels in $\hat{\mathcal{N}}(p)$ is independent of the color of v-points. To establish the proposition we shall show that the number of tunnels in $\hat{\mathcal{N}}(p)$ is independent of the color of e-points of $surface(x, p)$. Let S denote the set of white s-points of $\hat{\mathcal{N}}(p)$ and let S' denote the set of white s-points and e-points of $\hat{\mathcal{N}}(p)$. Let y be an e-point of $surface(x, p)$. According to Theorem 2.1 the number of tunnels in $\hat{\mathcal{N}}(p)$ is equal to one less than the number of 6-components of S in S'. We shall show that the number of 6-components of S in $S' - \{y\}$ is the same as that of S in $S' \cup \{y\}$.

It follows from $\mathcal{N}(p)$ that no two s-points are 6-adjacent and also no two e-points are 6-adjacent. This implies that a 6-path of s-points and e-points must be an alternating sequence of s-points and e-points. Thus, a 6-path of s-points and e-points between two s-points through y must contain two s-points of $\mathcal{N}(p)$ which are 6-adjacent to y. It follows from $\mathcal{N}(p)$ that y being an e-point, it is 6-adjacent to exactly two s-points of $\mathcal{N}(p)$. By assumption x is black i.e. $x \notin S' \cup \{y\}$ and $y \in$

$surface(x,p)$ i.e. y is 6-adjacent to x. Thus, there exists no 6-path in $S' \cup \{y\}$ between two s-points of S through y. Hence, two s-points of S are 6-connected in $S' \cup \{y\}$ implies that they are 6-connected in $S' - \{y\}$. Also, it is obvious that two s-points of S are 6-connected in $S' - \{y\}$ implies that they are 6-connected in $S' \cup \{y\}$. Hence, the number of 6-components of S in $S' - \{y\}$ is the same as that of S in $S' \cup \{y\}$.

□

In Chapter 2, we have presented an expression for the number of cavities in $\hat{\mathcal{N}}(p)$ by Equation 2.1. Here, we are repeating the same expression for a better reference.

$$\delta(p) = \begin{cases} 1 & \text{if six } s\text{-points of } \mathcal{N}(p) \text{ are black;} \\ 0 & \text{otherwise.} \end{cases} \tag{3.5}$$

Thus, $\delta(p)$ is a function of s-point configuration of $\mathcal{N}(p)$. According to Proposition 3.1 and Proposition 3.2, $\xi(p)$ as well as $\eta(p)$ are independent of the color of the points of $surface(x,p)$, when the s-point x is black.

Definition 3.1 *For an s-point $s \in \mathcal{N}(p)$, $surface(x,p)$ is defined as a dead-surface of $\mathcal{N}(p)$ if x is black. A v-point or an e-point is defined as an effective point of $\mathcal{N}(p)$ if it does not belong to any dead-surface.*

Corollary 3.1 *With a known s-point configuration of $\mathcal{N}(p)$, we can compute $\xi(p)$, $\eta(p)$, and $\delta(p)$ from the effective point configuration of $\mathcal{N}(p)$.*

Corollary 3.2 *With a known s-point configuration of $\mathcal{N}(p)$, we can compute $\eta(p)$ from the effective e-point configuration of $\mathcal{N}(p)$.*

Corollary 3.3 *With a known s-point configuration of $\mathcal{N}(p)$, the effective point configuration of $\mathcal{N}(p)$ determines whether the point p is a simple point or not.*

Corollary 3.1 is a straightforward consequence of Proposition 3.1 and Proposition 3.2 and Equation 3.5 while Corollary 3.2 is a straightforward consequence of Corollary 2.3 and Proposition 3.2. Corollary 3.3 is a straightforward consequence of Characterization 2.3, Proposition 3.1 and Proposition 3.2.

Proposition 3.3 *If an e-point x is black in $\hat{\mathcal{N}}(p)$ then $\xi(p)$ is independent of the color of other points of $edge(x,p)$.*

Proof: Let S denote the set of black points of $\hat{\mathcal{N}}(p)$ and let $y \neq x$ be a point of $edge(x,p)$. We establish the proposition by showing that the number of 26-components of $S - \{y\}$ and that of $S \cup \{y\}$ are the same. If this is not true then one of the following two cases must occur.

Case 1: None of the points of $S - \{y\}$ is 26-adjacent to y. In other words, the number of 26-components of $S \cup \{y\}$ is greater than that of $S - \{y\}$.

Case 2: Two or more 26-components of $S - \{y\}$ are 26-adjacent to y. In other words, the number of 26-components of $S - \{y\}$ is greater than that of $S \cup \{y\}$.

By assumption x is black i.e. $x \in S - \{y\}$ and $y \in edge(x,p)$ i.e. y is 26-adjacent to x. Hence, Case 1 never occurs. About Case 2, let us assume that two points $q, r \in S - \{y\}$ belong to two different 26-components of $S - \{y\}$ and q, r are 26-adjacent to y. Since, q, r are 26-adjacent to y they are also 26-adjacent to x (see Property 3.2). Thus, q, r are 26-connected in $S - \{y\}$ by the 26-path q, x, r. Hence the contradiction that q, r belong to two different 26-components of $S - \{y\}$. Thus, neither Case 1 nor Case 2 may occur and hence the number of 26-components of $S - \{y\}$ and that of $S \cup \{y\}$ are the same.

□

According to Corollary 2.3, Equation 3.5 and Proposition 3.3 we see that $\xi(p)$, $\eta(p)$ and $\delta(p)$ are independent of the color of other points of $edge(x,p)$ when the e-point

x is black.

Definition 3.2 *For an e-point $x \in \mathcal{N}(p)$, edge(x,p) is defined as a dead-edge of $\mathcal{N}(p)$ if x is black. A v-point is defined as an isolated point of $\mathcal{N}(p)$ if it neither belongs to a dead-surface of $\mathcal{N}(p)$ nor it belongs to a dead-edge of $\mathcal{N}(p)$. A v-point is defined as a dead-point of $\mathcal{N}(p)$ if it belongs to a dead-surface or it belongs to a dead-edge of $\mathcal{N}(p)$.*

Proposition 3.4 *Let y be a black isolated point of $\mathcal{N}(p)$. Then $\{y\}$ is a black component of $\hat{\mathcal{N}}(p)$.*

Proof: We shall prove this proposition by contradiction. Let us assume that $\{y\}$ is not a black component of $\hat{\mathcal{N}}(p)$. Hence, $\{y\}$ is 26-adjacent to some other black point of $\hat{\mathcal{N}}(p)$, say x. By definition, the set of black points of $\hat{\mathcal{N}}(p)$ is a subset of $\mathcal{N}^*(p)$ and hence $x \in \mathcal{N}^*(p)$. It follows from $\mathcal{N}(p)$ that no two v-points are 26-adjacent. Thus, $x \in \mathcal{N}^*(p)$ and x is 26-adjacent to y together imply that either x is an s-point or an e-point of $\mathcal{N}(p)$. Let us consider that x is an s-point. Thus $surface(x,p)$ is a dead-surface of $\mathcal{N}(p)$. Again it follows from $\mathcal{N}(p)$ that if a v-point is 26-adjacent to some s-point z then the v-point must belong to $surface(z,p)$. Thus y belongs to $surface(x,p)$ and hence y is not an isolated point. Contradiction!! Considering x as an e-point we can reach to the same contradiction in the same way. Hence, $\{y\}$ is a black component of $\hat{\mathcal{N}}(p)$.

□

Proposition 3.5 *Let all the six s-points of $\mathcal{N}(p)$ be white. Then $\xi(p)$ is equal to the number of black isolated points plus the number of 26-components in the set of black e-points of $\mathcal{N}(p)$.*

Proof: According to Proposition 3.4 each black isolated point is a black component of $\hat{\mathcal{N}}(p)$. By assumption, the s-points of $\mathcal{N}(p)$ are all white. Thus the number

of black components of $\hat{\mathcal{N}}(p)$ equals to the number of black isolated points plus the number of 26-components in the set of black e-points and black dead-points. It is a straightforward consequence of Proposition 3.1, Proposition 3.3 and Definition 3.2 that the number of black components in $\hat{\mathcal{N}}(p)$ is independent of the color dead-points. Thus the number of 26-components in the set of black e-points and black dead-points is equal to the number of 26-components in the set of black e-points of $\mathcal{N}(p)$. Hence $\xi(p)$ equals to the number of black isolated points plus the number of 26-components in the set of black e-points of $\mathcal{N}(p)$.

□

3.3.1 Geometric Class

We describe an interesting observation on $\mathcal{N}(p)$. Let us consider an image $\mathcal{P}_1$ with the set of black points $\mathcal{B}_1$. Let us consider another image $\mathcal{P}_2$ with the set of black points $\mathcal{B}_2$ such that the points of $\mathcal{B}_2 \cap \mathcal{N}(p)$ are obtained by some rotation (integral multiples of 90°) in three dimension about different axes with p as origin on the points of $\mathcal{B}_1 \cap \mathcal{N}(p)$. It is interesting to note that p is a simple point in $\mathcal{P}_1$ if and only if p is a simple point in $\mathcal{P}_2$. Moreover, the changes in the numbers of black components, tunnels and cavities in $\mathcal{N}(p)$ under binary transformation of p are exactly the same for both $\mathcal{P}_1$ and $\mathcal{P}_2$. For example, let us consider that $\mathcal{B}_1 \cap \mathcal{N}(p) = \{p, p_E, p_{SW}, p_{NW}, p_{TW}, p_{BW}\}$ and $\mathcal{B}_2 \cap \mathcal{N}(p) = \{p, p_N, p_{SE}, p_{SW}, p_{TS}, p_{BS}\}$. It may be noted that the points of $\mathcal{B}_2 \cap \mathcal{N}(p)$ is obtained by anti-clockwise rotation of 90° about y axis with p as origin to the corresponding points of $\mathcal{B}_1 \cap \mathcal{N}(p)$. It is easy to verify using Characterization 2.3 that p is not a simple point in both $\mathcal{P}_1$ and $\mathcal{P}_2$. Also both for $\mathcal{P}_1$ and $\mathcal{P}_2$ the deletion of p creates exactly two black components and one tunnel in $\mathcal{N}(p)$. Thus all possible configurations of $\mathcal{N}(p)$ may be grouped such that two configurations belong to the same group if and only if one can be transformed to the other by some three dimensional rotation in integral multiple of 90° about different axes with p as origin. In that case we only need to know the topological information of one member of each group. However, the number of groups becomes very large

when we consider all possible configurations of $\mathcal{N}(p)$. So, we only concentrate to all possible s-point configurations of $\mathcal{N}(p)$ and name each group as 'geometric class'. Geometric classes of s-point configurations of $\mathcal{N}(p)$ are defined as follows:

Definition 3.3 *Two s-point configurations of $\mathcal{N}(p)$ belong to the same geometric class if and only if one can be transformed to the other by some three dimensional rotation in integral multiples of* 90° *about different axes with p as origin.*

Possible geometric classes of s-point configurations, corresponding numbers of effective points (n_e) and the number of s-point configurations belonging to each geometric class are described as follows:

Class 0: Six s-points are black. The number of effective points (n_e) is zero. Only one s-point configuration belongs to this geometric class.

Class 1: Five s-points are black. The number of effective points (n_e) is zero. Six s-point configurations belong to this geometric class.

Class 2: Two pairs of opposite s-points are black. The number of effective points (n_e) is zero. Three s-point configurations belong to this geometric class.

Class 3: One pair of opposite s-points and two non-opposite s-points are black. The number of effective points (n_e) is one. Twelve s-point configurations belong to this geometric class.

Class 4: One pair of opposite s-points and another s-point are black. The number of effective points (n_e) is two. Twelve s-point configurations belong to this geometric class.

Class 5: Three non-opposite s-points are black. The number of effective points (n_e) is four. Eight s-point configurations belong to this geometric class.

Class 6: One pair of opposite s-points are black. The number of effective points (n_e) is four. Three s-point configurations belong to this geometric class.

Class 7: Two non-opposite s-points are black. The number of effective points (n_e) is seven. Twelve s-point configurations belong to this geometric class.

Class 8: One s-point is black. The number of effective points (n_e) is twelve. Six s-point configurations belong to this geometric class.

Class 9: No s-point is black. The number of effective points (n_e) is twenty. Only one s-point configuration belongs to this geometric class.

According to Corollary 3.3 and Corollary 3.1, simple point as well as topological parameters of $\mathcal{N}(p)$ are functions of effective point configuration of $\mathcal{N}(p)$. Thus, if $n_e = 0$ as in Classes 0–2, we at once know the topological parameters of $\mathcal{N}(p)$ and also we can say whether p is a simple point or not. In other cases as in Classes 3–9 where $n_e > 0$, we use a look_up_table. For a given s-point configuration there are 2^{n_e} possible effective point configurations. An effective point configuration can be thought of as an n_e-bit binary number. For example, consider a Class 5 situation with e_0, e_1, e_2, e_3 denoting the four effective points. Then a 4-bit binary number is generated such that its ith bit denotes the color of e_i (*i.e.* '1' when e_i is black and '0' otherwise). For example, a 4-bit binary number '1010' denotes an effective point configuration where e_0 and e_2 are white while e_1 and e_3 are black. For each such effective point configuration there is an entry in the look_up_table which contains the necessary topological information.

3.4 Detection of Simple Point

According to Corollary 3.3, after finding the s-point configuration of $\mathcal{N}(p)$ we can decide whether p is a simple point or not from the effective point configuration of $\mathcal{N}(p)$. Depending on the s-point configuration we actually switch to one of the possible sixty four cases. However, from the point of view of actions to be taken, all the sixty four cases may be classified into three groups as follows:

Group 3.4.1: (s-point configuration belonging to Class 0–2)
The number of effective points is zero. So we can at once know whether p is a simple point or not. For Class 0 and Class 2, p is never a simple point while p is always a simple point for Class 1.

Group 3.4.2: (s-point configuration belonging to Class 3–8)
The number of effective points is non-zero. A look_up_table is used for each geometric class. Since different s-point configurations may belong to the same geometric class, we consider one s-point configuration $base_i$ (a set of black s-points) from Class i. Let $base_i$ has n_i number of effective points. An ordered set $EFO(base_i)$ of these n_i effective points is defined as follows:

$$EFO(base_i) = \{e_0, e_1, \cdots, e_{n_i-1}\}$$

where $e_0, e_1, \cdots, e_{n_i-1}$ are the effective points of $\mathcal{N}(p)$ with the s-point configuration $base_i$. An effective point configuration for the s-point configuration $base_i$ is denoted by an n_i bit binary number whose jth bit denotes the color of e_j. For each such configuration of effective points there is an entry in the look_up_table. Each entry needs one bit that contains a '0' or '1' (one bit) flag to denote whether p is a simple point or not. The look_up_table needs 2^{n_i} entries i.e. 2^{n_i} bits (here n_i is the number of effective points for ith geometric class). Only one look_up_table is sufficient for all s-point configurations belonging to the same geometric class. Let us call the look_up_table for ith geometric class as $LUT\_simple\_point_i$. To illustrate the fact let us consider an s-point configuration Υ belonging to Class i such that:

$$\Upsilon = Rot(\mu, base_i)$$

where $Rot(\mu, base_i)$ is a function that generates a set from $base_i$ such that the jth element of the set is obtained from the jth element of $base_i$ after the rotation μ with p as origin (here, μ is a sequence of rotations about different axes in integral multiples of 90°). The same look_up_table may be used for the s-point configuration Υ with its ordered set of effective points $EFO(\Upsilon)$ as follows:

$$EFO(\Upsilon) = Rot(\mu, EFO(base_i))$$

That is jth element of $EFO(\Upsilon)$ is obtained from the jth element of $EFO(base_i)$ after the rotation μ. It is worthy to mention that computation of $EFO(\Upsilon)$ is not required during runtime. Instead, it is precalculated and implicitly stored in the program. More specifically, within the program there is a case for a particular s-point configuration Υ. At that place the ordered set of effective points $EFO(\Upsilon)$ is known to the program and it calculates the effective point configuration value accordingly.

Group 3.4.3: (s-point configuration belonging to Class 9)
As described in Section 3.3.1 only one s-point configuration belongs to this class. Here, the number of effective points is twenty. A straightforward application of the look_up_table described in Group 3.4.2 needs 2^{20} bits i.e. 128 Kbytes. So, we modify the form of the look_up_table. We classify Group 3.4.3 into two sub-groups and proceed as follows:

Sub-group 3.4.3a: (all e-points are white)
All v-points are isolated points. According to Proposition 3.5, $\xi(p)$ equals to the number of black v-points. Also $\hat{\mathcal{N}}(p)$ never contains a tunnel. Hence p is a simple point if and only if exactly one v-point is black.

Sub-group 3.4.3b: (at least one e-point is black)
Here, p is not a simple point if any of the following situations occurs — 1) the set of black e-points is not 26-connected, 2) there is a tunnel in $\hat{\mathcal{N}}(p)$, or 3) there is a black isolated point.

At first we find a black e-point of $\hat{\mathcal{N}}(p)$. If an e-point x is black then there may be at most 2^{11} possible configurations of other e-points and hence the look_up_table $LUT\_simple\_point_9$ contains 2^{11} entries. An ordered set $EEO(x)$ of these eleven e-points is used to calculate their configuration value. The address of an entry of $LUT\_simple\_point_9$ corresponds to a distinct configuration of $EEO(x)$. At each entry of $LUT\_simple\_point_9$ we store the following information — 1) whether the set of black e-points contains more than one 26-components or if there exists a

tunnel in $\hat{\mathcal{N}}(p)$, and 2) the set of isolated points. Since x is black at most six v-points can be isolated points. An ordered set of these six v-points is named $ISO(x)$. For each entry of $LUT\_simple\_point_9$ a one byte word l is used in which (0–5) bit positions denote the set of isolated points in $ISO(x)$. The 6th bit position of l is '1' if the set of black e-points contains more than one 26-components or if there is a tunnel. The 7th bit position always contains a '0'. To determine whether p is a simple point we generate a one byte word w whose (0–5) bit positions denote the configuration of $ISO(x)$ while 6th and 7th bits are '1' and '0' respectively. Thus p is a simple point if and only if the *bitwise AND* operation between l and w leads to zero. The look_up_table $LUT\_simple\_point_9$ now needs only 2^{11} bytes *i.e.* 2 Kbytes, instead of 128 Kbytes in its earlier form.

An e-point can be rotated in integral multiples of 90^o about different axes (with p as origin) to reach another e-point. Thus we can use single look_up_table for different e-points in the same fashion we have described for different s-point configurations belonging to the same geometric class. However, here we need the rotational transformation on both $EEO(x)$ and $ISO(x)$. At this point it should be made clear that rotation is not required at runtime to evaluate $EEO(X)$ and $ISO(X)$. In contrast, for each e-point X, $EEO(X)$ and $ISO(X)$ are precalculated and implicitly stored in the program.

3.4.1 The Algorithm (*simple_point*)

As described above our procedure of simple point detection has two parts, which are — (a) *a priori knowledge*, (b) *run-time computation*. The a priori knowledge includes the precalculation and storage of all the look_up_tables $LUT\_simple\_point_i$, $3 \leq i \leq 9$. Also, for each s-point configuration Υ belonging to Class i, $3 \leq i \leq 8$, the ordered set of effective points $EFO(\Upsilon)$ is precalculated as discussed earlier and implicitly stored in the program to compute the entry value of $LUT\_simple\_point_i$. Similarly, in case of Class 9, for every e-point x, $EEO(x)$ and $ISO(x)$ are precalcu-

lated and implicitly used in the program. It should be mentioned that the a *priori* knowledge is independent of the input image to be processed. Thus once generated, the knowledge can be used for any other image later on.

During the runtime, for any point $p \in Z^3$ of an input 3D image P, we use the following procedure (*simple_point*) to detect whether p is a simple point or not. Here bitwise_AND(x, y) is a function that returns the result of bitwise AND operation between two bytes x, y.

procedure *simple_point* (p)
Υ = s-point configuration value of $\mathcal{N}(p)$;
switch(Υ)
Group 1.a: /* Υ belongs to Class 0 */
flag = 0;
Group 1.b: /* Υ belongs to Class 1 */
flag = 1;
Group 1.c: /* Υ belongs to Class 2 */
flag = 0;
Group 2: /* Υ belongs to Class 3–8 */
let Υ belong to Class i, $3 \leq i \leq 8$;
j = configuration value of $EFO(\Upsilon)$;
flag = $LUT\_simple\_point_i[j]$;
Group 3: /* Υ belongs to Class 9 */
if an e-point of $\mathcal{N}(p)$, say x, is black then
i = configuration value of $EEO(x)$;
w = configuration value of $ISO(x) + 2^6$;
r = bitwise_AND$(w, LUT_simple_point_9[i])$;
if $r = 0$ then
flag = 1;
else
flag = 0;

```
else /* all e-points are white */
        if exactly one isolated point of N̂(p) is black then
            flag = 1;
        else
            flag = 0;
return(flag);
end procedure simple_point;
```

In the above algorithm there are sixty four cases for all possible s-point configurations. For convenience we do not mention all the sixty four cases. Instead, we mention different groups where each group is a representative of all cases of s-point configuration with corresponding geometric class.

3.5 Computation of Local Topological Parameters

As discussed in Section 2.5, the measure of topological changes in the $3 \times 3 \times 3$ neighborhood of a point $p \in Z^3$ under its binary transformation essentially computes the numbers of black components, tunnels and cavities in $\hat{\mathcal{N}}(p)$. The numbers of components, tunnels and cavities in $\hat{\mathcal{N}}(p)$ i.e. $\xi(p)$, $\eta(p)$ and $\delta(p)$ respectively, are also referred as topological parameters of p. In this section we shall describe an efficient approach of computing these parameters. According to Corollary 3.1, after finding the s-point configuration of $\mathcal{N}(p)$ we can compute $\xi(p)$, $\eta(p)$ and $\delta(p)$ from the effective point configuration of $\mathcal{N}(p)$. The algorithm switches on the s-point configuration. Similar to Section 3.4, all the sixty four cases of s-point configurations are classified into three groups as follows:

Group 3.5.1: (s-point configuration belonging to Class 0–2)
The number of effective point is zero. The values of $\xi(p)$, $\eta(p)$, $\delta(p)$ are stated as follows:

Class 0: $\xi(p) = 1, \eta(p) = 0, \delta(p) = 1$;

Class 1: $\xi(p) = 1, \eta(p) = 0, \delta(p) = 0$;

Class 2: $\xi(p) = 1, \eta(p) = 1, \delta(p) = 0$.

Group 3.5.2: (s-point configuration belonging to Class 3–8)
This case is similar to Group 3.4.2 of Section 3.4. The only difference lies in the structure of look up tables. There are only six s-points in $\mathcal{N}(p)$. So, $\hat{\mathcal{N}}(p)$ may contain at most five tunnels and it occurs only when all s-points are white while all e-points are black (see Theorem 2.1). Also $\hat{\mathcal{N}}(p)$ may contain at most eight black components and it occurs only when all v-points are black and all other points are white. Moreover, for Classes 3–8, $\delta(p)$ is always zero. Thus, for each entry of the look_up_table one byte is used whose lower order four bits store the value of $\xi(p)$ and higher order four bits store the value of $\eta(p)$. The look_up_table of ith geometric class needs 2^{n_i} entries i.e. 2^{n_i} bytes and it is referred as $LUT\_topo\_para_i$ (here n_i is the number of effective points for ith geometric class).

Group 3.5.3: (s-point configuration belonging to Class 9)
Similar to Group 3.4.3 of Section 3.4 one of the following two sub-groups is followed:

Sub-group 3.5.3a: (all e-points are white)
Here, $\eta(p) = 0$, $\delta(p) = 0$, and $\xi(p) =$ the number of black v-points.

Sub-group 3.5.3b: (at least one e-point is black)
Let us consider that an e-point x is black. Let $\mathcal{B}_e(p)$ denote the set of black e-points of $\hat{\mathcal{N}}(p)$. To compute $\xi(p)$ and $\eta(p)$ (here, $\delta(p) = 0$) we allocate two bytes for each entry of $LUT\_topo\_para_9$ that store the following information:

1. the number of tunnels in $\hat{\mathcal{N}}(p)$,

2. the number of 26-components of $\mathcal{B}_e(p)$,

3. the set of isolated points of $\mathcal{N}(p)$.

The higher order four bits of the first byte store the value of $\eta(p)$ while the lower order four bits of the same byte store the number of 26-components of $\mathcal{B}_e(p)$. The lower order six bits of the second byte denote the set of isolated points (6th and 7th bits are always zero). For example, if the first and second bytes of certain entry of $LUT\_topo\_para_9$ is '00110010' and '00010001' respectively, then $\eta(p) = 3$ and the number of 26-components of $\mathcal{B}_e(p)$ is 2 while 0th and 4th points of $ISO(x)$ are isolated points.

The look_up_table $LUT\_topo\_para_9$ needs only 2×2^{11} bytes *i.e.* 4 Kbytes. Let w be the configuration value of the points of $ISO(x)$. A bitwise 'AND' operation between w and the 2nd byte of corresponding entry of $LUT\_topo\_para_9$ results in the set of black isolated points of $\hat{\mathcal{N}}(p)$.

3.5.1 The Algorithm (*topo_para*)

During the runtime, for any point p of an input 3D image P, we use the following procedure (*topo_para*) to compute the topological parameters $\xi(p)$, $\eta(p)$, and $\delta(p)$. In the following algorithm $LUT\_topo\_para_9[j][0]$ denotes the first byte of jth entry of $LUT\_topo\_para_9$ while $LUT\_topo\_para_9[j][1]$ denotes the second byte of jth entry of $LUT\_topo\_para_9$. Also x_l/x_h denote the value of lower/higher four bits of the byte x.

```
procedure topo_para (p)
Υ = s-point configuration of N(p);
switch(Υ)
Group 1.a: /* Υ belongs to Class 0 */
```

$\xi(p) = 1$; $\eta(p) = 0$; $\delta(p) = 1$;

Group 1.b: /* Υ belongs to Class 1 */

$\xi(p) = 1$; $\eta(p) = 0$; $\delta(p) = 0$;

Group 1.c: /* Υ belongs to Class 2 */

$\xi(p) = 1$; $\eta(p) = 1$; $\delta(p) = 0$;

Group 2: /* Υ belongs to Class 3–8 */

let Υ belong to Class i, $3 \leq i \leq 8$;

j = configuration value of $EFO(\Upsilon)$;

$\xi(p) = LUT\_topo\_para_i[j]_l$;

$\eta(p) = LUT\_topo\_para_i[j]_h$;

$\delta(p) = 0$;

Group 3: /* Υ belongs to Class 9 */

if an e-point of $\mathcal{N}(p)$, say x, is black then

i = configuration value of $EEO(x)$;

w = configuration value of $ISO(x)$;

r = bitwise_AND(w, $LUT\_topo\_para_i[j][1]$);

$\xi(p) = LUT\_topo\_para_i[i][0]_l$ + number of '1' bits in r;

$\eta(p) = LUT\_topo\_para_i[i][0]_h$;

$\delta(p) = 0$;

else /* all e-points are white */

$\xi(p)$ = the number of black v-points;

$\eta(p) = 0$;

$\delta(p) = 0$;

return$(\xi(p), \eta(p), \delta(p))$;

end procedure *topo_para*;

3.6 The Euler Characteristic

A review on the Euler characteristic of 3D digital image is presented in Section 1.2.9 and Section 1.3.5. Here we present a new approach [116] of computing the Euler characteristic of 3D digital image in a parallel mode. We use following two propositions [115,116] to compute the Euler characteristic of a 3D digital image.

Proposition 3.6 *For a 3D digital image P, the Euler characteristic $\chi(P)$ equals to the number of black components minus the number of tunnels plus the number of cavities in P.*

Proposition 3.7 *Let $P = (Z^3, 26, 6, B)$ be a 3D digital image and let $p \in B$ be a black point of P. Under this assumption, the Euler characteristic of P is equal to the Euler characteristic of $(V, 26, 6, B - \{p\})$ plus the change in the Euler characteristic in $N(p)$ due to the deletion of p.*

Both Propositions 3.6 and 3.7 are important in our approach of computing the Euler characteristic of a 3D digital image. While Proposition 3.6 is motivated by the discussion in Section 1.2.9, Proposition 3.7 is considered by others [51,69]. The change in the Euler characteristic in the $3 \times 3 \times 3$ neighborhood of a black point p due to its deletion is equal to the Euler characteristic of $\dot{N}(p)$ minus the Euler characteristic of $\hat{N}(p)$. A recursive definition of $\chi(V, 26, 6, B)$ is stated as follows:

1. $\chi(V, 26, 6, B) = 0$ if $B = \phi$;
2. for any point $p \in B$, (3.6)

$$\chi(V, 26, 6, B) = \chi(V, 26, 6, B - \{p\}) + \chi(\dot{N}(p)) - \chi(\hat{N}(p)).$$

3.6.1 The Euler Characteristic in $3 \times 3 \times 3$ Neighborhood

As mentioned in Section 2.4, the *numbers of black components*, tunnels and cavities in $\dot{\mathcal{N}}(p)$ are '1', '0' and '0' respectively. Hence, $\chi(\dot{\mathcal{N}}(p)) = 1 - 0 + 0 = 1$. Thus our work boils down to the computation of the Euler characteristic of $\hat{\mathcal{N}}(p)$ which then leads to the estimation of the numbers of black components, tunnels and cavities in $\hat{\mathcal{N}}(p)$. According to Corollary 3.1, after finding the s-point configuration of $\mathcal{N}(p)$, the change in the Euler characteristic in the $3 \times 3 \times 3$ neighborhood of p can be computed from the effective point configuration of $\mathcal{N}(p)$. The algorithm switches on the s-point configurations. Similar to Section 3.4, all the sixty four s-point configurations are classified into three groups as follows:

Group 3.6.1: (s-point configuration belonging to Class 0–2)
The number of effective points is zero. The changes in the Euler characteristic are as stated follows:

$$\begin{aligned}
&\text{Class 0:} \quad \chi(\dot{\mathcal{N}}(p)) - \chi(\hat{\mathcal{N}}(p)) = -1, \\
&\text{Class 1:} \quad \chi(\dot{\mathcal{N}}(p)) - \chi(\hat{\mathcal{N}}(p)) = 0, \\
&\text{Class 2:} \quad \chi(\dot{\mathcal{N}}(p)) - \chi(\hat{\mathcal{N}}(p)) = 1.
\end{aligned}$$

Group 3.6.2: (s-point configuration belonging to Class 3–8)
This case is similar to Group 3.4.2 of Section 3.4. The only difference lies in the structure of look up tables. Each entry of a look_up_table stores $\chi(\dot{\mathcal{N}}(p)) - \chi(\hat{\mathcal{N}}(p))$ that needs single byte. The look_up_table of ith geometric class needs 2^{n_i} bytes and it is referred as $LUT\_euler\_change_i$ (where n_i is the number of effective points for ith geometric class).

Group 3.6.3: (s-point configuration belonging to Class 9)
Similar to Group 3.4.3 of Section 3.4 one of the following two sub-cases is followed.

Sub-group 3.6.3a: (all e-points are white)
Here, $\chi(\dot{\mathcal{N}}(p)) - \chi(\hat{\mathcal{N}}(p))$ is computed as follows:

$$\chi(\dot{\mathcal{N}}(p)) - \chi(\hat{\mathcal{N}}(p)) = 1 - \text{the number of black } v\text{-points.}$$

Sub-group 3.6.3b: (at least one e-point is black)
To compute $\chi(\dot{\mathcal{N}}(p)) - \chi(\hat{\mathcal{N}}(p))$, each entry of $LUT\_euler\_change_9$ needs two bytes which store the following information:

1. 1 − the number of 26-components of $\mathcal{B}_e(p)$ + the number of tunnels in $\hat{\mathcal{N}}(p)$, and

2. the set of isolated points of $\hat{\mathcal{N}}(p)$.

The first byte of each entry stores the value of '1 − the number of 26-components of $\mathcal{B}_e(p)$ + the number of tunnels in $\hat{\mathcal{N}}(p)$'. The lower order six bits of the second byte denote the set of isolated points (6th and 7th bits are always zero). The look_up_table $LUT\_euler\_change_9$ needs only 4 Kbytes. A bitwise 'AND' operation between the configuration value w of $ISO(x)$ and the 2nd byte of corresponding entry of $LUT\_euler\_change_9$ results in the set of black isolated points of $\hat{\mathcal{N}}(p)$. Hence, $\chi(\dot{\mathcal{N}}(p)) - \chi(\hat{\mathcal{N}}(p))$ = value of first byte of $LUT\_euler\_change_9$ − the number of black isolated points. For example, let configuration value of $EEO(x)$ be i and the 1st and 2nd bytes of ith entry of $LUT\_euler\_change_9$ be '00000001' and '011000100' respectively. Let configuration value w of $ISO(x)$ be '00000100'. Then the number of black isolated points is '1' and $\chi(\dot{\mathcal{N}}(p)) - \chi(\hat{\mathcal{N}}(p)) = 1 - 1 = 0$.

The Algorithm (*euler_change*)

For any point p of an input 3D image P, we use the following procedure (*euler_change*) to compute $\chi(\dot{\mathcal{N}}(p)) - \chi(\hat{\mathcal{N}}(p))$.

```
procedure euler_change (p)
Υ = s-point configuration of N(p);
switch(Υ)
Group 1.a: /* Υ belongs to Class 0 */
        el_ch = −1;
Group1.b: /* Υ belongs to Class 1 */
        el_ch= 0;
Group1.c: /* Υ belongs to Class 2 */
        el_ch = 1;
Group 2: /* Υ belongs to Class 3–8 */
        let Υ belong to Class i,  3 ≤ i ≤ 8;
        j = configuration value of EFO(Υ);
        el_ch = LUT_euler_change_i[j];
Group 3: /* Υ belongs to Class 9 */
        if an e-point of N(p), say x, is black then
                i = configuration value of EEO(x);
                w = configuration value of ISO(x);
                r = bitwise_AND(w, LUT_euler_change_i[j][1]);
                el_ch = LUT_topo_para_i[i][0] - number of '1' bits in r;
        else /* all e-points are white */
                el_ch = 1 - the number of black v-points;
return(el_ch);
end procedure euler_change;
```

3.6.2 The Euler Characteristic of Digital Image

In Section 3.6.1 we have described an efficient algorithm to compute the change in the Euler characteristic in the $3 \times 3 \times 3$ neighborhood of a point p that occurs

due to its deletion. Using the algorithm *euler_change*, the Euler Characteristic of a 3D digital image can be computed according to Equation 3.6. A parallel implementation of the method is possible using the concept of sub-fields [28]. The parallelization is based on the following concept.

If two points $p, q \in B$ are not 26-adjacent then

$$\chi(\mathcal{V}, 26, 6, B) = \chi(\mathcal{V}, 26, 6, B - \{p, q\}) + \chi(\dot{\mathcal{N}}(p)) - \chi(\hat{\mathcal{N}}(p)) + \chi(\dot{\mathcal{N}}(q)) - \chi(\hat{\mathcal{N}}(q))$$

To conceive maximum parallelization in the algorithm eight sub-fields $O_0, O_1, \cdots, O_7$ are defined as follows:

$$O_l = \{(2 \times i + f, 2 \times j + g, 2 \times k + h) \mid i, j, k = 0, \pm 1, \pm 2, \cdots, \\ f, g, h \in \{0, 1\} \text{ and } 2^2 \times f + 2^1 \times g + 2^0 \times h = l\} \tag{3.7}$$

such that two points $p, q \in O_l$ are never 26-adjacent. The Euler Characteristic of a 3D digital image can be computed in eight steps and at each step the algorithm uses the following equation:

$$\chi(\mathcal{V}, 26, 6, B) = \chi(\mathcal{V}, 26, 6, B - O_l) + \sum_{p \in O_l \cap B} \chi(\dot{\mathcal{N}}(p)) - \chi(\hat{\mathcal{N}}(p)) \tag{3.8}$$

where $\sum_{p \in O_l \cap B} \chi(\dot{\mathcal{N}}(p)) - \chi(\hat{\mathcal{N}}(p))$ can be computed in a parallel manner.

3.7 Conclusion

In this chapter we have given algorithmic forms of three important topological operators *simple_point*, *topo_para*, and *euler_change*. The algorithm *simple_point* detects whether a point is a simple point or not; *topo_para* computes local topological parameters of a point p i.e. the numbers of black components, tunnels and cavities in $\hat{\mathcal{N}}(p)$ while *euler_change* computes the change in the Euler characteristic in the

$3 \times 3 \times 3$ neighborhood of a point due to its deletion. The most naive and trivial approach for these operations is to prepare a look_up_table for all possible black/white configurations of the $3 \times 3 \times 3$ neighborhood that needs 2^{26} entries. In other words the look_up_table for *simple_point* needs 2^{26} bits i.e. 8 Mbytes and the look_up_table for *topo_para* or *euler_change* need 2^{26} bytes i.e. 64 Kbytes. On the other hand, in our approach the look_up_table needs 2 Kbytes for *simple_point* and 4 Kbytes for *topo_para* or *euler_change*. Moreover, only for Class 9 these operations need the configuration of all the twenty six points of the $3 \times 3 \times 3$ neighborhood. For Classes 0–8 they need the configuration of lesser number of points (see Groups 3.4.1–2, Groups 3.5.1–2, and Groups 3.6.1–2 in Section 3.4, Section 3.5, and Section 3.6.1 respectively).

Application of *simple_point* in 3D object thinning is discussed in Chapter 4 while the application of *topo_para* in 3D object segmentation is discussed in Chapter 5. In this chapter we have described an application of *euler_change* to develop a parallel algorithm for computing the Euler characteristic of a 3D digital image.

Chapter 4

Parallel Thinning For 3D Objects

4.1 Introduction

This chapter is concerned with a new parallel thinning algorithm for three dimensional (3D) digital images. Many image processing techniques such as smoothing, filtering, thinning and segmentation are of interest in various applications to 3D image processing. The objective of 3D image thinning is to produce a medial surface representation (sometimes an arc representation) that preserves the topology and maintains the shape of an object as much as possible. Thinning makes a compact representation of an object and hence is computationally attractive for future analysis. However thinning is not guaranteed to produce a meaningful representation of an object unless the object is piecewise "elongated" or "flat-shaped". That is the object is composed of parts each of which has the property that (at least) one of its dimension is much less than the others.

One of the important uses of thinning is to decompose an object into meaningful segments [115]. In Section 1.3.8 we have studied previous works on 3D thinning [32,28,69,79,122,131,70,71]. Unfortunately none of the previous researchers

studied the behavior of their algorithms around different types of corners. Also they did not study the robustness of their algorithms under noise or rotation. In this chapter we describe a parallel thinning algorithm based on our works [114,117,118]. We consider the aspects of our thinning algorithm stressing its behavior and robustness under pseudo random noise and rotation.

Theoretical aspect of the proposed thinning approach that produces a medial surface representation of 3D object is described in Section 4.2. At the end of this section we discuss an approach that produces a medial arc representation of an object from its surface representation. The parallel thinning algorithm is described and the experimental results are presented in Section 4.3. The robustness of the proposed algorithm under pseudo random contour noise as well as rotation is studied with respect to shape properties. The results are described in Section 4.4. A comparative study between our approach and the existing approaches is presented in Section 4.5.

4.2 The Thinning Approach

We initially consider thinning as an approach of producing a medial surface representation of a 3D digital object that preserves the topology and maintains the shape of the object to the maximum extent. It may be necessary in some applications to produce a medial arc representation of an object. We call this transformation process as arc-thinning and consider it at the end of this section. The proposed thinning approach producing a medial surface representation is an iterative erosion process that consists of two steps namely primary-thinning and final-thinning. The results of these steps are called primary-skeleton and final-skeleton respectively.

Our thinning approach exploits the information from two versions of an image implicitly stored throughout the thinning procedure. One image version denotes the black/white configuration before the current iteration while the other denotes the current stage of the processed image. Here, it is worthy to mention that simple

points are always detected on the current version of the image while the shape preserving constraints are mostly defined on the image version before each current iteration. This idea is quite different from other works [131,32] where only one version of image is used for thinning. In this context we particularly note that only one image is physically stored throughout the thinning algorithm, although we refer to two image versions. Two image versions are realized from one physical image by the way of interpreting the values of image points. This concept will be more clear from the subsequent discussion. At the beginning of the algorithm when we read an image, every white point is assigned a large negative number, say $-maxint$ and each black point is assigned '0'. At the beginning of execution all black points are unmarked. As the erosion continues, some of the black points are deleted and some are marked. Once a point is marked it is never deleted in subsequent steps of erosion during primary-thinning. Each iteration is denoted by an iteration number i. A threshold value thr is defined during ith iteration as follows:

$$thr = -maxint + i.$$

If during ith iteration a point is found deletable then it is assigned the value thr. Thus a point having value greater than or equal to thr is black before the iteration. Otherwise, the point is white before the iteration. A point with negative value is currently white while a point with non-negative value is currently black. In this way, two image versions are realized from single physical image. A point with zero value is an unmarked black point. A point is marked by assigning the iteration number i. Thus a point with non-zero positive value is a marked point.

At this point it should be made clear that in this work, iteration and scan are two completely different concepts. A scan is a (point by point) traversal of the entire image when subjected to the thinning process. On the other hand, an iteration is completed after considering the entire outer-layer of an object through proper topology and shape constraints. An iteration may consist of one or more scans in which case the operation in each scan is generally different. The set of points considered for erosion during an iteration defines the outer-layer for that iteration.

Before we describe the thinning procedure let us present some definitions and conditions in this context. In the following definitions and conditions (a, d), (b, e) and (c, f) denote three distinct unordered pairs of opposite s-points of $\mathcal{N}(p)$ unless stated otherwise.

Definition 4.1 *During an iteration a black point p is an s-open point if at least one s-point of $\mathcal{N}(p)$ is white before the iteration.*

Definition 4.2 *During an iteration a black point p is an e-open point if p is not an s-open point and an e-point $e(a, b, p)$ is white while the points $f_1(a, p)$, $f_1(b, p)$ are black before the iteration.*

Definition 4.3 *During an iteration a black point p is a v-open point if p is neither an s-open point nor an e-open point and a v-point $v(a, b, c, p)$ is white while the points $f_1(a, p)$, $f_1(b, p)$, $f_1(c, p)$ are black before the iteration.*

The set of s-open, e-open and v-open points defines the outer-layer in an iteration. It is understood from the above definitions that the labeling of points as s-open, e-open and v-open points is made once before each iteration. In the definition of e-open points, the extra condition '$f_1(a, p)$,$f_1(b, p)$ are black' is used to include the points marked as 'e' in Figure 4.1 while to exclude the points marked as '$\times$' in Figure 4.2. If the points marked as '$\times$' are included as e-open points i.e. considered for erosion in the particular iteration then the sharpness of the corner is lost in the next iteration. Similarly, the extra condition '$f_1(a, p)$,$f_1(b, p)$, $f_1(c, p)$ are black' is used in the definition of v-open points to preserve the sharpness at the meeting corner of three surfaces.

Condition 4.1 *During an iteration a point p satisfies Condition 4.1 if there exist two opposite s-points $a, d \in \mathcal{N}(p)$ such that $\mathcal{E}\,\mathcal{M}(a, d, p)$ contains a 6-closed path*

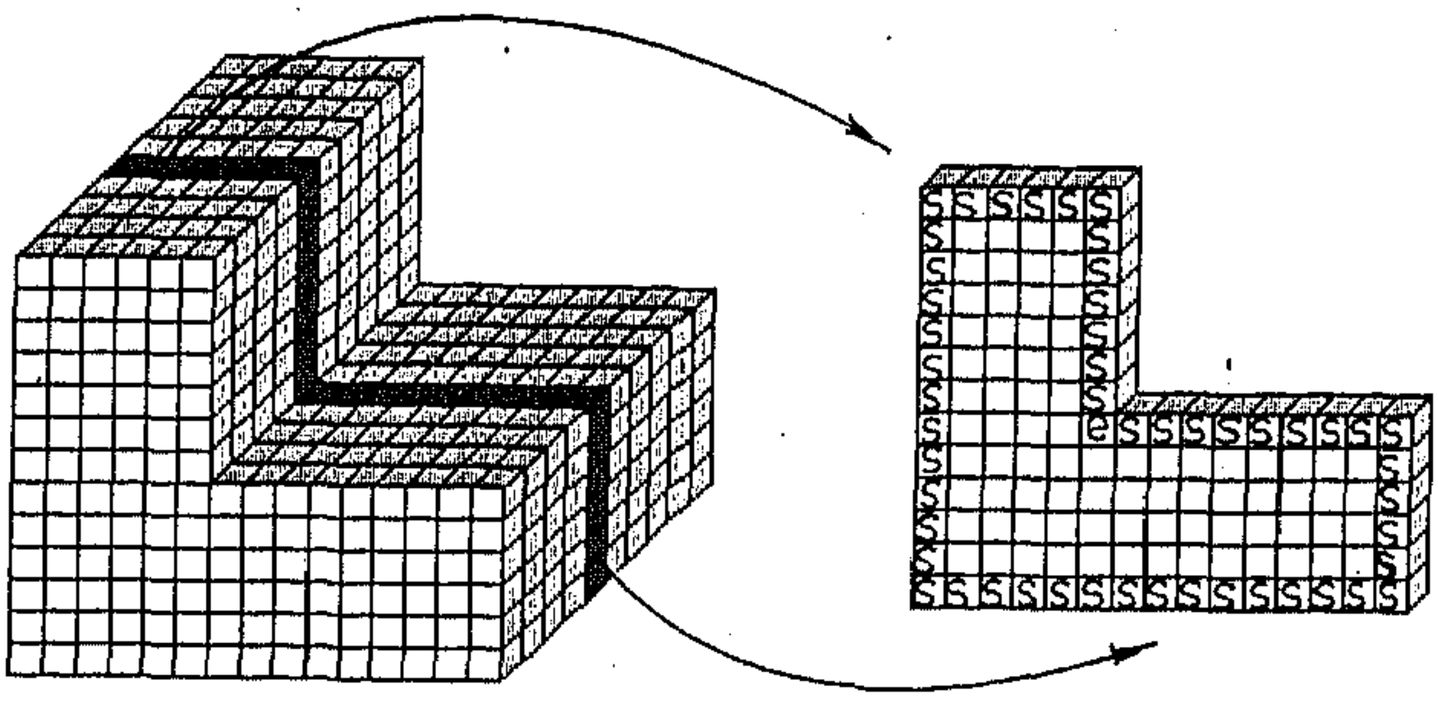

Figure 4.1: Demonstration of *e*-open points. The point marked as '*e*' is an *e*-open point. Here, points marked as '*s*' are *s*-open points.

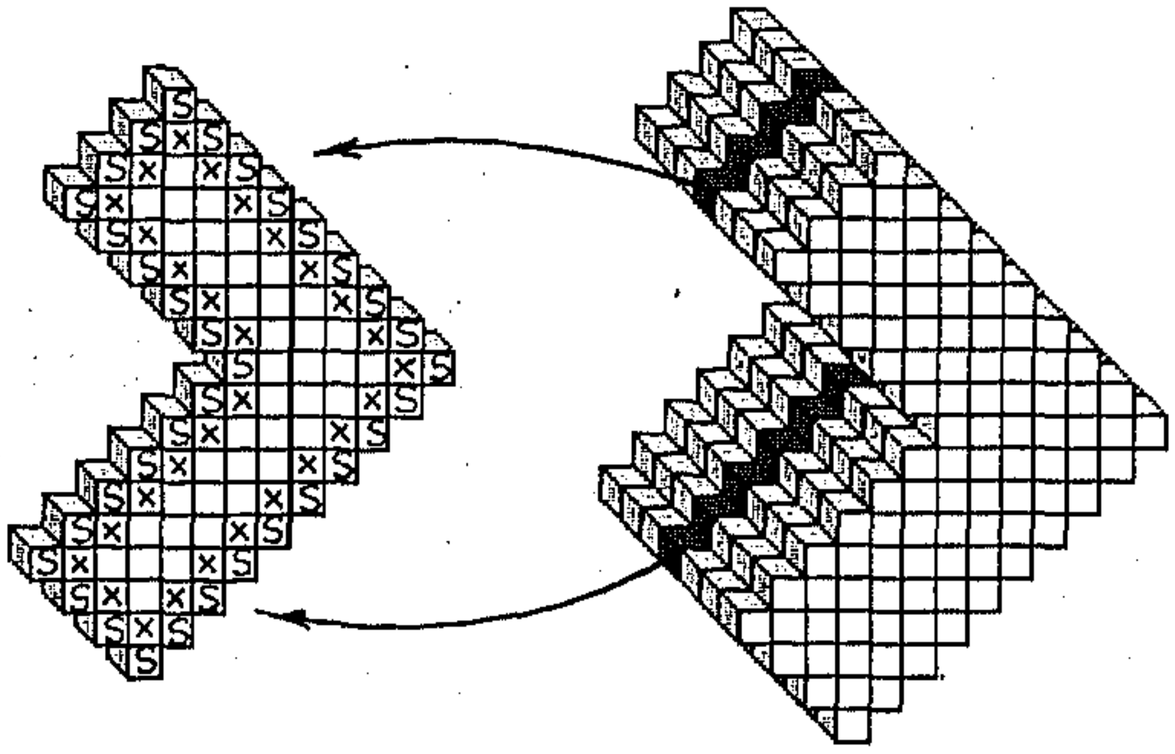

Figure 4.2: The points marked as '×' are excluded as *e*-open points to preserve the sharpness of the corner. Here, points marked as '*s*' are *s*-open points.

of white points encircling p and each of $surface(a,p)$ and $surface(d,p)$ contains at least one black point before the iteration.

A 6-closed path of $\mathcal{E}M(a,d,p)$ encircles p if it contains two points of $\mathcal{E}M(a,d,p) \cap \{p_T, p_N, p_E\}$. It is worthy to mention that in this thesis a path or a closed path is a sequence of distinct points (see Section 1.2.7). It may also be noted that a 6-path of white points encircling p defines a tunnel [111,113,114,115] in the background. Thus one may guess that this condition characterizes an arc-like shape. The second part of the condition ensures that the arc-like shape must be at least three points elongated.

Condition 4.2 *During an iteration a point p satisfies Condition 4.2 if there exists a pair of opposite s-points (a,d) such that $d \in \{p_B, p_S, p_W\}$, a is white, d or $f_1(d,p)$ is white and each of the sets $\{e(a,b,p), b, e(b,d,p)\}$, $\{e(a,c,p), c, e(c,d,p)\}$, $\{e(a,e,p), e, e(d,e,p)\}$, $\{e(a,f,p), f, e(d,f,p)\}$, $\{v(a,b,c,p), e(b,c,p), v(b,c,d,p)\}$, $\{v(a,b,f,p), e(b,f,p), v(b,d,f,p)\}$, $\{v(a,c,e,p), e(c,e,p), v(c,d,e,p)\}$, $\{v(a,e,f,p), e(e,f,p), v(d,e,f,p)\}$ contains at least one black point before the iteration.*

Condition 4.2 characterizes a surface-like shape and the second part of this condition that each of the eight sets (mentioned in the condition) contains a black point, ensures that the surface must be at least of size 3×3 points.

Definition 4.4 *During an iteration a black point is a shape point if it satisfies Condition 4.1 or Condition 4.2.*

Thus a shape point is either an arc-like shape or a surface-like shape. It may also be noted that shape points are labeled once before each iteration.

Condition 4.3 *During an iteration a point p satisfies Condition 4.3 if for each middle plane $M(a,d,p)$ of $\mathcal{N}(p)$ — either all e-points in $M(a,d,p)$ are black before*

the iteration or the current black points of $M(a,d,p)$ generate single 26-component without any tunnel [114,115].

The black points of the middle plane $M(a,d,p)$ generate a tunnel if and only if all the s-points of $N(p)$ belonging to $M(a,d,p)$ are currently black.

Definition 4.5 *During an iteration a function is defined on the black/white configuration before the iteration as follows:*

$$thick(a,d,p) = \begin{cases} true & \text{if } a \text{ and } f_1(d,p) \text{ are white while } d \text{ is black,} \\ false & \text{otherwise.} \end{cases}$$

Condition 4.4 *A point p satisfies Condition 4.4 if $thick(a,d,p)$, where $d \in \{p_B, p_S, p_W\}$, is true and the current black points of each of $M(b,e,p)$ and $M(c,f,p)$ generate single 26-component without any tunnel.*

Condition 4.5 *A point p satisfies Condition 4.5 if $thick(a,d,p)$ and $thick(b,e,p)$, where $d,e \in \{p_B, p_S, p_W\}$, are true and the current black points of $M(c,f,p)$ generate single 26-component without any tunnel.*

Condition 4.6 *A point p satisfies Condition 4.6 if $thick(a,d,p)$, $thick(b,e,p)$ and $thick(c,f,p)$, where $d,e,f \in \{p_B, p_S, p_W\}$, are true.*

Definition 4.6 *During an iteration a black point is an erodable point if it is a simple point and satisfies any of the Conditions 4.4, 4.5 or 4.6.*

4.2.1 Primary-Thinning

As mentioned earlier primary-thinning is an iterative procedure and iterations are continued as long as any point is deleted in the last iteration. Each iteration is

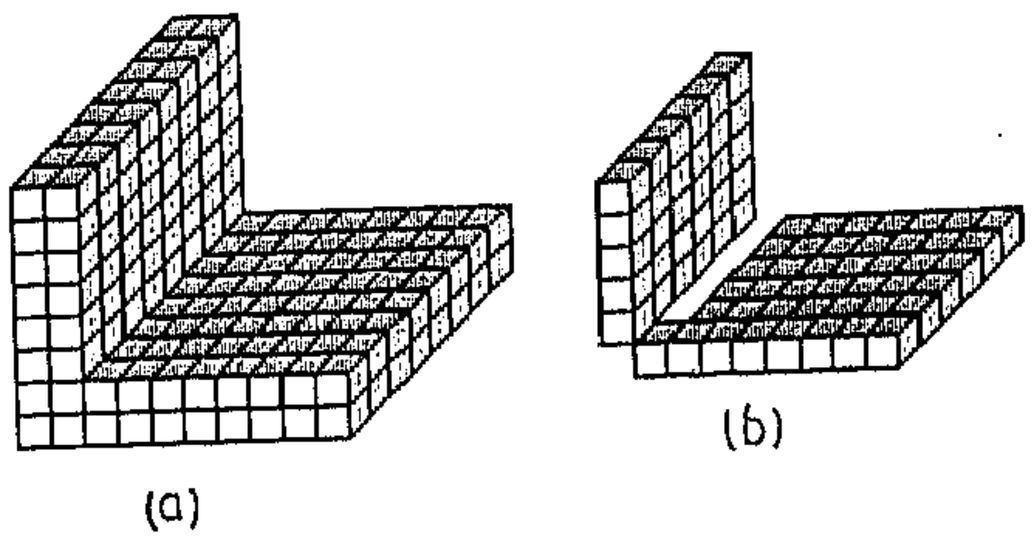

Figure 4.3: Problem of eroding all simple *e*-open points. (a) Original object. (b) Surface-skeleton when all simple *e*-open points are eroded.

completed in three successive scans. During the first scan the set of unmarked *s*-open points is used for erosion. An unmarked *s*-open point is marked if it is a shape point. When it is not a shape point, it is deleted if it is a simple point, otherwise it is left unmarked. During the second scan the set of unmarked *e*-open points is used for erosion. It may be observed from Definitions 4.2 and 4.4 that an *e*-open point can never be a shape point and hence is never marked. However an undesired situation may occur as shown in Figure 4.3 when all unmarked *e*-open points satisfying the constraints of simple points [111,113,114] are deleted. To overcome this problem an additional constraint, namely Condition 4.3, is imposed on the deletion of *e*-open points. It may be noted that the Condition 4.3 basically checks 2D topology preservation in each co-ordinate plane passing through the candidate point and containing one of its white (before the iteration) *e*-points. Thus in the second scan an unmarked *e*-open point is deleted if it is a simple point and satisfies Condition 4.3. During the third scan the set of unmarked *v*-open points is used for erosion. An unmarked *v*-open point is deleted if it is a simple point.

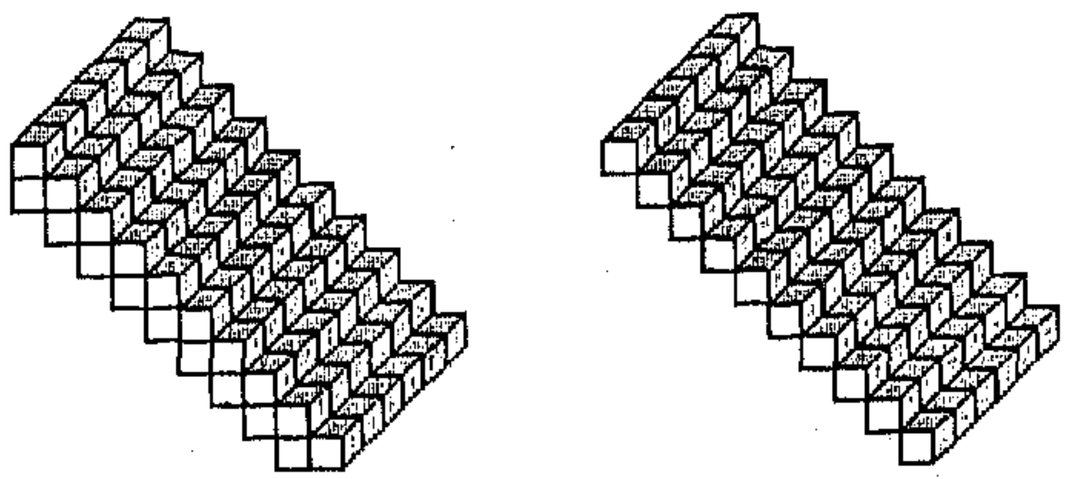

(a) (b)

Figure 4.4: (a) An output of primary-thinning. (b) Properly thinned output after final thinning.

4.2.2 Final-Thinning

From the definition of shape point it may be understood that a two-point thick slanted surface may occur in primary-skeleton. Final-thinning is necessary to get a proper skeleton for such cases. This is a single iteration procedure and the iteration consists of single scan. During this scan a black point p (irrespective of whether p is marked or unmarked) is deleted if it is an erodable point. In Figure 4.4.(a), we show an output of primary-thinning. The output of final thinning for corresponding pattern which is properly thinned is shown in Figure 4.4.(b). Also, final-thinning produces similar thinned output for two-point thick slanted surfaces (like Figure 4.4.(a)) in different directions.

4.2.3 Shape Preservation Around Corners

Intuitively it is obvious that the quality of skeleton gets affected by the sequence in which the points are deleted when outer-layer is defined on the current version of the processed image. This problem does not occur when the image before each current iteration is oonsidered to label the outer-layer. It is already mentioned that in the proposed algorithm the outer-layer i.e. the set of different open points are labeled

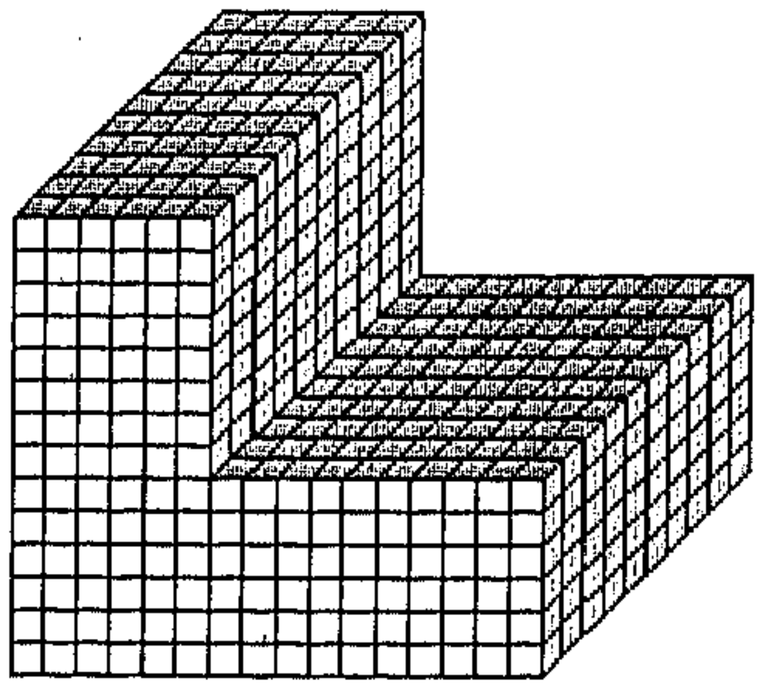

(a)

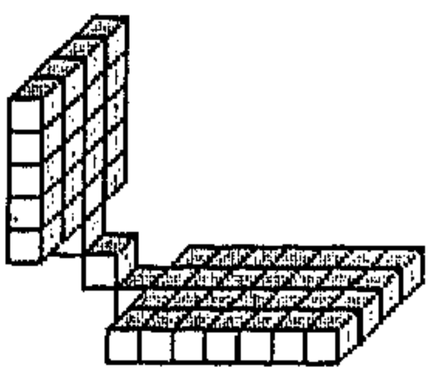

(b)

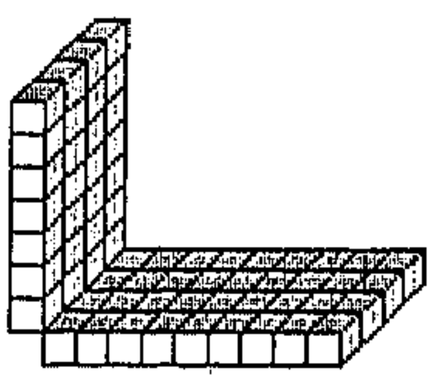

(c)

Figure 4.5: Problem of considering 6-contour points for erosion during each iteration. (a) Original object. (b) Skeleton using 6-contour points. (c) Skeleton using *s*-open, *e*-open and *v*-open points separately for erosion.

before each current iteration. Even if the outer-layer is labeled before each current iteration, it may improperly behave around different corners. For example, if the set of 6-contour points[1] is used as outer-layer then an undesired situation may arise as shown in Figure 4.5. On the other hand, if the set of 26-contour points[2] is used as outer-layer then it produces a proper skeleton for the object of Figure 4.5.(a) but fails to do so for the object of Figure 4.6.(a) (see Figure 4.6.(b)). The approach of using *s*-open points, *e*-open points and *v*-open points for erosion in three successive

[1]a black point having a white 6-neighbor before the current iteration is a 6-contour point

[2]a black point having a white 26-neighbor before the current iteration is a 26-contour point

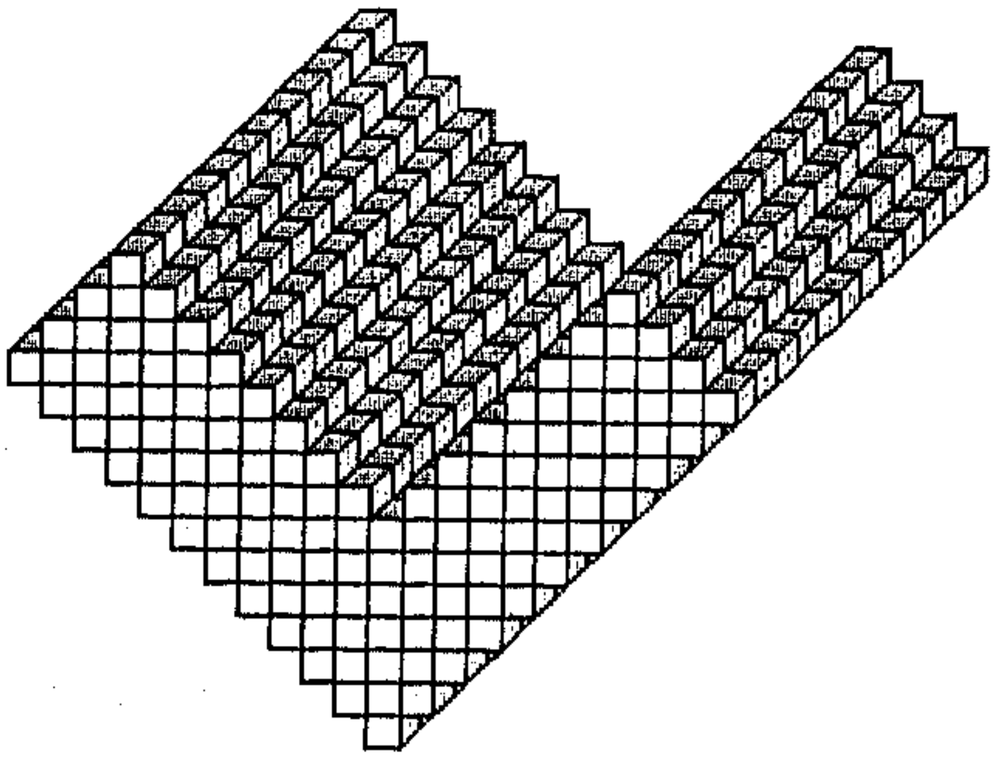

(a)

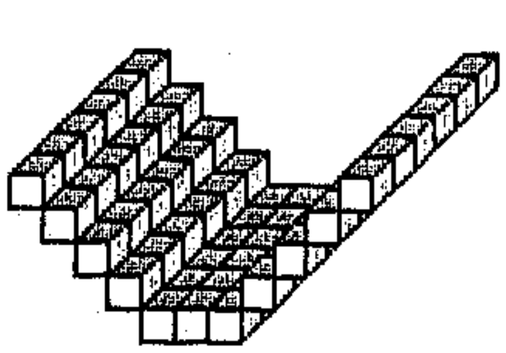

(b)

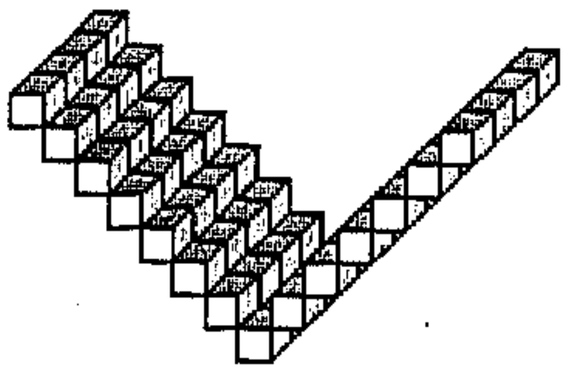

(c)

Figure 4.6: Problem of considering 26-contour points for erosion during each iteration. (a) Original object. (b) Skeleton using 26-contour points. (c) Skeleton using p-open, e-open and v-open points separately for erosion.

scans of each iteration as described in Section 4.2.1, produces proper skeletons for both the objects as shown in Figures 4.5.(c) and 4.6.(c) respectively. Proper skeleton means that the sharpness of meeting corners of two or more surfaces is preserved. Our approach is applied on different other types of junctions with varied angles and rotations and the skeletons obtained are quite satisfactory. A quantitative study on the behavior of the algorithm under rotation is demonstrated in Section 4.4.2.

4.2.4 Contour Noise Handling

Since noise is a part of real life, a good thinning algorithm should be robust enough to preserve the shape of skeleton under noise. Unfortunately it is not easy to specify the noise points from an image. We consider a model of noise which consists of adding simple points of the background to the object or deleting simple points from the object. The probability to change the type of a point is the measure of the noise. Thus single point protrusions or dents on the contour are created as noise in the proposed model and we ensure that they do not produce undesired skeletal parts or branches. The definition of shape point serves the purpose. Branches are allowed to grow only from the shape points. Conditions 4.1 and 4.2 for shape point arrest the creation of undesired branches from a single point protrusion or dent. Our technique of contour noise handling is supported by experimental results shown in Figures 4.7–4.11. Also, a quantitative study on the behavior of the algorithm under pseudo random contour noise is demonstrated in Section 4.4.1.

4.2.5 Arc Thinning

Depending on the applications we may need arc representation of an object. We present a schematic description of the procedure that produces a medial arc representation of an object from its surface representation. To avoid ambiguity we call this procedure as arc-thinning. Arc-thinning is also an iterative procedure with

two steps, namely primary-arc-thinning and final-arc-thinning. The results of these steps are called primary-arc-skeleton and final-arc-skeleton respectively. Here too we memorize two image versions in the same way described earlier. At first, we put forward some definitions in this context. In the following definitions $(a, d), (b, e)$ and (c, f) denote three distinct unordered pairs of opposite s-points of $\mathcal{N}(p)$.

Definition 4.7 *During an iteration a black point p is an s-open-surface point if the points a, $e(a, b, p)$, b, $e(b, d, p)$, d are all white before the iteration.*

Definition 4.8 *During an iteration a point p is an e-open-surface point if it is not an s-open-surface point and at least one point from each of the sets $\{a\}$, $\{e(a, b, p),\ e(a, c, p)\}$, $\{v(a, b, c, p)\}$, $\{e(b, c, p)\}$, $\{v(b, c, d, p)\}$, $\{e(b, d, p),\ e(c, d, p)\}$, $\{d\}$ is white while each of the sets $\{f_2(a, b, p),\ f_3(a, b, p),\ f_2(b, a, p),\ f_1(b, p),\ f_2(b, d, p),\ f_3(b, d, p),\ f_2(d, b, p)\}$ and $\{f_2(a, c, p),\ f_3(a, c, p),\ f_2(c, a, p),\ f_1(c, p),\ f_2(c, d, p),\ f_3(c, d, p),\ f_2(d, c, p)\}$ contains at least one black point before the iteration.*

During arc-thinning, the set of s- and e-open-surface points define the outer-layer and they are labeled once before each iteration. It may be noted from the above definitions that for an s-open-surface point there is a 6-path of white points between two opposite s-points through another s-point. For e-open-surface points there is a 6-path of white points between two opposite s-points through an e-point. In case of e-open-surface points the second condition is imposed to preserve the sharpness of corners during thinning (similar to the reasons explained for Definitions 4.2 & 4.3).

Definition 4.9 *A black point is an arc-shape point if it satisfies Condition 4.1.*

Thus an arc-shape point is an arc-like shape which is at least three-point elongated. Similar to shape points arc-shape points are also labeled once before each iteration.

Definition 4.10 *A black point p is an arc-erodable point if — i) every middle plane of $\mathcal{N}(p)$ contains at least one currently black point, and ii) p is a simple point.*

Each iteration of primary-arc-thinning is completed in two scans. During the first scan an unmarked s-open-surface point p is marked if it is an arc-shape point. Otherwise, if p is a simple point then it is deleted else it is left unmarked. During the second scan an unmarked e-open-surface point is deleted if it is a simple point. Otherwise, the point is left unmarked. Final arc-thinning is a single scan procedure. During this scan a black point p is deleted if p is an arc-erodable point.

4.3 The Parallel Thinning Approach

In this section we describe a parallel thinning algorithm based on the approach discussed in Section 4.2. Some shape and topology constraints are checked to mark or to delete a point. The most important problem faced by a parallel thinning algorithm is that two points p, q individually satisfy the necessary topology constraints of deletion but if both of them are deleted together then the topology constraints may be violated [130]. This condition may occur only when p, q are 26-adjacent. This is because the topology constraints for a point p are defined in its 26-neighborhood $\mathcal{N}(p)$ only. So, if two points p, q are not 26-adjacent then $\mathcal{N}(p) \cap q = \phi$, $\mathcal{N}(q) \cap p = \phi$, and obviously $p \cap q = \phi$. To solve this problem we use the concept of sub-fields [28,32]. An image is partitioned into eight disjoint subsets such that no two members p, q in the same subset are 26-adjacent. Hence the members of each subset may be used for parallel erosion. Eight subsets $O_0, O_1, \cdots O_7$ are defined as follows:

$$O_l = \{(2 \times i + f, 2 \times j + g, 2 \times k + h) \mid i, j, k = 0, \pm 1, \pm 2, \cdots; \\ f, g, h \in \{0, 1\} \text{ and } 2^2 \times f + 2^1 \times g + 2^0 \times h = l\} \tag{4.1}$$

such that two points $p, q \in O_l$ are never 26-adjacent. Each scan of the thinning algorithm may be completed in eight cycles and at lth cycle the image subset O_l

is subjected to parallel erosion. The parallel algorithm requires $m^3/8$ processors for an image of size $m \times m \times m$ and it needs 8 cycles to complete each scan. The image size means the size of the smallest rectangular parallelepiped that encloses the set of black points. It is also possible to implement the algorithm with $m^3/8n$ processors for an integer n and in that case each scan requires $8n$ cycles instead of 8. The concept of sub-fields in two dimensional hexagonal tessellation was earlier proposed by Golay [28] where he used three sub-fields to carry out one scan of topology preserving skeletonization. This concept was further studied by Hafford and Preston [32] in three dimensional tetradecahedral tessellation. They used six sub-fields to carry out one scan of topology preserving skeletonization. However they used only one version of image while thinning. On the other hand we use two versions of image throughout the thinning algorithm.

To test the effectiveness of the proposed algorithm it is applied on synthetically generated 3D objects as shown in Figures 4.7–4.11. In Figures 4.8–4.11 the background is made dark to render a better visual effect. The 3D objects in Figures 4.7–4.11 may be enclosed in minimum rectangular space of size $44 \times 41 \times 44$, $63 \times 136 \times 35$, $79 \times 79 \times 31$, $81 \times 42 \times 62$ and $72 \times 116 \times 72$ respectively. Figure 4.7 contains typical additive and subtractive noises. Figures 4.8–4.11 have both noiseless and noisy versions. The noise in Figures 4.8–4.11 is generated in a pseudo random manner while the noise in Figure 4.7 is imparted manually to incorporate all typical possibilities. Arc-thinning is considered on Figures 4.7–4.8 only (meaningful result cannot be obtained by arc-thinning for Figures 4.9–4.11). In Figure 4.7 the thinned surface and arc representations show the desirable shape despite noise. The surface and arc representations of both noiseless and noisy versions of Figure 4.8 as well as the surface representations of Figures 4.9–4.11 are visually satisfactory.

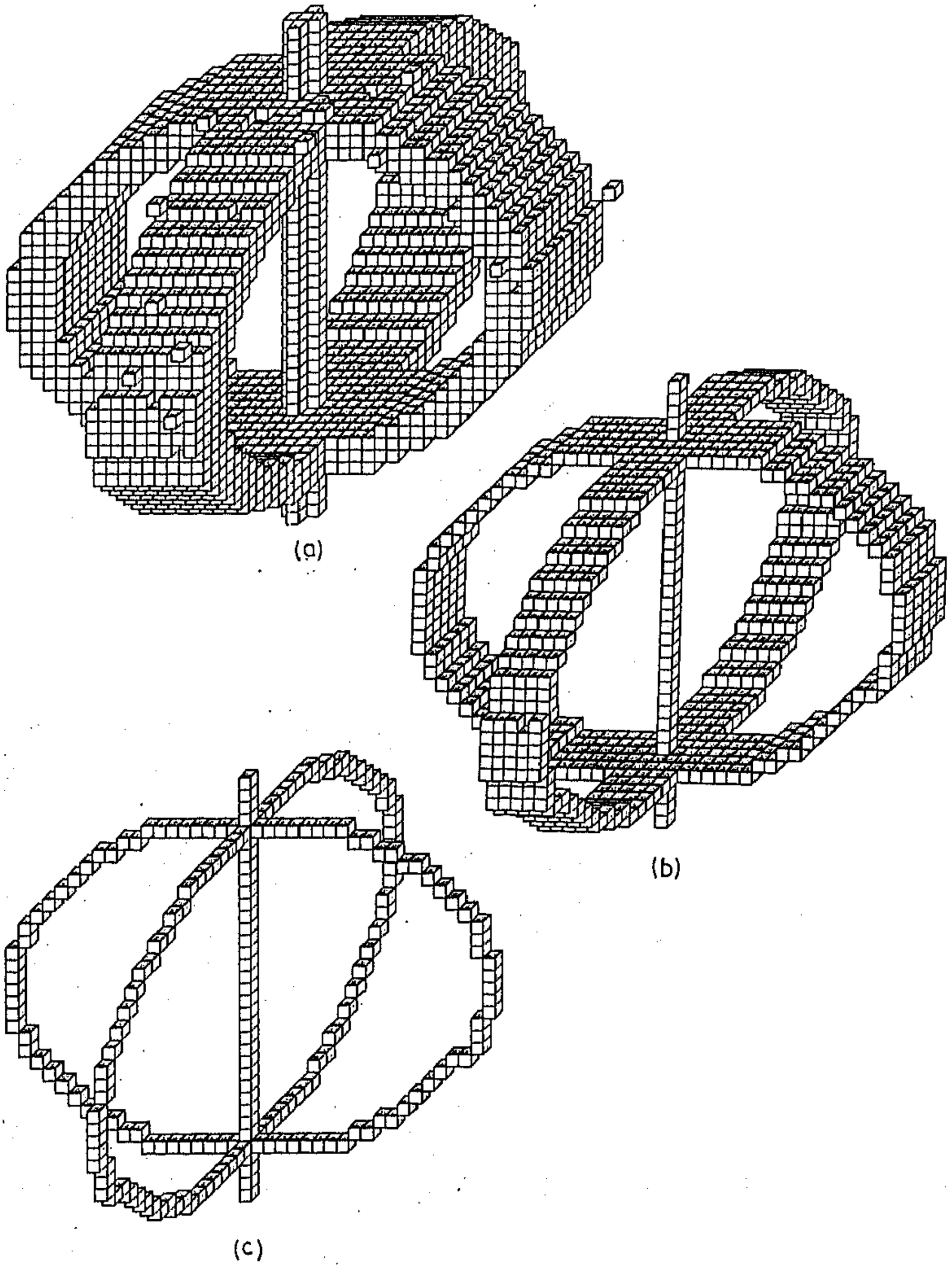

Figure 4.7: Results of thinning. (a) Original object. (b) Skeleton. (c) Arc-skeleton.

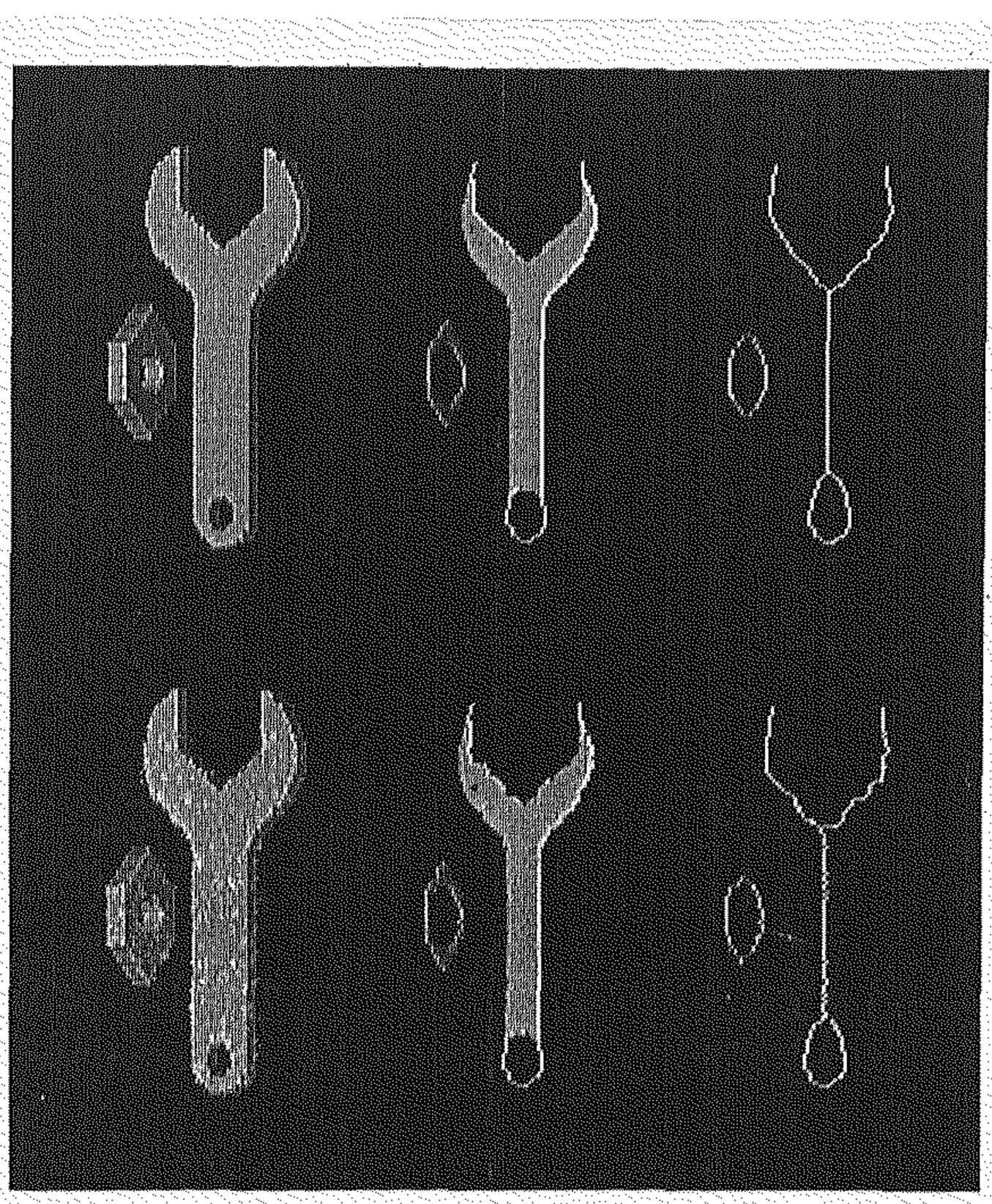

Figure 4.8: Results of thinning. Top row (from left to right): original object, skeleton and arc-skeleton. Bottom row (from left to right): original object with noise, skeleton and arc-skeleton.

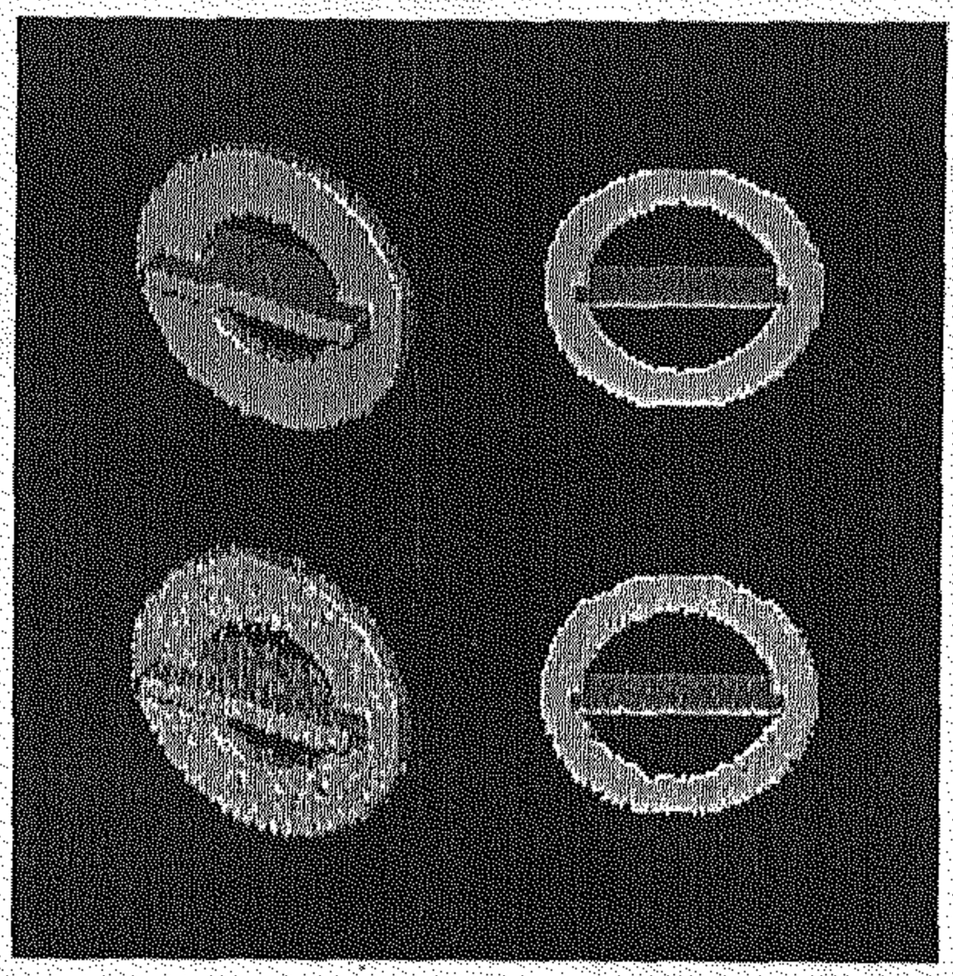

Figure 4.9: Results of thinning. Top row (from left to right): original object and skeleton. Bottom row (from left to right): original object with noise and skeleton (here, objects and skeletons are shown from different angle to produce a better view).

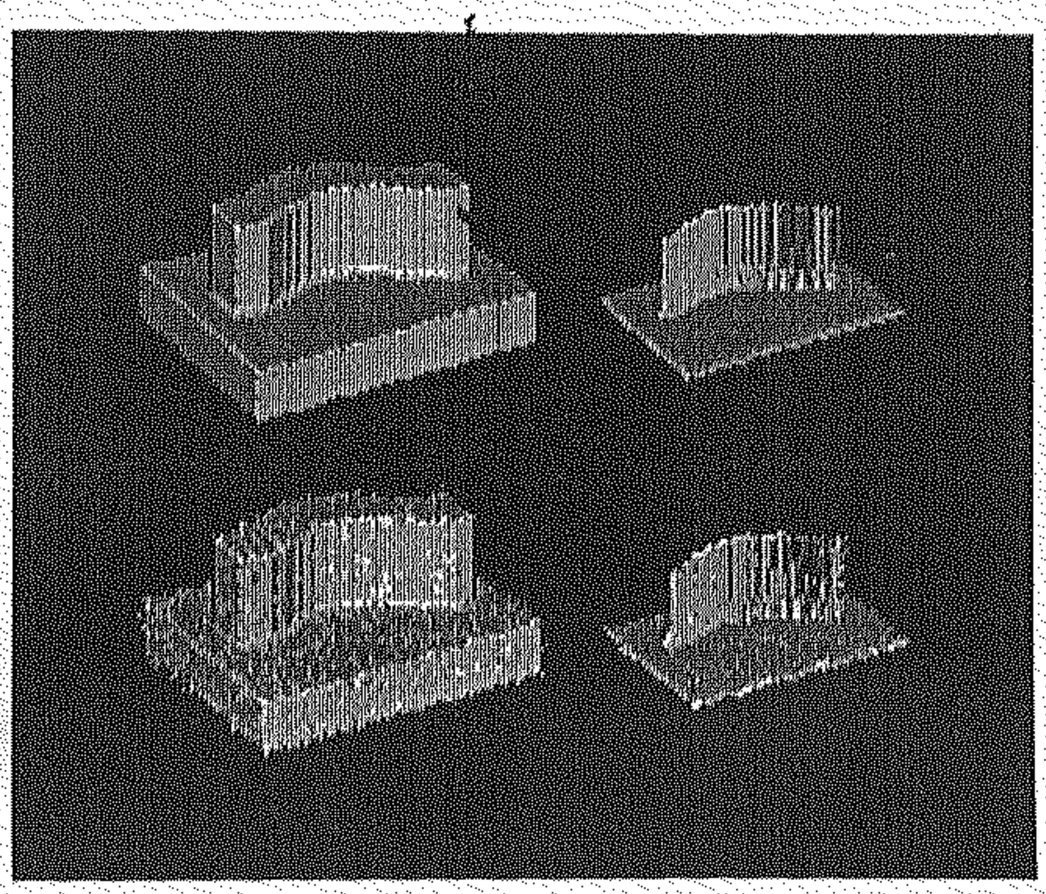

Figure 4.10: Results of thinning. Top row (from left to right): original object and skeleton. Bottom row (from left to right): original object with noise and skeleton.

4.3.1 Utility of Two Image Versions

Consider the ith cycle of certain iteration in which the image subset O_i is used for erosion. During the erosion of ith cycle some of the points of O_i will be deleted. Since the points of O_i are not 26-adjacent, undesired local spikes may be created in the current image. If the shape constraints are defined on the current image while eroding the points of O_{i+1} in the next cycle then undesired branches may occur from the local spikes created in the current image version. This fact suggests that a prior version of the image should be memorized to define the shape constraints. It may be interesting to note that different open points and shape points are labeled once before each current iteration in the proposed thinning approach. As a result of this the local spikes in the current image do not affect the skeleton.

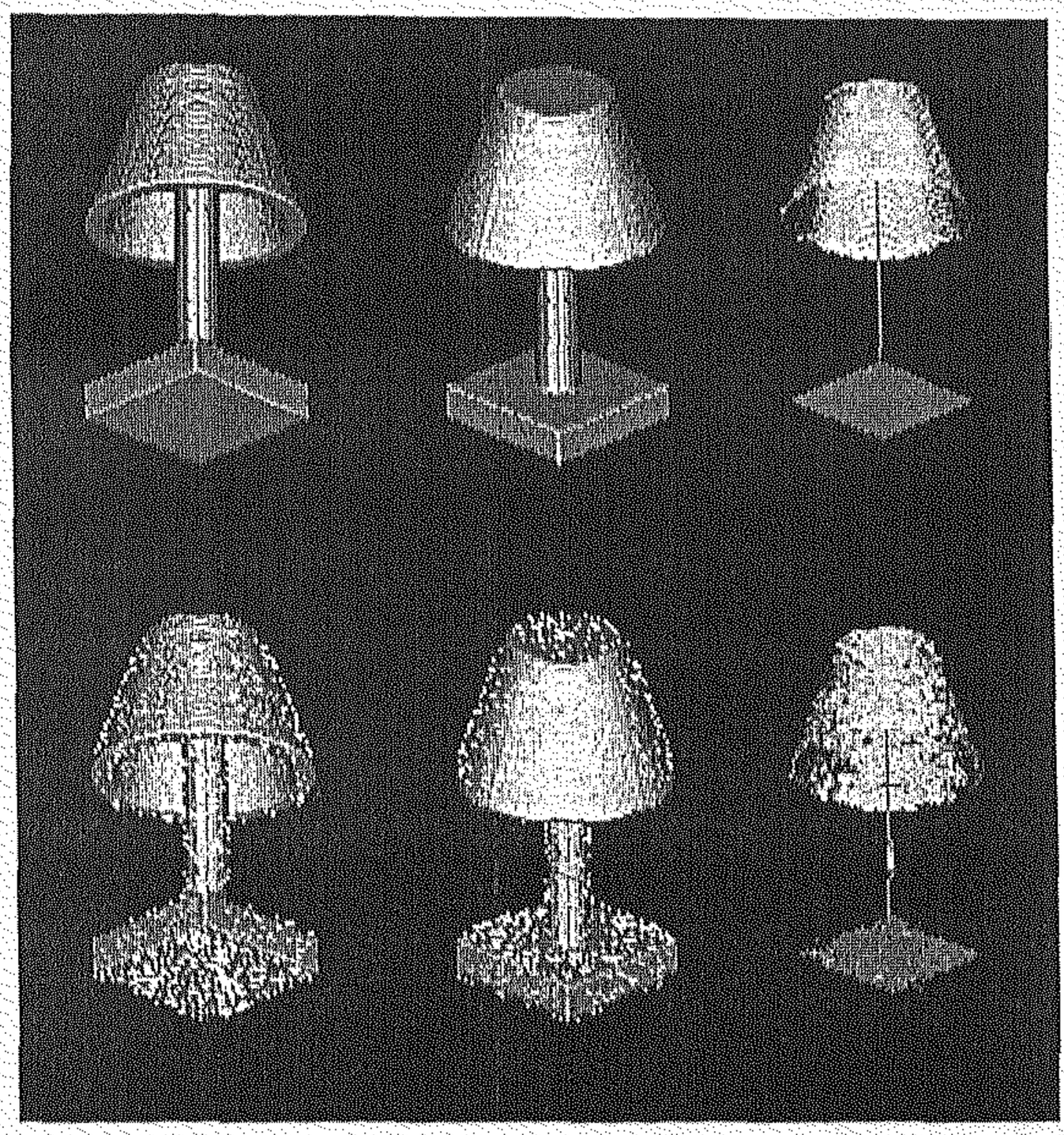

Figure 4.11: Results of thinning. Top row (from left to right): original object, original object with different angle of view, skeleton. Bottom row (from left to right): original object with noise, noisy object with different angle of view and skeleton.

4.4 Shape Analysis Under Noise and Rotation

To study the behavior of the proposed algorithm under noise and rotation we define a shape distance function for 3D digital objects that will be useful in this context. A shape distance metric for 3D objects in E^3 was proposed by Banerjee et. al. [12] and Dutta Majumder [72]. They considered a subset A in E^3 as an object if — 1) A is compact, 2) Interior(A) is non-empty and connected, and 3) Closure(Interior(A)) $= A$. The shape distance is defined as follows: let C be the class of all objects in E^3 which have the center of gravity at the origin (0,0,0) and have unit volume. Any rotation of an object in E^3 about the origin (0,0,0) is determined by the corresponding rotation of the system of axes. This rotation is specified by three angles θ, ω and ψ in $[0^o, 360^o]$ where θ is the angle between the new and the old x-axis, ω is the angle between the new and the old y-axis and ψ is the angle between the new and the old z-axis. Let $A_{\theta\omega\psi}$ denote the rotated form of an object A in C, where θ, ω and ψ determine the new system of axes. It is clear that $A_{\theta\omega\psi}$ is in C. Rotation defines an equivalence relation on C. This equivalence relation is denoted by $\mathcal{R}$. The shape of an object is defined as an equivalence class generated by $\mathcal{R}$ in C. Let τ be the family of all such equivalence classes i.e. of all shapes. D_1 is a distance function on C such that for $A, B \in C$

$$D_1(A, B) = Leb_3\left((A - B) \cup (B - A)\right),$$

where Leb_3 is the Lebesgue measure in E^3. As shown in [12] D_1 defines a metric on C. D_2 is a distance function on C such that for $A, B \in C$

$$D_2(A, B) = \min_{\theta,\omega,\psi} D_1(A, B_{\theta,\omega,\psi})$$

D_2 is a metric on τ.

We propose a modified shape distance function between two objects in a 3D digital space that may be useful for estimation of shape distortion in thinning under noise and rotation. According to our requirement we restrict ourselves to the assump-

tion that the distance function is applied on the objects with normalized size and rotation.

Definition 4.11 *DT_1 is a distance function between two points $p_1 = (x_1, y_1, z_1)$ and $p_2 = (x_2, y_2, z_2)$ as follows:*

$$DT_1(p_1, p_2) = \sqrt{(x_1 - x_2)^2 + (y_1 - y_2)^2 + (z_1 - z_2)^2}$$

DT_1 is the Euclidean distance function between two points of E^3.

Definition 4.12 *DT_2 is a distance function between a point p and a finite set of points S as follows:*

$$DT_2(p, S) = \min_{q \in S} DT_1(p, q)$$

Definition 4.13 *The center of gravity $(\overline{x}, \overline{y}, \overline{z})$ of a finite set of points $S = \{(x_i, y_i, x_i) \mid i = 0, \cdots, n\}$ is defined as follows:*

$$\overline{x} = \frac{\sum_{i=0}^{n} x_i}{\mid S \mid}; \qquad \overline{y} = \frac{\sum_{i=0}^{n} y_i}{\mid S \mid}; \qquad \overline{z} = \frac{\sum_{i=0}^{n} z_i}{\mid S \mid}$$

where $\mid S \mid$ denotes the number of points in S.

Definition 4.14 *A position normalized set $norm(S)$ is derived from a finite set of points S as follows:*

$$norm(S) = \{(x_i - \overline{x}, y_i - \overline{y}, z_i - \overline{z}) \mid (x_i, y_i, z_i) \in S\}$$

where $(\overline{x}, \overline{y}, \overline{z})$ is the center of gravity of S.

Definition 4.15 *DT_3 is a distance function between two finite sets of points S_1 and S_2 as follows:*

$$DT_3(S_1, S_2) = \frac{\sum_{p \in norm(S_1)} DT_2(p, norm(S_2))}{\mid S_1 \mid} + \frac{\sum_{p \in norm(S_2)} DT_2(p, norm(S_1))}{\mid S_2 \mid}$$

We are noting that DT_3 is not a metric because it does not satisfy the triangle inequality. The issue of investigating alternative distance function of DT_3 that are metrics, is listed in Chapter 6 as an important future work.

4.4.1 Shape Distortion Under Noise

To find shape distortion by a thinning algorithm under pseudo random contour noise we add random noise on a 3D digital object according to the model presented in Section 4.2.4 and then estimate the shape distortion in the skeleton. Let $Sk(X)$ denote the skeleton of a 3D object X. Let $\ddot{X}$ denote the noisy version of X. To find the distortion of shape in the skeleton under noise we compute $DT_3(Sk(X), Sk(\ddot{X}))$. A comparative study between the percentage of noise in $\ddot{X}$ and $DT_3(Sk(X), Sk(\ddot{X}))$ gives a quantitative sense about the robustness of a thinning algorithm under noise. A comparative study on the objects of Figures 4.8–4.11, under different amount of noise, is shown in Figure 4.12.

4.4.2 Shape Distortion Under Rotation

We study the shape distortion by the thinning algorithm under rotation. Let $[X]_{\theta\omega\psi}$ denote the 3D digital object obtained from a 3D digital object X by a rotation where θ, ω, ψ determines the new system of axes with the center of gravity of X as the origin. Let $Sk(X)_{\theta\omega\psi}$ denote the rotated form of $Sk(X)$ where θ, ω, ψ determines the new system of axes with the center of gravity of $Sk(X)$ as the origin. It is worthy to mention that $[X]_{\theta\omega\psi}$ is a rotation in digital space while $Sk(X)_{\theta\omega\psi}$ is a rotation in the Euclidean 3-space. Even if the digital rotation introduces error, we need to map the rotation of input image in digital space as it is subjected to thinning subsequently. However, for skeleton the Euclidean rotation suffices as shape distance is measured between two finite sets of points in Euclidean space. To estimate the shape distortion under rotation we compute $DT_3(Sk(X)_{\theta\omega\psi}, Sk([X]_{\theta\omega\psi}))$. An experimental study of

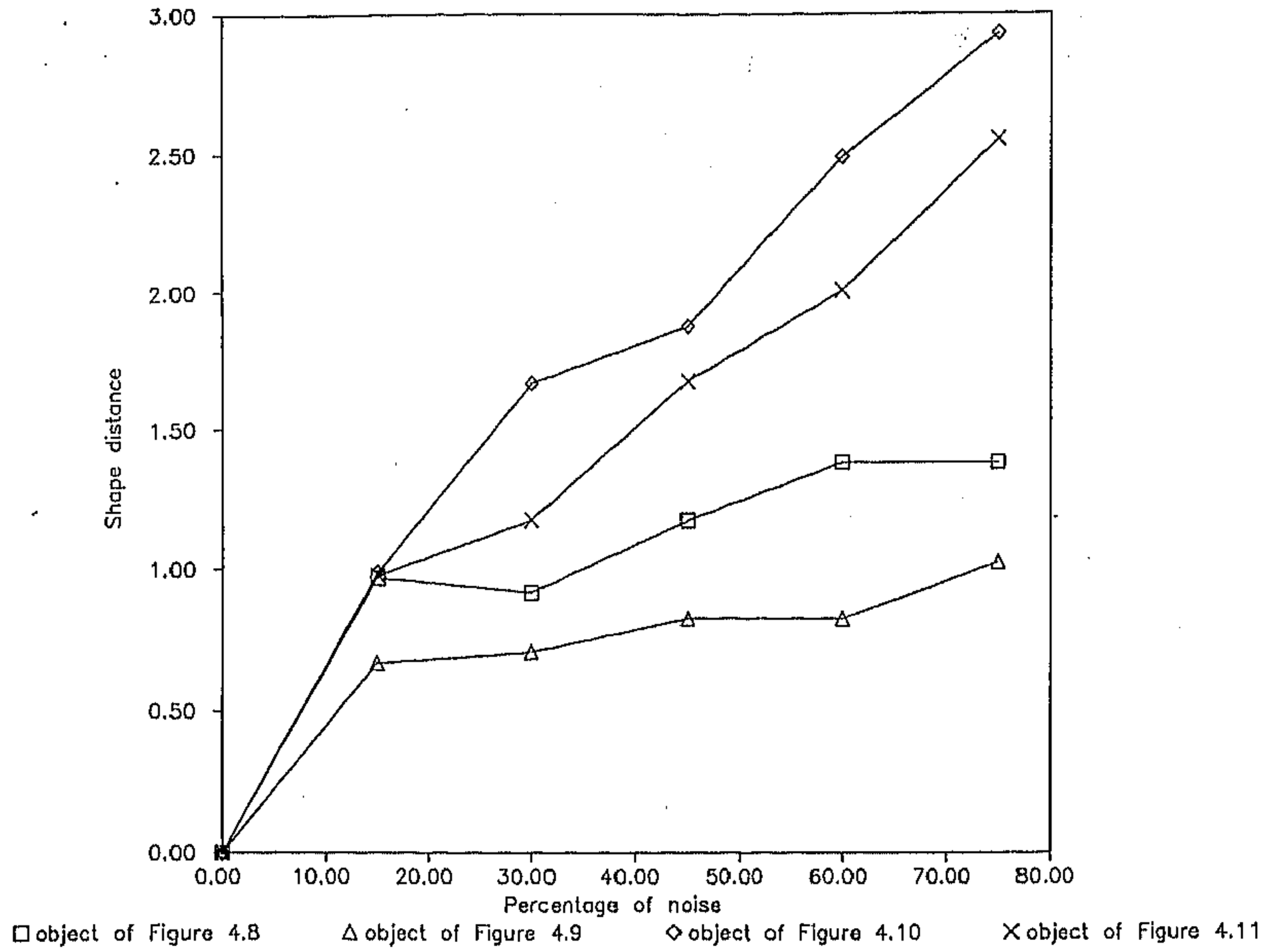

Figure 4.12: Shape distortion analysis under pseudo random contour noise for the objects of Figures 4.8–4.11.

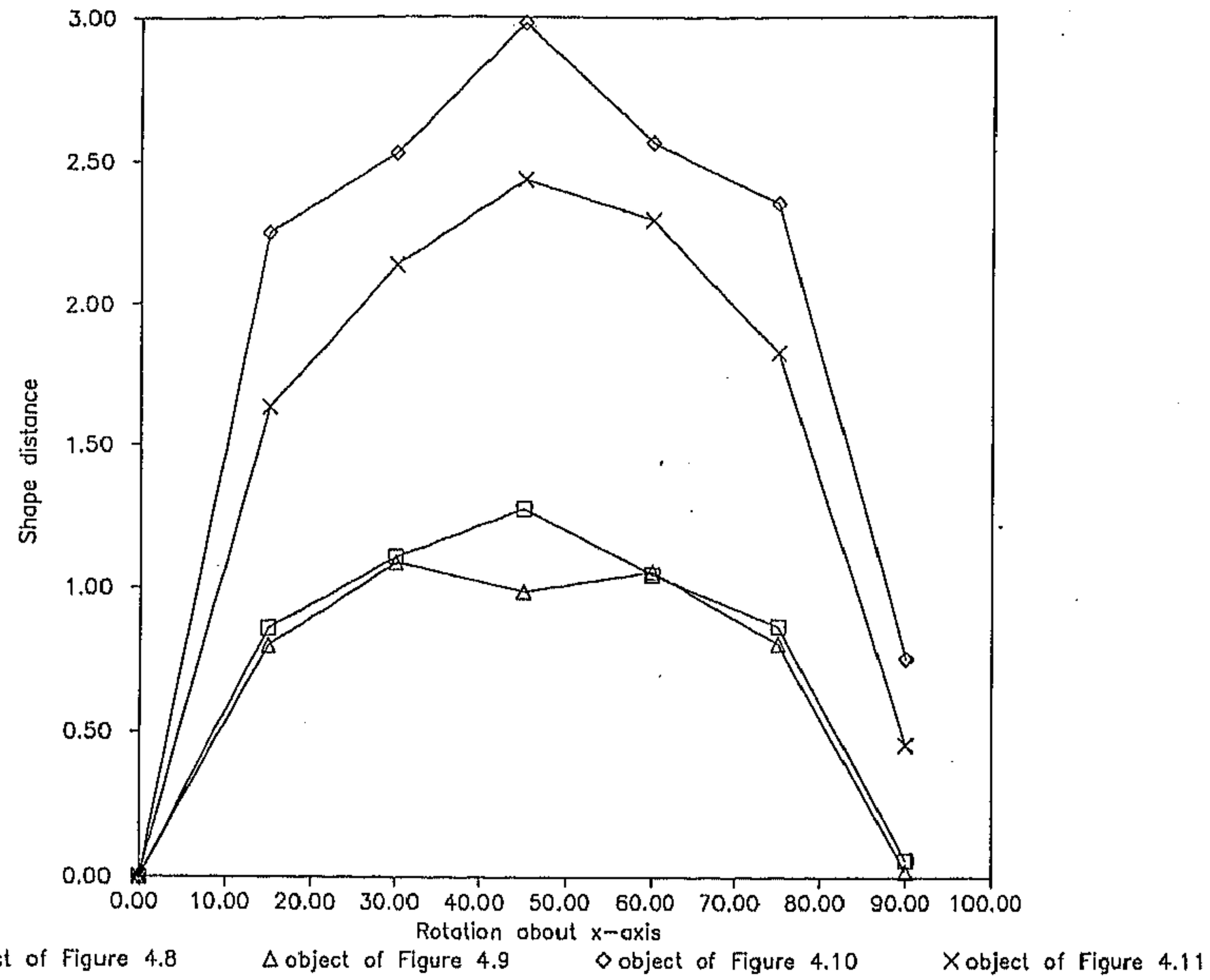

Figure 4.13: Shape distortion analysis under rotation about the x-axis for the objects of Figures 4.8–4.11.

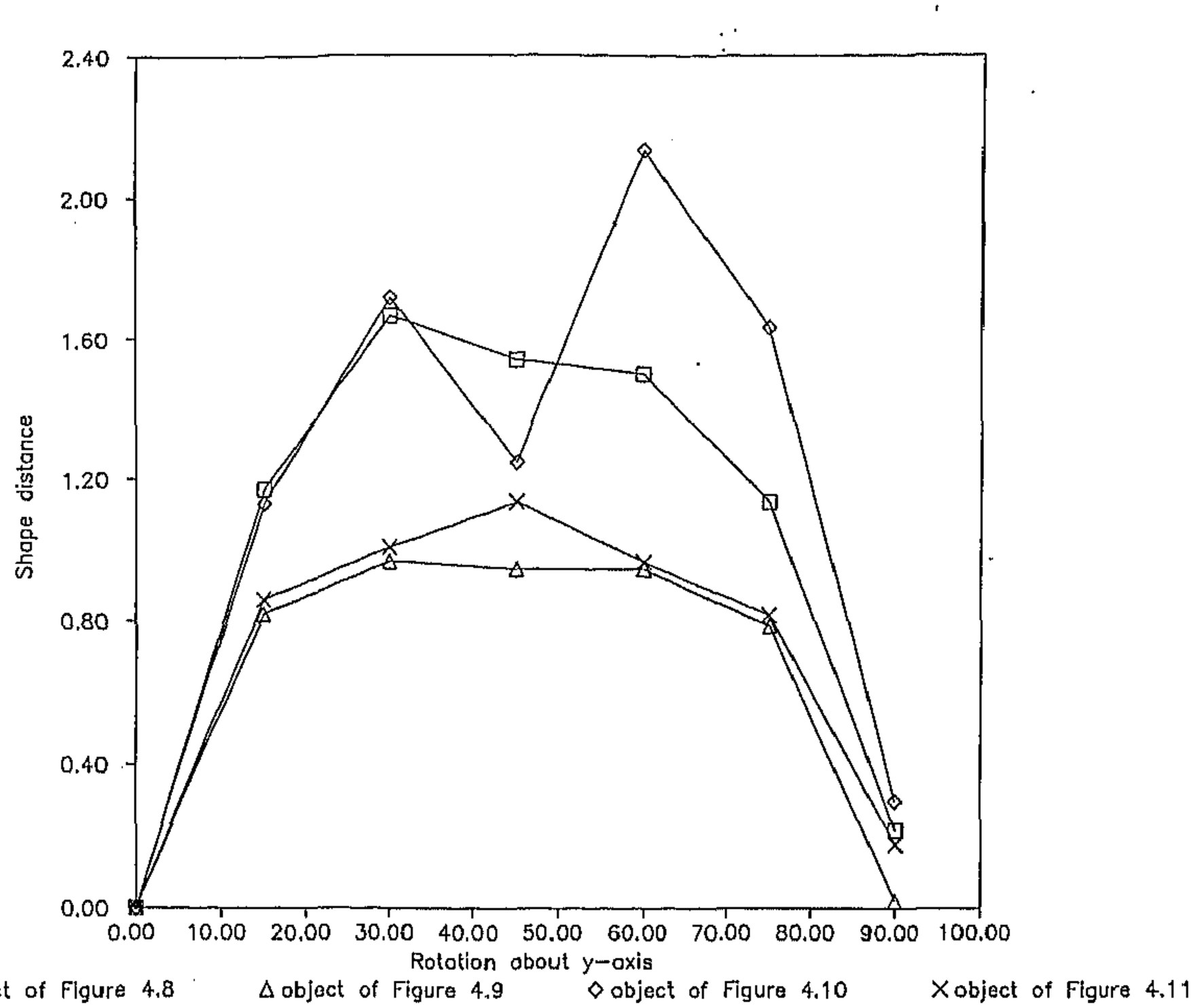

Figure 4.14: Shape distortion analysis under rotation about the y-axis for the objects of Figures 4.8–4.11.

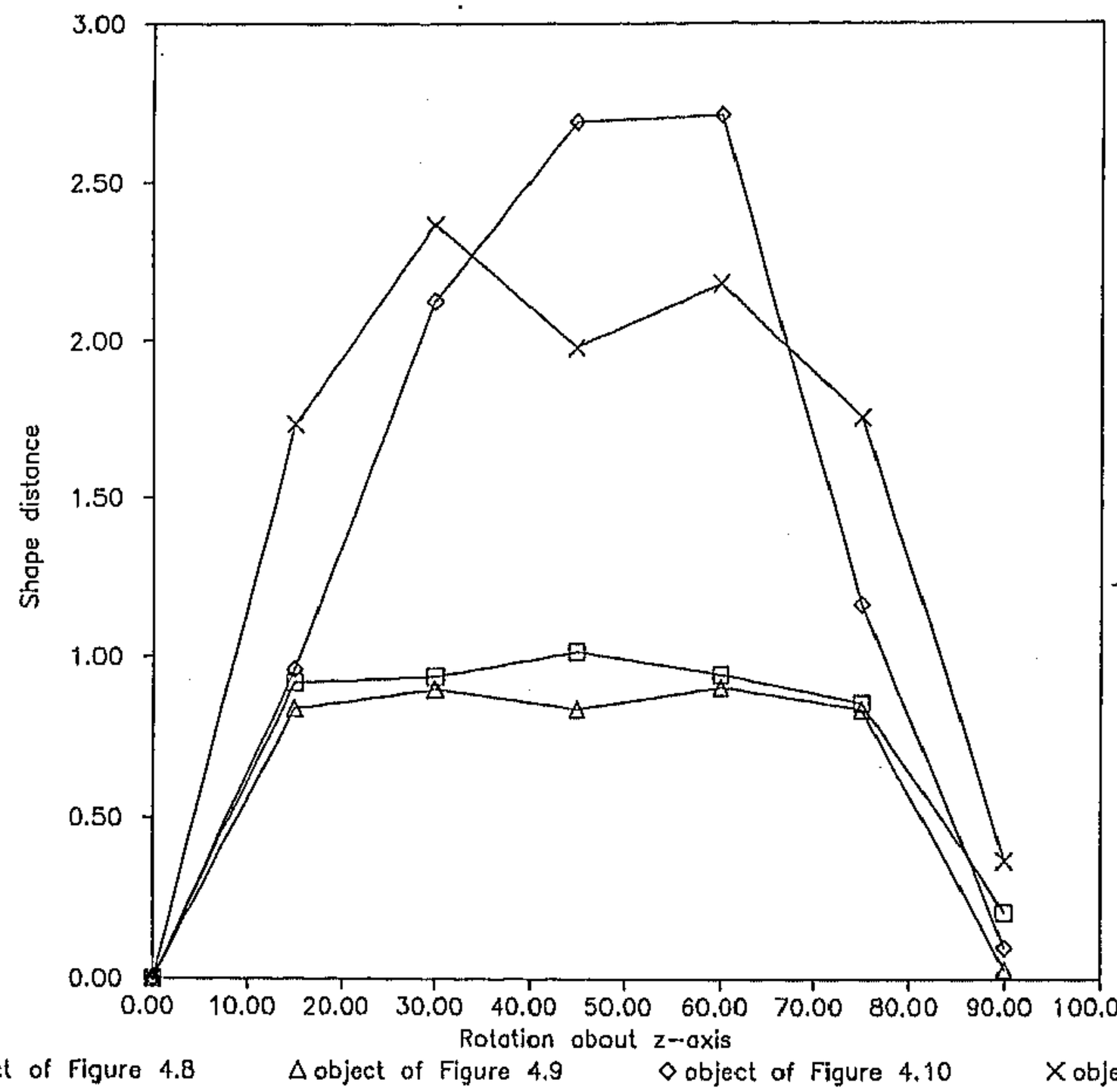

Figure 4.15: Shape distortion analysis under rotation about the z-axis for the objects of Figures 4.8–4.11.

shape distortion on the objects of Figures 4.8–4.11, under different rotation about the x-, y- and z-axes, are shown in Figures 4.13, 4.14 and 4.15 respectively.

4.5 Comparative Study

In the literature of 3D thinning there are publications [32,28,69,79,122,130,131,70,71] where the topology preservation is ensured during thinning. On the other hand, shape preservation has received less attention, especially in noisy images. Tsao and Fu [130] in particular considered the issues of parallel thinning in 3D cubic grid. Hafford and Preston [32] considered parallel thinning in tetradecahedral tessellation using the concept of sub-fields. Lobregt et. al. [69] and Ma [70,71] considered the issues related to topology preservation in parallel thinning. However, they have not discussed the issues of shape preservation. Mukherjee et. al. [79] and Shrihari [122] considered the issues of sequential thinning. Therefore, it is logical to compare our method with Tsao and Fu [130]. They considered path connectivity and surface connectivity for topology preservation. While they introduced the concept of end points to avoid excessive erosion, their methodology lacks the treatment of noisy images with no special mention of shape preservation about corners.

In contrast we have introduced the concept of open points that produces desired skeletons around corners as discussed in Section 4.2.3. The idea of shape points, detailed in Section 4.2, have helped us to tackle the noises in particular. Subjectively, the methodology of utilizing two image versions have generated significantly improved result over Tsao and Fu [130]. The Figure[3] 4.16 (the original image and its thinned versions following Tsao and Fu's algorithm [130]) and Figure 4.17 (thinned versions following our algorithm) are the experimental evidence in support of our claim.

[3]Reprinted from Tsao and Fu [130]

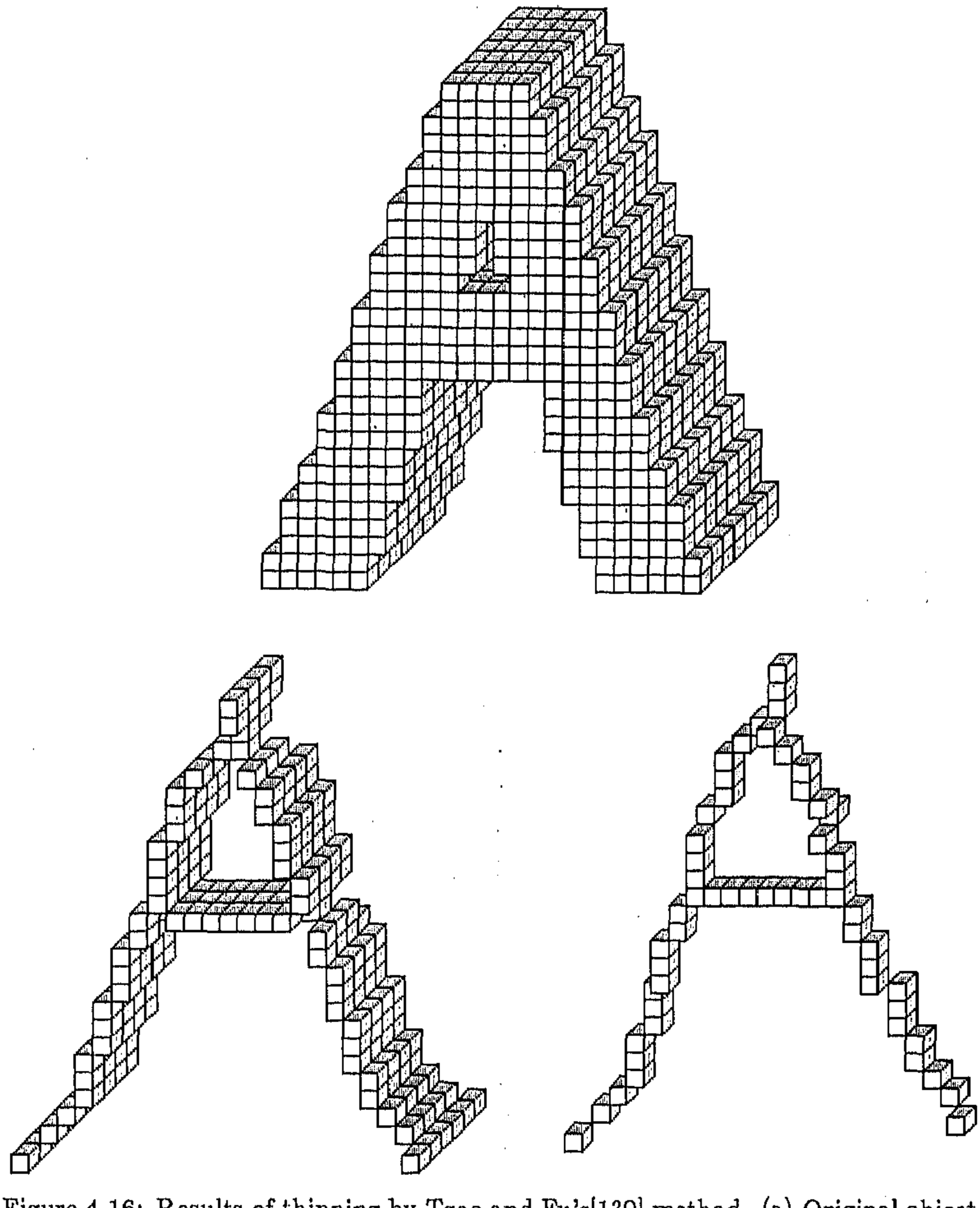

Figure 4.16: Results of thinning by Tsao and Fu's[130] method. (a) Original object. (b) skeleton obtained by Tsao and Fu's method. (c) Arc-skeleton obtained by Tsao and Fu's method.

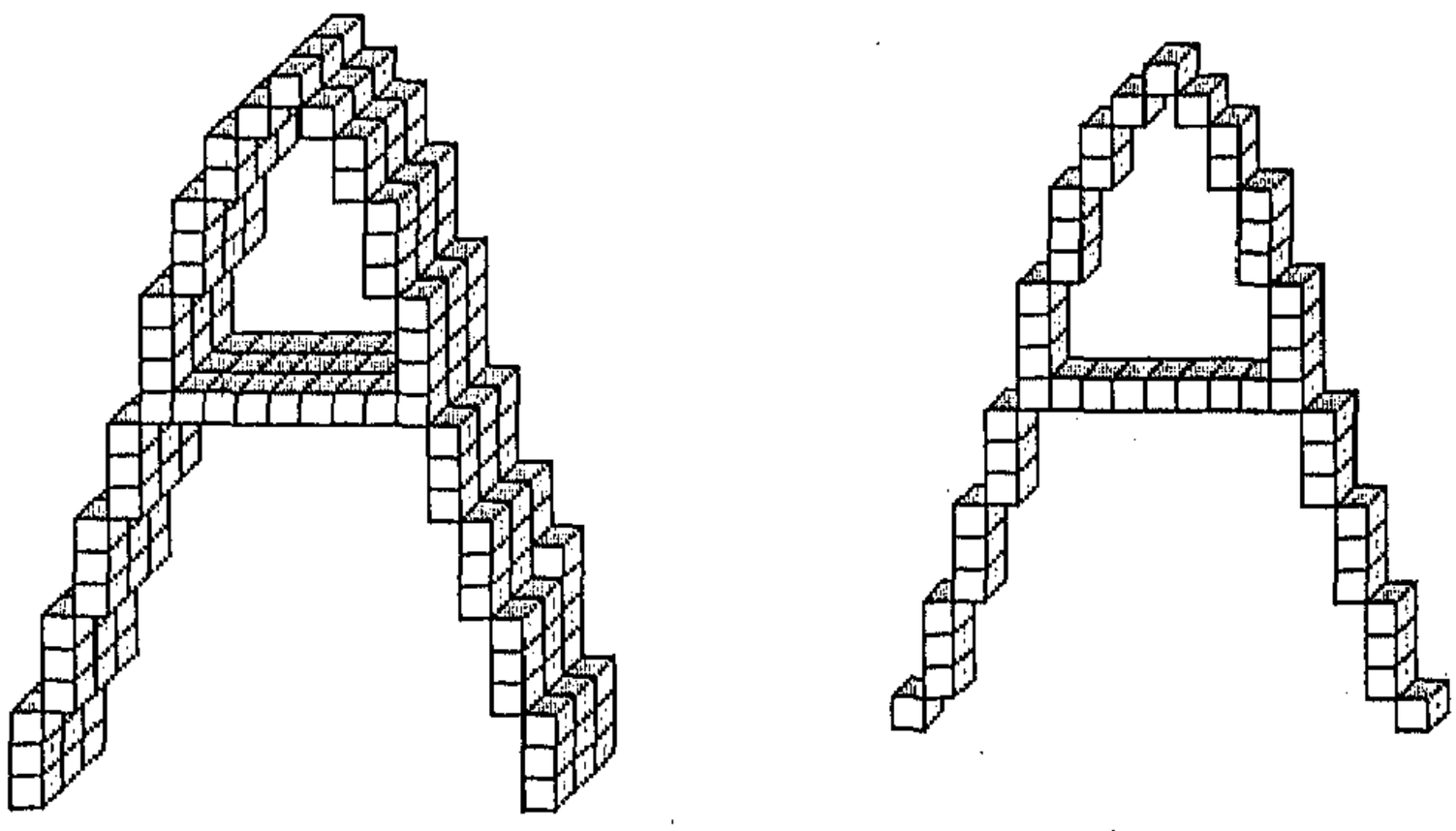

Figure 4.17: Results of thinning by our method on Tsao and Fu's[130] object. (a) Skeleton obtained by our method. Compare this with Figure 16.(b). (b) Arc-skeleton obtained by our method. Compare this with Figure 16.(c)

4.6 Discussion and Conclusion

A new parallel thinning algorithm of 3D digital images with topology and shape preserving properties has been developed in this chapter. To preserve topology we have applied the concept of simple points [111,113,114]. On the other hand the concept of sub-fields [28] has been used for parallel implementation. The concepts of open points and shape points have been introduced and applied to 3D thinning. The role of open points in producing proper skeleton around different types of corners has been justified. Also, the shape points are found to be robust under noise.

We have used two versions of the image — one before the current iteration while the other being the currently processed image. The necessity of two image versions in parallel thinning has been justified. This concept has made a major improvement in the quality of thinned image. The results of application of the parallel thinning algorithm on several synthetically generated 3D objects and their noisy versions have been presented. We have also described an algorithm that produces a medial arc representation of an object from its surface representation.

In practice the shape of a skeleton gets distorted under noise and rotation. The distortion, among others, characterizes the goodness of an algorithm. To estimate the degree of distortion we have used the concept of shape distance. The robustness of our algorithm under pseudo random contour noise and rotation has been studied and presented with examples. Because of digital nature of the image space, a shape may be distorted under rotation. This distortion is also reflected in the skeleton. A part of the skeletal distortion shown in Figures 4.13–4.15 is because of this reason. It is understood from Figures 4.13–4.15 that shape distortion is maximum for a rotation around 45° and it is quite expected. Also for this thinning algorithm the shape distortion increases more or less linearly with the percentage of noise. This work can be applied for finding meaningful parts of 3D objects.

Chapter 5

Topology and 3D Object Segmentation

5.1 Introduction

Recent developments of three dimensional images as an effective interactive media (e.g. 3D imaging in medical science) have motivated scientists in exploring three dimensional image processing to a greater detail. An automatic interpretation of 3D digital images is a challenging and definitely an important step for many applications. Since 3D digital images involve a large volume of data, feasible steps toward an automatic interpretation demand a compact and well structured representation of 3D images. In the previous chapter, a parallel 3D thinning approach has been described that produces a compact representation of an object while maintaining the topology as well as the shape. While thinning produces a compact representation, segmentation helps in producing a structured representation of an object.

In this chapter we describe a segmentation process [115] based on topological properties. The major steps of this segmentation process are as follows:

1. Derivation of surface skeletal representation of an object.
2. Computation of local topological parameters of surface skeletal points.
3. Classification of surface skeletal points into different types of points (e.g. curve inner point, curve edge point, surface inner point and surface edge point) and detection of different types of junction points (e.g. junction points between curves, between curves and surface and also between surfaces).
4. Segmentation of surface skeletal representation into meaningful parts.

The proposed approach segments a surface skeletal representation into surfaces and curves without junction. More specifically, a segmented part belongs to one of the following categories:

1. a simple surface patch (topologically equivalent to a rectangular sheet),
2. a simple cylindrical surface (topologically equivalent to a hollow cylinder),
3. a simple closed surface (topologically equivalent to a hollow sphere),
4. a simple curve (topologically equivalent to a straight line segment), and
5. a simple closed curve (topologically equivalent to a circle).

The segmented parts along with their depth information may be used to represent an object as a compact structure of simple geometric feature restricted by a predetermined feature set.

The steps of thinning an object to a surface skeleton is discussed and a parallel algorithm is developed in Chapter 4 while an efficient algorithm of computing the

local topological parameters is described in Chapter 3. In this chapter, we first describe the method of point classification [115] in Section 5.2. The segmentation approach [115] is discussed in Section 5.3. A comparative study between our approach and that due to Malandain et. al. [73] has been presented in Section 5.4. Finally the results of application of the segmentation process to several synthetically generated 3D objects are presented in Section 5.5.

5.2 Point Classification

In Chapter 3 an efficient procedure *topo_para* is developed that computes the topological parameters $\xi(p)$, $\eta(p)$, and $\delta(p)$ corresponding to a point p. It is worthy to recapitulate that $\xi(p)$, $\eta(p)$, and $\delta(p)$ represent the numbers of black components, tunnels and cavities in $\hat{\mathcal{N}}(p)$ respectively. We describe their applications to the classification [115] of different types of points as surface edge point, curve end point, surface or curve inner point and different types of junction points in a surface skeleton representation. The results of this classification method are applied for a meaningful segmentation of 3D objects.

In a 2D skeleton we can imagine only three types of points namely curve end point, curve inner point and junction point of curves. However, in a surface skeleton of 3D object, different types of junction points may occur (e.g. junction of surfaces, junction of surfaces and curves, and junction of curves).

As an example, let us consider a surface skeleton representation shown in Figure 5.1 where different points of importance are marked as p_i, $i = 1, 2, \cdots, 8$. These points along with their $\xi(p)$, $\eta(p)$, and $\delta(p)$ values are described as follows:

- p_1 is an edge point of surface (SE-type),
  $\xi(p_1) = 1, \eta(p_1) = 0, \delta(p_1) = 0$;

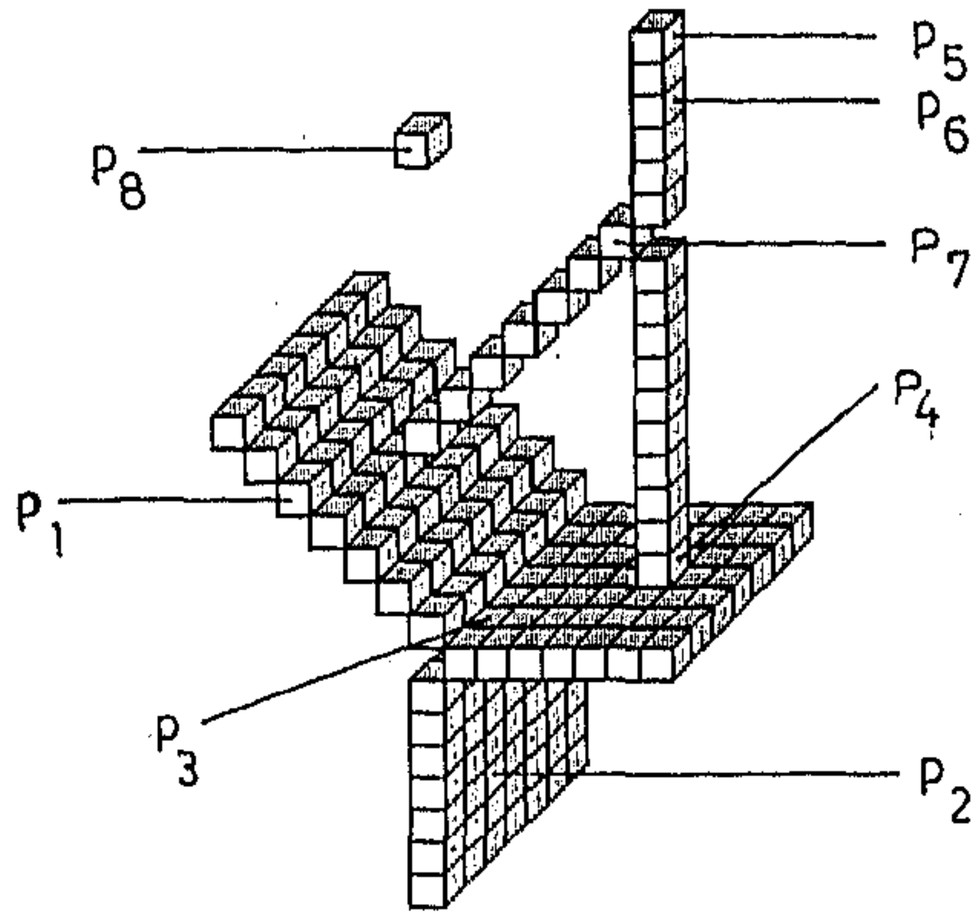

Figure 5.1: Demonstration of different types of points in a surface skeleton representation (see the text for details).

Table 5.1: Initial decision table for skeleton point classification.

$\xi(p)$	$\eta(p)$	$\delta(p)$	Point type	Name assigned
0	0	0	I-type	N_1
1	0	0	SE-type or CE-type	N_2
2	0	0	C-type	N_3
>2	0	0	CC-type	N_4
1	1	0	S-type or CC-type	N_5
>1	≥1	0	SS-type or SC-type or CC-type	N_6
1	>1	0	SS-type or SC-type or CC-type	N_7
1	0	1	SS-type or SC-type or CC-type	N_8

Table 5.2: Final decision table for skeleton point classification. In this table 'ASP' is an abbreviation of '26-adjacent skeleton point'.

Name	Neighborhood analysis	Point type
N_2	exactly one ASP	CE-type
N_2	more than one ASPs	SE-type
N_5	all ASPs are N_3 or N_4	CC-type
N_5	not all ASPs are N_3 or N_4	S-type
N_6	all ASPs are N_3 or N_4	CC-type
N_6	not all but some ASPs are N_3 or N_4	SC-type
N_6	no ASP is N_3 or N_4	SS-type
N_7	all ASPs are N_3 or N_4	CC-type
N_7	not all but some ASPs are N_3 or N_4	SC-type
N_7	no ASP is N_3 or N_4	SS-type
N_8	all ASPs are N_3 or N_4	CC-type
N_8	not all but some ASPs are N_3 or N_4	SC-type
N_8	no ASP is N_3 or N_4	SS-type

- p_2 is an inner point of surface (S-type),
  $\xi(p_2) = 1, \eta(p_2) = 1, \delta(p_2) = 0$;

- p_3 is a junction point of surfaces (SS-type),
  $\xi(p_3) = 1, \eta(p_3) = 2, \delta(p_3) = 0$;

- p_4 is a junction point of surfaces and curves (SC-type),
  $\xi(p_4) = 2, \eta(p_4) = 1, \delta(p_4) = 0$;

- p_5 is an curve end point (CE-type),
  $\xi(p_5) = 1, \eta(p_5) = 0, \delta(p_5) = 0$;

- p_6 is an inner point of curve (C-type),
  $\xi(p_6) = 2, \eta(p_6) = 0, \delta(p_6) = 0$;

- p_7 is a junction point of curves (CC-type),
  $\xi(p_7) = 3, \eta(p_7) = 0, \delta(p_7) = 0$;

- p_8 is an isolated point (I-type),
  $\xi(p_8) = 0, \eta(p_8) = 0, \delta(p_8) = 0$.

From the above example it may appear that $\delta(p)$ does not have any discriminating power. However, as shown in Table 5.1, there is a situation (last row of the table) where $\delta(p)$ takes a value '1' and hence discriminates against other cases. By analyzing all feasible combinations of $\xi(p)$, $\eta(p)$, and $\delta(p)$ we develop Table 5.1 for automatic detection of different types of points.

It may be noted from Table 5.1 that N_1, N_3, N_4 signify unique point type while N_2, N_5, N_6, N_7, N_8 signify two or more point types. Therefore, using Table 5.1 we can get a partial classification of skeleton points in one scan. However, from this partial classification one can arrive at unique classification using another scan. During the second scan we observe the 26-neighborhood of any point not uniquely decided by Table 5.1 and use Table 5.2 for unique classification. Thus, in Table 5.2 only N_2, N_5, N_6, N_7, N_8 points are considered.

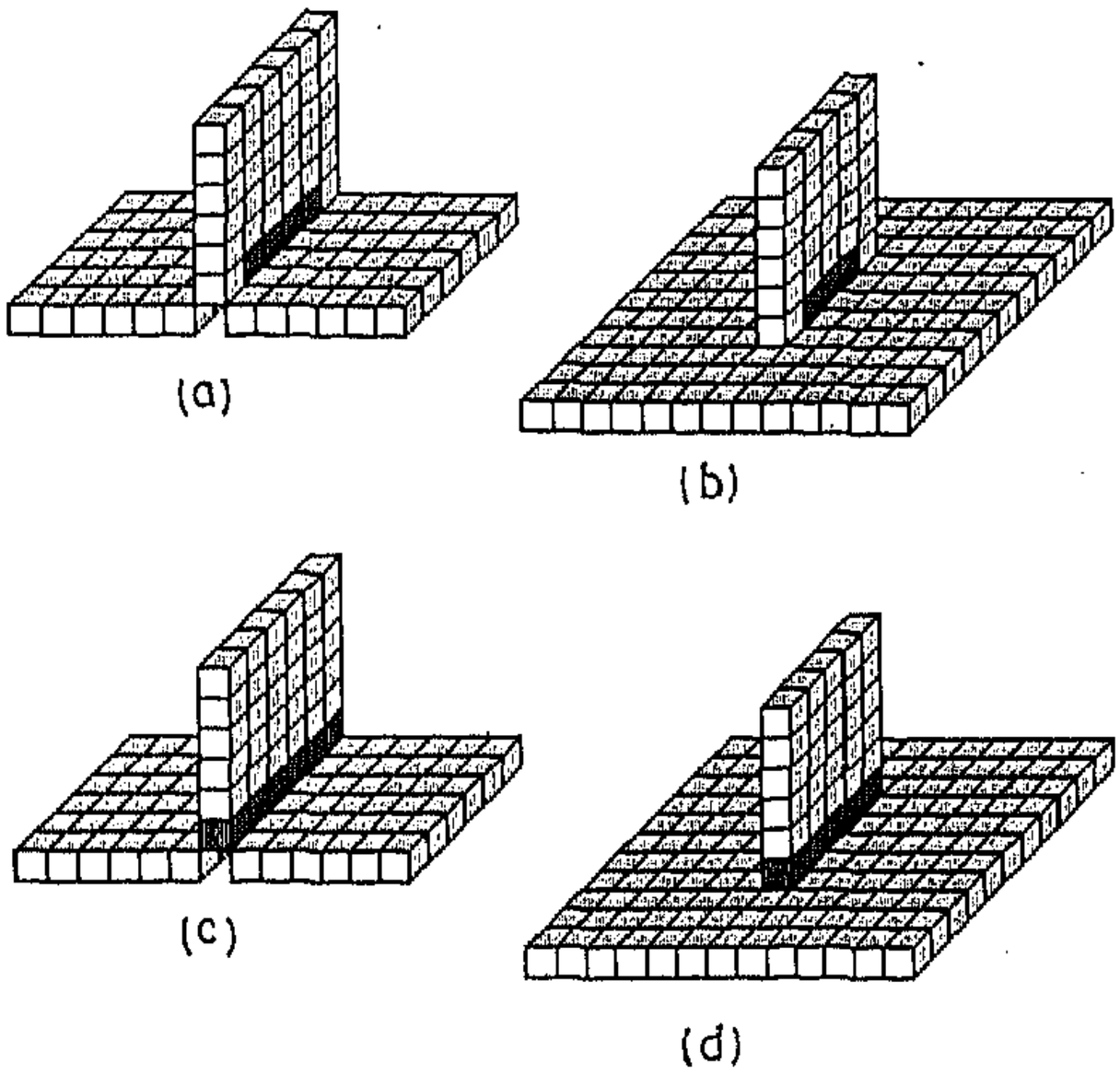

Figure 5.2: Extension of SS-lines. (a) and (b) The SS-line (shown black) obtained using Table 5.2. (c) and (d) The SS-line after the extension process.

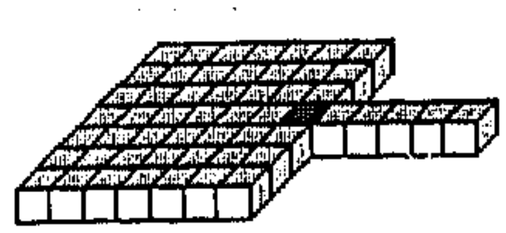

Figure 5.3: The SC-type junction point (shown black) cannot be detected using Table 5.2.

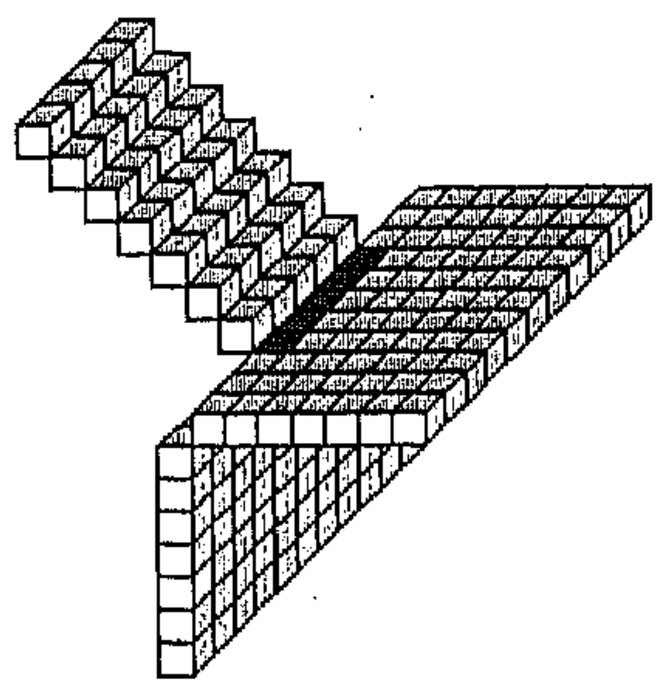

Figure 5.4: An example where the extension process is not needed.

At the end of second scan the classification process is completed except for a small problem illustrated by Figures 5.2 and 5.3. In Figures 5.2.(a) and 5.2.(c), the hidden points immediately below the vertical 6×6 rectangle are all white points. Also in Figures 5.2.(b) and 5.2.(d), the hidden points immediately below the vertical 5×6 rectangle are all white points. In Figures 5.2.(a) and 5.2.(b), the SS-line (a 26-path of SS-type points) should be extended to reach surface edges as shown in Figures 5.2.(c) and 5.2.(d) respectively. In Figure 5.3, the curve-line (a 26-path of C-type or CC-type points) meets the surface and we have to find out the junction point between the curve-line and the surface. On the other hand, in another example shown in Figure 5.4, the SS-line should not be extended at two ends. However, as discussed below it is possible to identify these cases and act accordingly.

Extension of SS-lines

At first we put forward some definitions.

Definition 5.1 *A function D is defined on two points p, q as follows:*

$$D(p,q) = \begin{cases} 0 & \text{if } p = q; \\ 1 & \text{if } p \text{ is an s-point of } \mathcal{N}(q); \\ 2 & \text{if } p \text{ is an e-point of } \mathcal{N}(q); \\ 3 & \text{if } p \text{ is a v-point of } \mathcal{N}(q); \\ \infty & \text{if } p \notin \mathcal{N}(q); \end{cases}$$

Let S be a finite set of points. Using the above function we define q as one of the nearest points of p in S if $\forall r \in S$, $D(p,r) \geq D(p,q)$. It should be noted that a point may have more than one nearest points in a set of points.

Let S_{SE} denote the set of all SE-type points in a surface skeleton. Let p be an end point of an SS-line (an end point has at most one 26-adjacent SS-type point). Let SS_p denote the set of all SS-type points of $\mathcal{N}(p)$ excluding p and let S_p denote the set of all S-type points of $\mathcal{N}(p)$ excluding p. We observe every SE-type point $q \in (\mathcal{N}(p) - \mathcal{E}(SS_p)) \cap S_{SE}$ and flag according to the following algorithm:

if $S_{SE} \cap \mathcal{N}^*(q)$ contains more than two 26-components then
    flag q;
else
if the number of tunnels in $S_{SE} \cap \mathcal{N}^*(q)$ is greater than zero then
    flag q;
else
if $S_{SE} \cap \mathcal{N}^*(q)$ contains less than two 26-components then
    if $\exists r \in S_p \cap \mathcal{N}^*(q) - \mathcal{E}(SS_p)$ such that $D(q,r) < D(q,p)$ then
        select one of the nearest points of q in $S_p \cap \mathcal{N}^*(q) - \mathcal{E}(SS_p)$, say t;
        flag t;

Note that after the last 'else' statement the flagged point (if at all) is not q but a point t nearest to q in $S_p \cap \mathcal{N}^*(q) - \mathcal{E}(SS_p)$. Finally, all flagged points are renamed as SS-type points. If the algorithm is executed on Figures 5.2.(a) and (b) then we obtain Figures 5.2.(c) and (d) respectively.

Finding junctions between the curve and the surface

Let p be a C-type or CC-type point and let S be the set of S-type, SC-type and SS-type points of $\mathcal{N}(p)$. Let $S_1, S_2, \cdots, S_n$ be the 26-components of S. For each S_i such that S_i contains no SC-type or SS-type points, one of the nearest points of p in S_i is declared as an SC-type point. The SC-type junction point of Figure 5.3 is detected by this algorithm.

5.3 The Segmentation Method

Using the results of the point classification method described in Section 5.2, we detail a segmentation method [115] of three dimensional digital objects from their surface skeletal representations. Let S denote the set of all skeleton points and let J denote the set of all SS-type, SC-type, CC-type points (*i.e.* all junction points). Let $S' = S - (\mathcal{E}(J) \cup J)$. Two or more surfaces and curves meet each other at junction points. In other words more than one surfaces and curves are connected around junction points. Thus the set of 26-components of S' represents different segmented surfaces and curves of the surface skeleton. However, some undesired situations may occur for some surface representations. These situations along with their solutions are described below.

For a surface representation shown in Figure 5.5.(a) an undesired tunnel is created in S' as shown in Figure 5.5.(b). Moreover in Figure 5.6.(a) the tail-like part is lost as shown in Figure 5.6.(b). To solve these problems we use two more steps as follows:

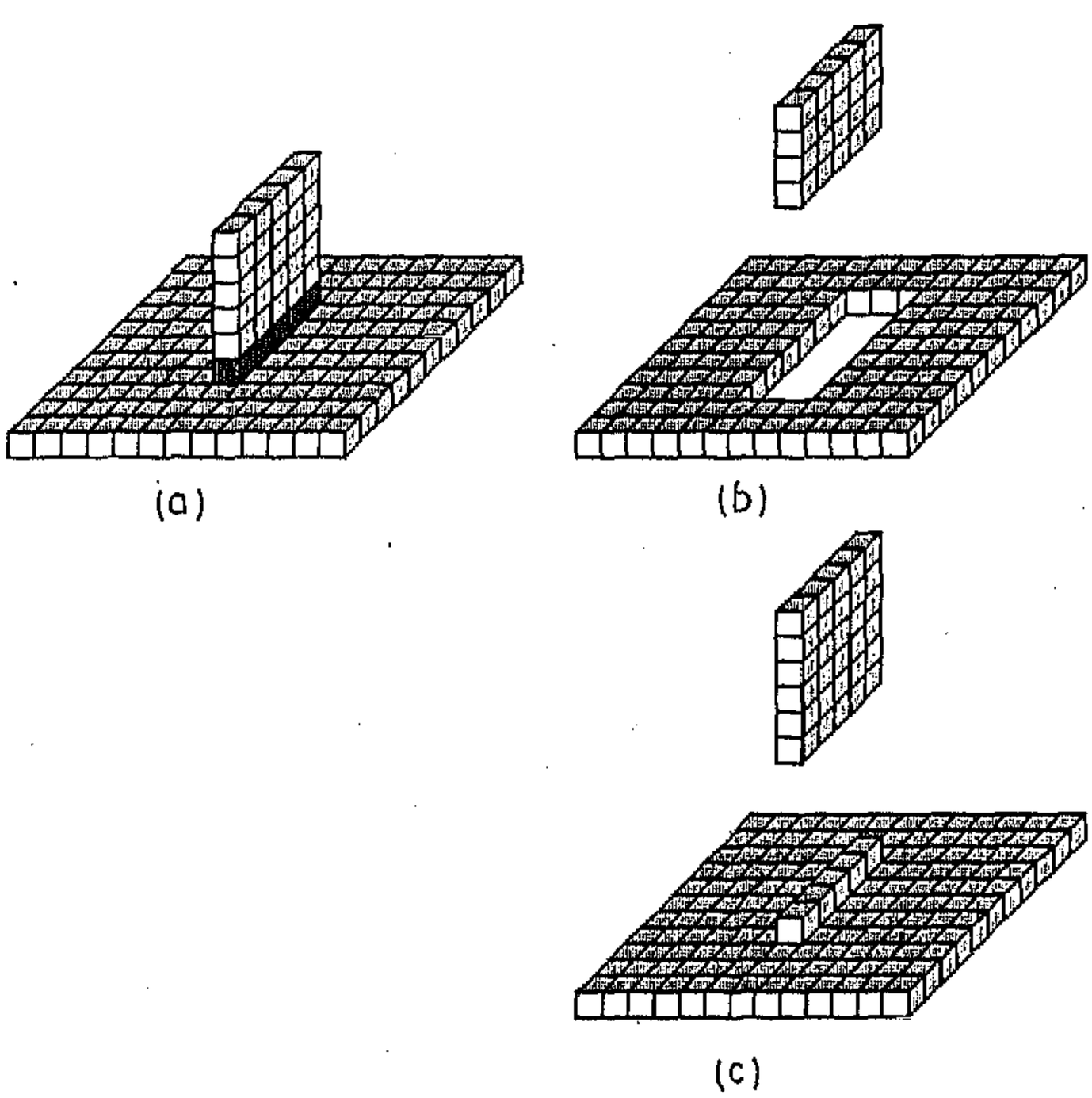

Figure 5.5: An example where an undesired tunnel is created in S' (see the text). (a) Original surface representation with the junction points shown black. (b) 26-components of S'. (c) Final segments.

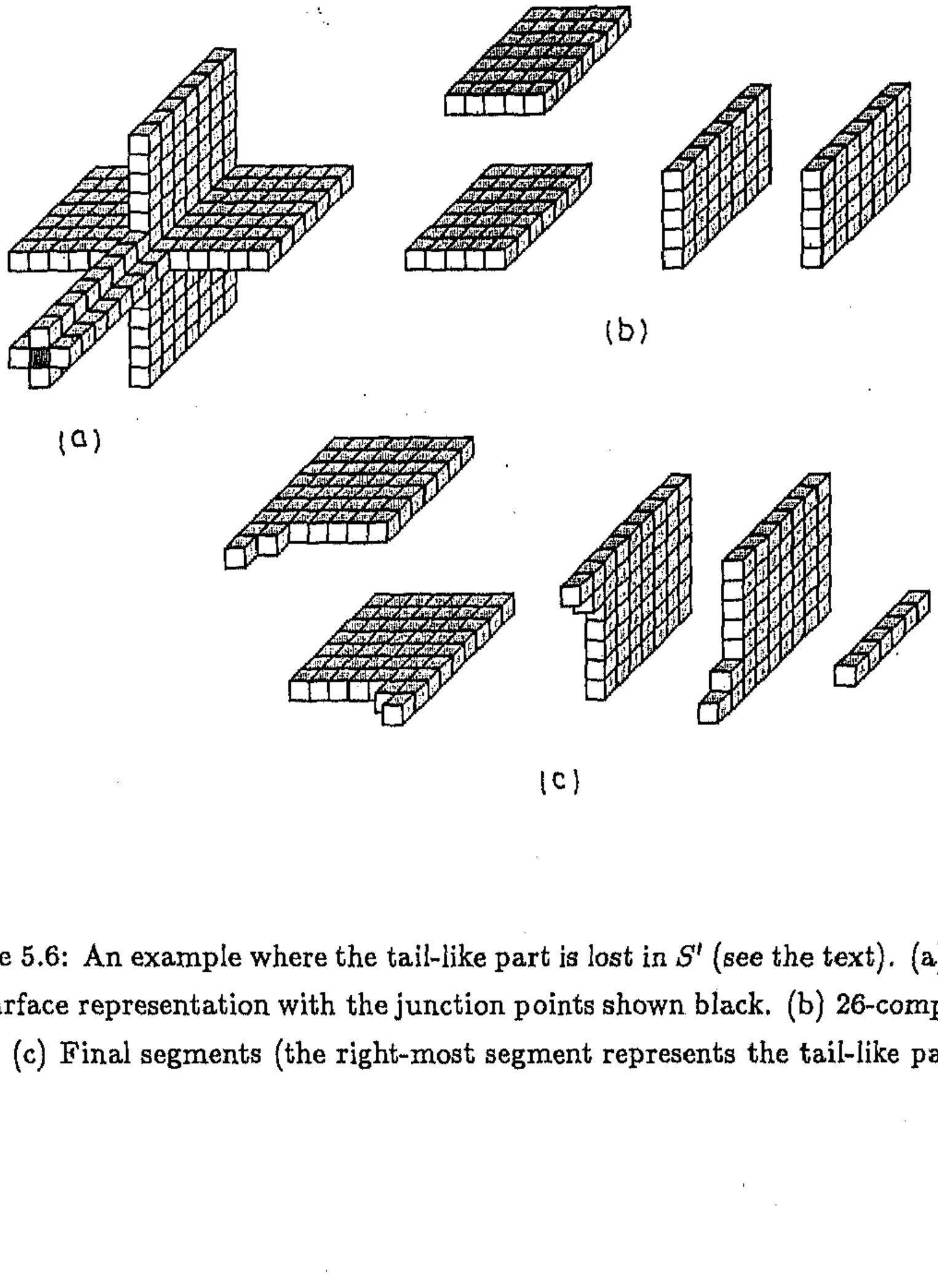

Figure 5.6: An example where the tail-like part is lost in S' (see the text). (a) Original surface representation with the junction points shown black. (b) 26-components of S'. (c) Final segments (the right-most segment represents the tail-like part).

Step 1 Let $S'_1, S'_2, \cdots, S'_n$ be the 26-components of S'. Each S'_i is extended to ES'_i as follows:

$$ES'_i = S'_i \cup (\mathcal{E}(S'_i) \cap S).$$

Step 2 Each extended component ES'_i is further extended to reach final components FS'_i as follows:

$$FS'_i = ES'_i \cup (\mathcal{E}(ES'_i) \cap J).$$

Finally all FS'_is as well as all 26-components of $J - \bigcup_{i=0}^{n} FS'_i$ are declared as segmented parts. Steps 1 and 2 are used to solve the problem of undesired tunnels shown in Figure 5.5.(b) while the 26-components of $J - \bigcup_{i=0}^{n} FS'_i$ restore the lost tail-like parts shown in Figure 5.6.(b). Figures 5.5.(c) and 5.6.(c) demonstrate the final outputs obtained using these steps.

5.4 Comparative Study

Malandain et. al. [73] also considered segmentation of 3D surface using topological features. They made some classification of points in E^3 where every point type classification is unique and applied the same classification in digital domain. The unique classification table creates undesired situations some of which were described by them. Also Figure 12 of [73] has a junction of surfaces which is not a curve but a surface of three-point width. This creates further problems in segmenting the surfaces. Such a situation does not arise in our approach. Also in [73] no mention was made to efficiently compute the numbers of adjacent object components (referred as C^* in [73]) and adjacent background components (referred as $\overline{C}$ in [73]) of a point in its $3 \times 3 \times 3$ neighborhood. On the other hand, our algorithm *topo_para* is an efficient approach of computing the parameters related to topological segmentation which are characterized by Table 5.1. The concept of using 18-neighborhood

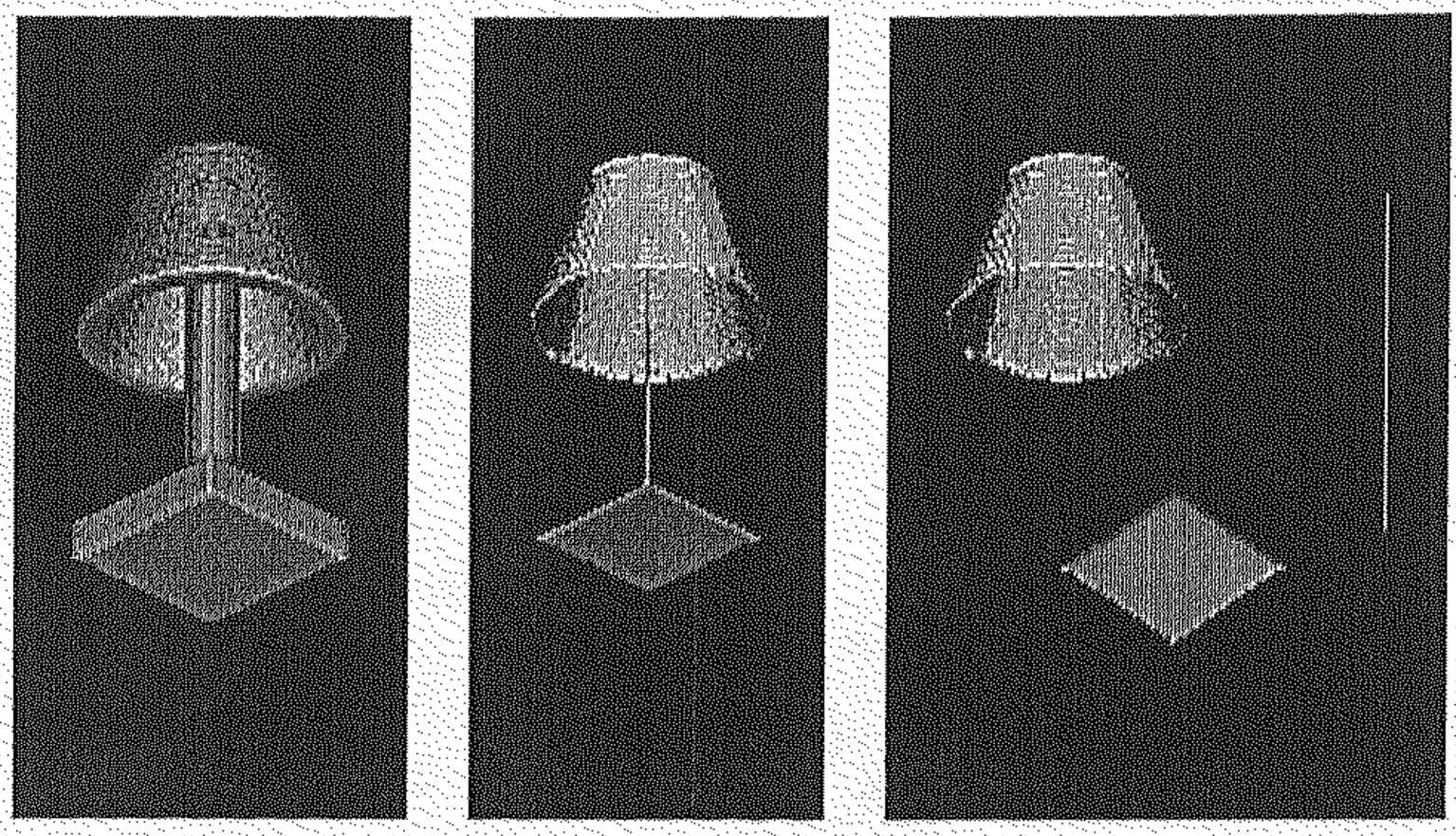

Figure 5.7: Results of segmentation. (a) Original object. (b) Surface skeleton representation. (c) Segmented parts.

in computing the number of 6-adjacent background components of a point in its $3 \times 3 \times 3$ neighborhood was first proposed by Saha et. al. [111].

Segmentation of surface representation is detailed in Section 5.3. Throughout the process of segmentation our algorithm emphasizes the preservation of topological features of sub-parts. For example, we provide methodologies which arrest creation of the undesired holes and restore lost tail-like parts demonstrated in Figures 5.5 and 5.6 respectively. On the other hand Malandain et. al. [73] had not mentioned about the preservation of topological features of sub-parts.

5.5 Results and Discussion

Based on digital topology a new approach of segmenting 3D digital images has been developed. This segmentation approach is applied on some 3D digital

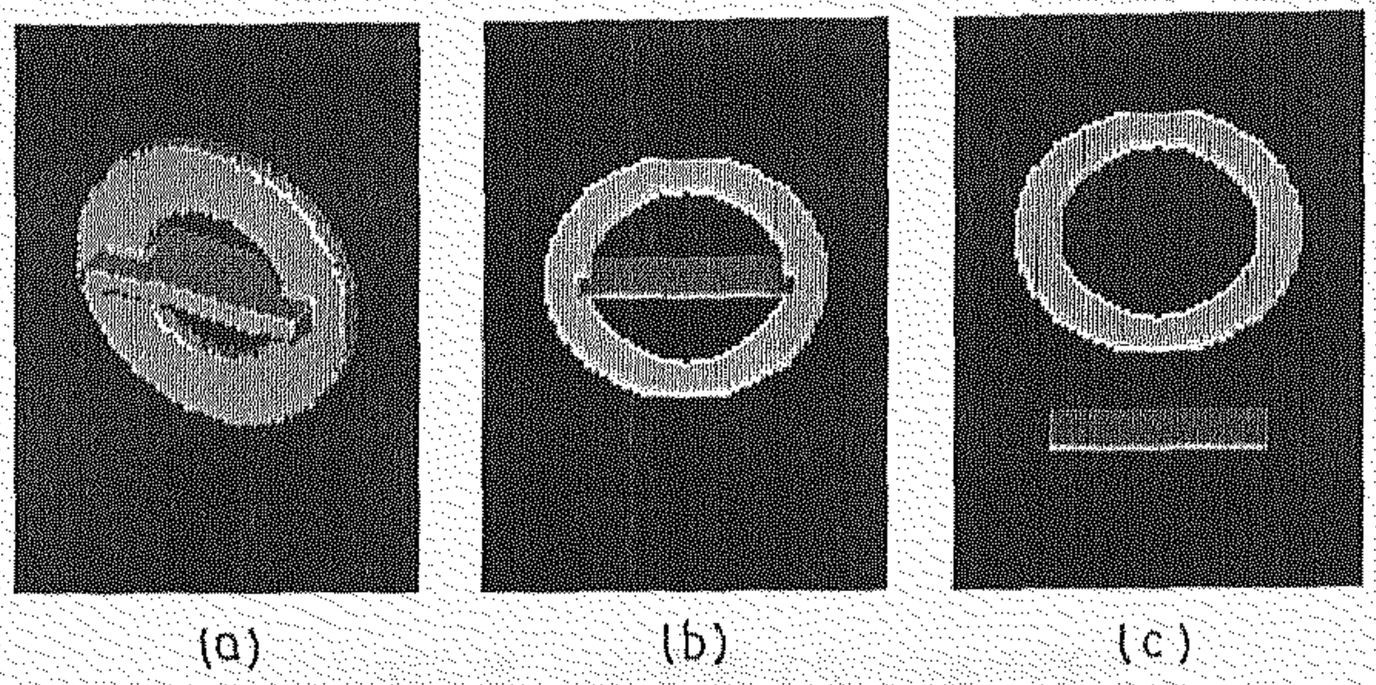

Figure 5.8: Results of segmentation. (a) Original object. (b) Surface skeleton representation. (c) Segmented parts.

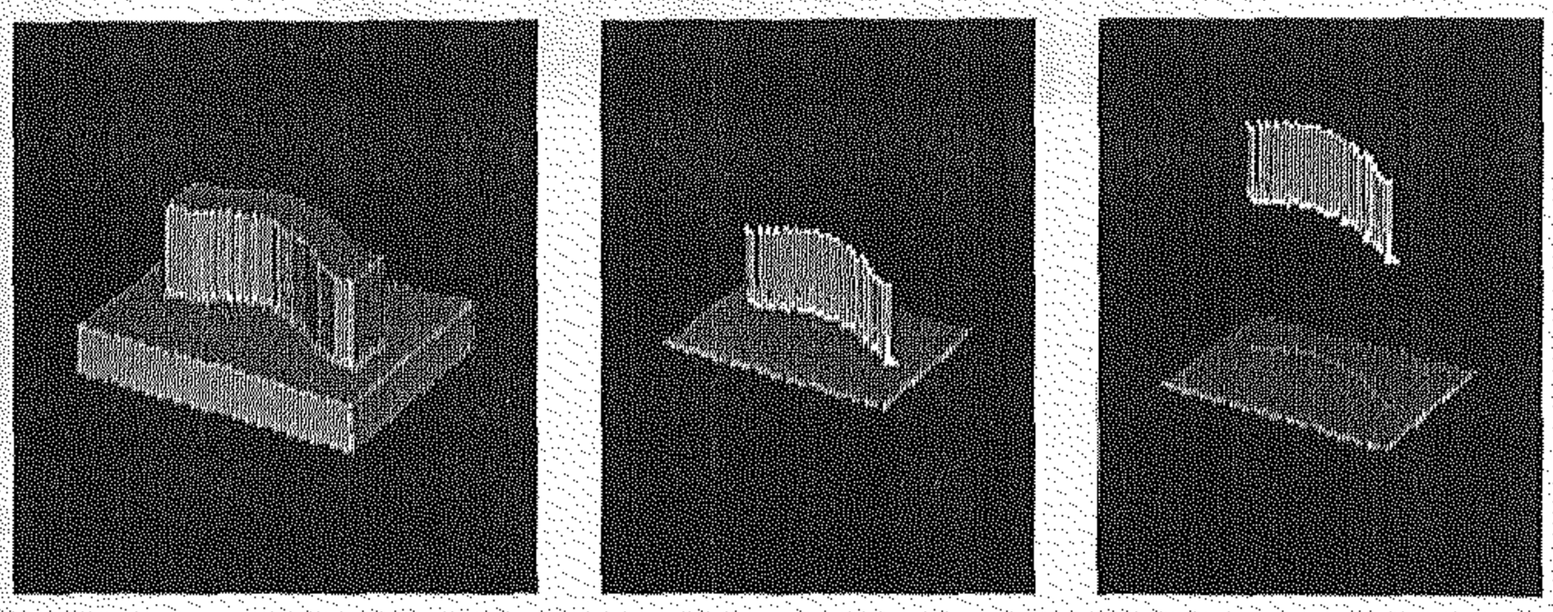

Figure 5.9: Results of segmentation. (a) Original object. (b) Surface skeleton representation. (c) Segmented parts.

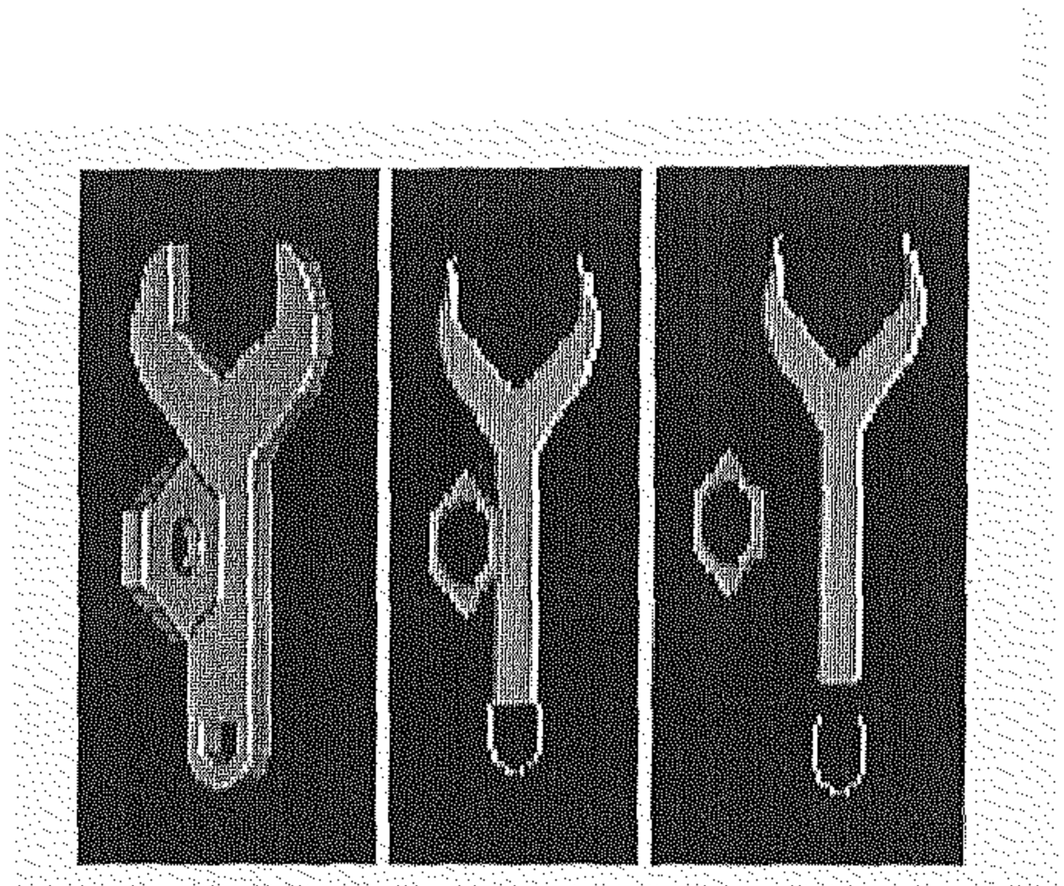

Figure 5.10: Results of segmentation. (a) Original object. (b) Surface skeleton representation. (c) Segmented parts.

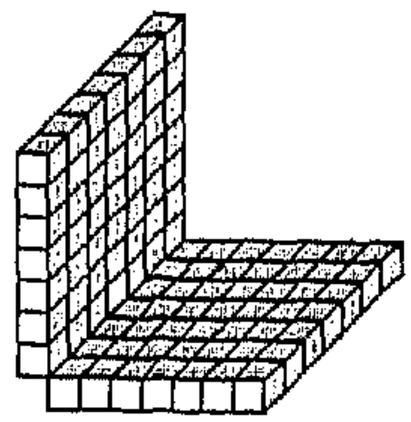

Figure 5.11: An example where two surfaces can not be segmented by the proposed method.

images and the results are illustrated in Figures 5.7–5.10. Figures 5.7.(a)–5.10.(a) are four binary images displayed by 3D surface rendering. The size of the smallest rectangular parallelepiped to enclose these images are $71 \times 114 \times 71$, $77 \times 77 \times 29$, $79 \times 40 \times 60$ and $72 \times 116 \times 72$ respectively. Backgrounds are made black to produce better visual effect. Figures 5.7.(b)–5.10.(b) are corresponding surface skeleton representations obtained by applying the thinning algorithm described in Chapter 4. In Figure 5.8 the original image and the skeleton are displayed from different angle to produce a better view. Figures 5.7.(c)–5.10.(c) demonstrate the corresponding segmented parts using the method described in Sections 5.2 and 5.3. These segmented parts along with the depth information derived from a thinning algorithm can be used to represent an object by a set of simple geometric features restricted by a predetermined feature set.

The segmentation process is based on observing topological junction points. Non-topological segmentation is not possible by this method. Figure 5.11 is an example where the two surfaces can not be separated. In this case the segmentation could be done by analyzing the abrupt change in surface normal direction.

Chapter 6

Conclusion

The work presented in the thesis is an attempt towards an advancement in the area of three dimensional digital topology. At the same time this work has tuned up the topological concepts with image processing applications. An in-depth study has been made on the current status of the digital topology. The basic concepts and useful definitions have also been presented.

First of all, the topological effects in a 3D digital image under binary transformation of a point has been considered. A theorem has been established that defines the number of tunnels in $3 \times 3 \times 3$ neighborhood which was definitely a 'bottleneck' in 3D digital topology. Based on this theorem a new and efficient characterization of (26,6) simple point has been presented. One of the attractive features of this characterization is that it only uses connectedness of points in $3 \times 3 \times 3$ neighborhood. Using the theorem defining the number of tunnels in $3 \times 3 \times 3$ neighborhood an effective measure of local topological changes due to binary transformation of single point has been developed.

In this thesis a set of interesting properties of $3 \times 3 \times 3$ neighborhood has been observed and an in-depth study has been made. This has resulted in new concepts like

'dead-surface', 'dead-edge', 'effective points', 'isolated points'. These concepts have been used to find out the don't care points (i.e. the points whose color can be ignored) while collecting local topological information of a point. Further, the concept of 'geometric class' has been introduced. All these concepts have been assembled to develop algorithmic forms of three useful topological operators: 1) simple point detection, 2) computation of local topological parameters (these parameters also define the local topological changes under binary transformation), and 3) change in the Euler characteristic under binary transformation. One important feature of these algorithms is that they need the configuration of all the 26-neighbors of a point only in the worst case and in most of the situations they need the configuration of lesser number of points. A parallel algorithm to compute the Euler characteristic of 3D digital images has been developed in this connection.

Subsequently an application of simple point concept in 3D thinning has been considered where we have developed a parallel thinning algorithm for 3D digital objects that preserves the topology as well as the shape. To preserve topology we have applied concepts of simple points while the concept of sub-fields has been used for parallelization. The concepts of 'open points', 'shape points' etc. have been introduced and applied to 3D thinning. The role of 'open points' in producing proper skeletons around different types of corners has been justified. Also, 'shape points' have been found to be quite robust under noise. We have introduced the concept of using two image versions in thinning and have justified its necessity in parallel thinning. This concept has made a marked improvement in the quality of thinned image. The results of application of the parallel thinning algorithm on several synthetically generated 3D objects and their noisy versions have been presented. We have also described an algorithm that produces a medial arc representation of an object from its surface skeleton representation. After studying the quality of skeletons around different types of corners, we have made an extensive study on the behavior of the algorithm under pseudo random contour noise and under rotation using shape distance. The study has revealed that shape distortion in skeleton increases more or less linearly with noise while in case of rotation, this distortion is

maximum around 45°.

Finally, we have described the role of digital topology in segmentation of 3D digital objects from their surface skeletal representations. After finding the surface skeleton of a 3D digital object and computing local topological parameters of surface skeleton points, the segmentation method has been completed in two steps: 1) point classification, and 2) segmentation into meaningful parts. Local topological parameters have been used to develop the point classification method which properly classifies the surface skeleton point and successfully detects different junction points. One important property of the point classification method is that it produces exactly one 26-curve of junction points when two or more surfaces meet. Also, exactly one junction point is generated when one or more curves meet with a surface or meet themselves. After detecting the junction points, the results have been applied to develop a segmentation method that produces meaningful segments of 3D digital objects. The results of application of the segmentation method on synthetically generated 3D objects have been presented. A limitation of the segmentation method has been pointed out that the method cannot segment the cases when two surfaces sharply meet at their edges producing no topological junctions.

We state the directions of future research that may evolve from this thesis:

1. Investigation of proof for the generalized version of Proposition 2.2.
2. Characterization of simple points that is valid in any regular 3D digital image space.
3. Measure of local topological parameters that is valid in any regular 3D digital image space.
4. Robust parallel thinning algorithm for 3D digital objects in a selected domain of application.
5. Thinning algorithm of 3D digital objects using distance transformation method.

6. Investigation of alternative distance function of DT_3 that are metrics.

7. Segmentation of surface skeletal representations analyzing the change in surface normal direction.

8. Representation of 3D objects by simple geometric features restricted by a predetermined feature set.

Appendix A

A.1 List of Notations

[1]

$3D$: three dimension.

α: adjacency relation.

β: adjacency relation.

$\delta(p)$: number of cavities in $\hat{\mathcal{N}}(p)$, see page 68.

$\eta(p)$: number of tunnels in $\hat{\mathcal{N}}(p)$, see page 68.

$\xi(p)$: number of components of $\hat{\mathcal{N}}(p)$, see page 68.

$\pi(\ )$: digital fundamental group, see page 8.

ϕ: null set.

[1]This list of notation is provided for better readability. This list is neither exhaustive nor the formal meaning of notations are always presented here.

$\chi(\ )$: the Euler Characteristic, see page 12.

Υ: s-point configuration, see page 76.

$(\mathcal{V}, \alpha, \beta)$: digital image space, see page 4.

$(\mathcal{V}, \alpha, \beta, \mathcal{B})$: digital image, see page 6.

$[X]_{\theta\omega\psi}$: an object in $\mathcal{Z}^3$ from the object $X \subset \mathcal{Z}^3$ after the rotation θ, ω, ψ, see page 112.

$A_{\theta\omega\psi}$: an object in E^3 from the object $A \subset E^3$ after the rotation θ, ω, ψ, see page 110.

$\mathcal{B}$: set of black points, see page 6.

$\mathcal{B}(p)$: the set of black points of $\hat{\mathcal{N}}(p)$, see page 49.

$\mathcal{B}'(p)$: the set of black points of $\hat{\mathcal{N}}'(p)$, see page 49.

$\mathcal{B}_e(p)$: the set of black e-points of $\hat{\mathcal{N}}'(p)$, see page 81.

$\mathcal{B}_i(p)$: the set of black points after the completion of ith steps of shrinking of $\hat{\mathcal{N}}(p)$, see page 51.

$C(\ )$: continuous analog, see page 8.

$D_1(\ )$: a distance function between two shapes, see page 110.

$D_2(\ )$: a distance function between two shapes, see page 110.

$DT_1(\ )$: a distance function between two points, see page 111.

$DT_2(\ )$: a distance function between a point and a finite set of points, see page 111.

$DT_3(\ )$: a distance function between two finite sets of points, see page 111.

e-point: an 18-adjacent point which is not 6-adjacent, see page 13.

$e(\ )$: a function from Z^3 to Z^3, see page 13.

edge( ): an edge of $3 \times 3 \times 3$ neighborhood, see page 13.

$\mathcal{E}(\ )$: 26-envelope, a function producing a finite subset of Z^3 from a finite subset of Z^3, see page 16.

E^3: the Euclidean 3-space

$EFO(\ )$: an ordered set of effective points, see page 76.

$EEO(\ )$: an ordered set of effective *e*-points, see page 77.

$\mathcal{E}M(\ )$: an extended middle plane of $3 \times 3 \times 3$ neighborhood, see page 15.

euler_change(p): computes the change in the Euler characteristic in $N(p)$ under deletion of p, see page 87.

$f_1(\ )$: a function from Z^3 to Z^3, see page 15.

$f_2(\ )$: a function from Z^3 to Z^3, see page 15.

$f_3(\ )$: a function from Z^3 to Z^3, see page 15.

$\mathcal{F}$: minimal separator, see page 39.

$\mathcal{F}(p)$: 26-minimal separator of $N(p)$, see page 39.

$ISO(\ )$: an ordered set of isolated points, see page 78.

$LUT\_simple\_point_i$: look up table of simple point detection for ith geometric

class, see page 76.

$LUT\_topo\_para_i$: look up table of topological parameter computation for ith geometric class, see page 81.

$LUT\_euler\_change_i$: look up table of the Euler change computation for ith geometric class, see page 85.

$M(\,)$: a middle plane of $3 \times 3 \times 3$ neighborhood, see page 15.

$\mathcal{N}_\alpha(p)$: the set of α-neighbors of p including p itself, see page 13.

$\mathcal{N}(p)$: $3 \times 3 \times 3$ neighborhood of p including p, see page 13.

$\mathcal{N}(p,q)$: the set of points α-adjacent to both p and q including p, q, see page 13.

$\mathcal{N}^*(\,)$: $3 \times 3 \times 3$ neighborhood of p excluding p, see page 13.

$\dot{\mathcal{N}}(p)$: $(Z^3, \alpha, \beta, (\mathcal{N}(p) \cap \mathcal{B}) \cup \{p\})$, here p is black, see page 15.

$\hat{\mathcal{N}}(p)$: $(Z^3, \alpha, \beta, (\mathcal{N}(p) \cap \mathcal{B}) - \{p\})$, here p is black, see page 15.

$\hat{\mathcal{N}}'(p)$: a shrunk version of $\hat{\mathcal{N}}(p)$, see page 49.

$\hat{\mathcal{N}}_i(p,p')$: $(Z^3, \alpha, \beta, (\mathcal{B}_{i-1}(p) \cap \mathcal{N}(p')) - \{p'\})$, see page 51.

$norm()$: a position normalized set, see page 111.

$\mathcal{P}$: digital image, see page 6.

$\overline{\mathcal{P}}$: inverse digital image of $\mathcal{P}$, see page 6.

$\mathcal{P}'$: a shrunk version of $\mathcal{P}$, see page 38.

p_B: a point of $\mathcal{N}(p)$, see Figure 1.1 in page 14.

p_{BE}: a point of $\mathcal{N}(p)$, see Figure 1.1 in page 14.

p_{BN}: a point of $\mathcal{N}(p)$, see Figure 1.1 in page 14.

p_{BNE}: a point of $\mathcal{N}(p)$, see Figure 1.1 in page 14.

p_{BNW}: a point of $\mathcal{N}(p)$, see Figure 1.1 in page 14.

p_{BS}: a point of $\mathcal{N}(p)$, see Figure 1.1 in page 14.

p_{BSE}: a point of $\mathcal{N}(p)$, see Figure 1.1 in page 14.

p_{BSW}: a point of $\mathcal{N}(p)$, see Figure 1.1 in page 14.

p_{BW}: a point of $\mathcal{N}(p)$, see Figure 1.1 in page 14.

p_{E}: a point of $\mathcal{N}(p)$, see Figure 1.1 in page 14.

p_{N}: a point of $\mathcal{N}(p)$, see Figure 1.1 in page 14.

p_{NE}: a point of $\mathcal{N}(p)$, see Figure 1.1 in page 14.

p_{NW}: a point of $\mathcal{N}(p)$, see Figure 1.1 in page 14.

p_{S}: a point of $\mathcal{N}(p)$, see Figure 1.1 in page 14.

p_{SE}: a point of $\mathcal{N}(p)$, see Figure 1.1 in page 14.

p_{SW}: a point of $\mathcal{N}(p)$, see Figure 1.1 in page 14.

p_{T}: a point of $\mathcal{N}(p)$, see Figure 1.1 in page 14.

p_{TE}: a point of $\mathcal{N}(p)$, see Figure 1.1 in page 14.

p_{TN}: a point of $\mathcal{N}(p)$, see Figure 1.1 in page 14.

p_{TNE}: a point of $\mathcal{N}(p)$, see Figure 1.1 in page 14.

p_{TNW}: a point of $\mathcal{N}(p)$, see Figure 1.1 in page 14.

p_{TS}: a point of $\mathcal{N}(p)$, see Figure 1.1 in page 14.

p_{TSE}: a point of $\mathcal{N}(p)$, see Figure 1.1 in page 14.

p_{TSW}: a point of $\mathcal{N}(p)$, see Figure 1.1 in page 14.

p_{TW}: a point of $\mathcal{N}(p)$, see Figure 1.1 in page 14.

p_{W}: a point of $\mathcal{N}(p)$, see Figure 1.1 in page 14.

$Rot(\ )$: a rotation function, see page 76.

$rt(x,y)$: $\{(z_1,z_2,z_3) \in Z^3$ and $\max(x_i,y_i) \geq z_i \geq \min(x_i,y_i)$ for $1 \leq i \leq 3\}$, here $x=(x_1,x_2,x_2), y=(y_1,y_2,y_3) \in Z^3$, see page 38.

$rti(x,y)$: the set of interior points of $rt(x,y)$, see page 38.

$rts(x,y)$: the set of border points of $rt(x,y)$, see page 38.

$rts^*(x,y)$: the set of border points of $rt(x,y)$ which are 6-adjacent to $rti(x,y)$, see page 38.

s-point: a 6-adjacent point, see page 13.

$simple\_point(p)$: detects whether p is a simple point or not, see page 79.

$spt(\alpha\text{-path})$: the set of points in the α-path, see page 10.

$surface(\ )$: a surface of $3 \times 3 \times 3$ neighborhood, see page 13.

$Sk(\ )$: surface skeleton of a digital object, see page 112.

thick( ): a function with true or false value, see page 96.

topo_para(p): computes topological parameters of p, see page 82.

v-point: a 26-adjacent point which is not 18-adjacent, see page 13.

v( ): a function from Z^3 to Z^3, see page 15.

$\mathcal{V}$: image set, see page 4.

$W(p)$: the set of white points of $N^*(p)$, see page 49.

$W_s(p)$: the set of white s-points of $\hat{N}(p)$, see page 49.

$W_e(p)$: the set of white e-points of $\hat{N}(p)$, see page 49.

$W_{se}(p)$: the set of white 18-neighbors of p, see page 49.

$W'_s(p)$: the set of white s-points of $\hat{N}'(p)$, see page 49.

$W'_e(p)$: the set of white e-points of $\hat{N}'(p)$, see page 49.

$W'_{se}(p)$: the set of white s-points and e-points of $\hat{N}'(p)$, see page 49.

$W^i_{se}(p)$: the set of white s-points and e-points after the completion of ith steps of shrinking of $\hat{N}(p)$, see page 51.

Z: the set of integers.

Z^3: $\{(i,j,k) \mid i,j,k \in Z\}$.

Bibliography

[1] P. Ahmed, P. Goyal, T. S. Narayanan, and C. Y. Suen, "Linear time algorithms for an image labelling machine," *Pattern Recognit. Lett.*, vol. 7, pp. 273–278, 1988.

[2] N. Ahuja, B. An, and B. Schachter, "Image representation using Voronoi tessellation," *Comput. Vision Graphics Image Process.*, vol. 29, pp. 286–295, 1985.

[3] N. Ahuja, "Dot pattern processing using Voronoi polygons as neighborhoods," *Proceedings, 5th International Conference on Pattern Recognition*, pp. 1122–1127, 1980.

[4] C. Arcelli, L. P. Cordella, and S. Levialdi, "From local maxima to connected skeletons," *IEEE Trans. Pattern Anal. Mach. Intell.*, vol. PAMI-3, pp. 134–143, 1981.

[5] C. Arcelli and G. S. di Baja, "On the sequential approach to medial line transformation," *IEEE Trans. Systems Man Cybernet.*, vol. SMC-8, pp. 139–144, 1978.

[6] C. Arcelli and G. S. di Baja, "A thinning algorithm based on prominence detection," *Pattern Recognit.*, vol. 13, pp. 225–235, 1981.

[7] C. Arcelli and G. S. di Baja, "A width-independent fast thinning algorithm," *IEEE Trans. Pattern Anal. Mach. Intell.*, vol. PAMI-7, pp. 463–474, 1985.

[8] C. Arcelli, "A condition for digital point removal," *Signal Process.*, vol. 1, pp. 283–285, 1979.

[9] C. Arcelli, "Pattern thinning by contour tracing," *Comput. Graphics Image Process.*, vol. 17, pp. 130–144, 1981.

[10] E. Artzy, G. Frieder, and G. T. Herman, "The theory, design, implementation, and evaluation of a three-dimensional boundary detection algorithm," *Comput. Graphics Image Process.*, vol. 15, pp. 1–24, 1981.

[11] H. H. Atkinson, I. Gargantini, and M. V. S. Ramanath, "Improvements to a recent 3D-border algorithm," *Pattern Recognit.*, vol. 18, pp. 215–226, 1985.

[12] D. K. Banerjee, S. K. Parui, and D. D. Majumder, "A shape metric for 3D objects," *Indian J. Pure Appl. Math.*, vol. 25 (1 & 2), pp. 95–111, Jan. & Feb., 1994.

[13] A. Bel-Lan and L. Montoto, "A thinning transform for digital images," *Signal Process.*, vol. 3, pp. 37–47, 1981.

[14] H. Bieri and W. Nef, "Algorithms for the Euler characteristic and related functionals of digital objects," *Comput. Vision Graphics Image Process.*, vol. 28, pp. 166–175, 1984.

[15] H. Bieri, "Computing the Euler characteristic and related additive functionals of digital objects from their bintree representation," *Comput. Vision Graphics Image Process.*, vol. 40, pp. 115–126, 1987.

[16] B. Bham, "Representation and shape matching of 3D objects," *IEEE Trans. Pattern. Anal. Mach. Intell.*, vol. PAMI-6, pp. 340–350, 1984.

[17] G. Bertrand, "Simple points, topological numbers and geodesic neighborhoods in cubic grids," *Pattern Recognition Letters*, vol. 15, pp. 1003–1011, 1994.

[18] H. Blum, "A transformation for extracting new descriptors of shape," in *Models for the Perception of Speech and Visual Form* (W. Wathen-Dunn, Ed.), pp. 362–380, MIT Press, Cambridge, MA. 1967.

[19] J. D. Boissonnat, "Shape recontruction from plannar cross-sections," *Comput. Vision Graphics Image Process.*, vol. 44, pp. 1–29, 1988.

[20] O. P. Buneman, "A grammer for the topological analysis of plane figures," in *Machine Intelligennce*, (B. Meltzer and D. Michie, eds.), pp. 383–393, Edinburgh Univ. Press., Edingurgh, 1969.

[21] M. Buen, "A flexible method for automatic reading of hand-written numerals," *Phillips Tech. Rev.*, vol. 31, pp. 130–137, 1973.

[22] B. B. Chaudhuri and D. D. Majumder, *Two Tone Image Processing and Recognition.* Wiley Eastern Limited, 1993.

[23] R. T. Chin, H. Wan, D. L. Stover, and R. D. Iverson, "A one-pass thinning algorithm and its parallel implementation," *Comput. Vision Graphics Image Process.*, vol. 40, pp. 30–40, 1987.

[24] W. Doyle, "Recognition of sloppy hand printed characters," *Proc. of West Joint Comp. Conf.*, vol. 17, pp. 133–142, 1960.

[25] R. O. Duda, P. E. Hart, and J. H. Munson, *Graphical Data Processing Research Study and Experimental Investigation.* AD650926, March, 1967.

[26] C. R. Dyer, "Computing the Euler number of an image from its quadtree," *Comput. Graphics Image Process*, vol. 13, pp. 270–276, 1980.

[27] C. R. Dyer and A. Rosenfeld, "Thinning algorithms for grayscale pictures," *IEEE Trans. Pattern Anal. Mach. Intell.*, vol. PAMI-1, pp. 88–89, 1979.

[28] M. J. E. Golay, "Hexagonal parallel pattern transformations," *IEEE Trans. Comput.*, vol. C-18, pp. 733–740, 1969.

[29] D. Gordon and J. K. Udupa, "Fast surface tracking in three-dimension binary images," *Comput. Vision Graphics Image Process.*, vol. 45, pp. 196–214, 1989.

[30] S. B. Gray, *Local Properties of Binary Images in Two and Three Dimensions.* Information International, Boston, 1970.

[31] A. Gudsen, "A quantitive analysis of preprocessing techniques for the recognition of hand-printed characters," *Pattern Recognition*, vol. 8, pp. 219–227, 1976.

[32] K. J. Hafford and K. Preston Jr., "Three-dimensional skeletonization of elongated solids," *Comput. Vision Graphics Image Process.*, vol. 27, pp. 78–91, 1984.

[33] E. L. Hall, *Computer Image Processing and Recognition*, ch. 7, pp. 423–425. Academic Press, New York, 1979.

[34] R. W. Hall, "Connectivity preserving parallel operators in 2D and 3D images," in *1992 SPIE Conference on Vision Geometry*, pp. 172–183, Boston, MA, 1992.

[35] G. T. Herman and D. Webster, "A topological proof of a surface tracking algorithm," *Comput. Vision Graphics Image Process.*, vol. 23, pp. 162–177, 1983.

[36] G. T. Herman and H. K. Liu, "Dynamic boundary surface detection," *Comput. Graphics and Image Process.*, vol. 7, pp. 130–138, 1978.

[37] G. T. Herman, "On topology as applied to image analysis," *Comput. Graphics and Image Process.*, vol. 52, pp. 409–415, 1990.

[38] G. T. Herman and D. Webster, "Surfaces of organs in discrete three-dimensional space," in *Mathematical Aspects of Computerized Tomography*, (G. T. Herman and F. Natherer, eds.), pp. 204–224, Springer-Verlag, Berlin, 1981.

[39] C. J. Hilditch, "Linear skeletons from square cupboards," in *Machine Itelligence*, vol. 4 (B. Meltzer and D. Michie Eds.), pp. 403–420, Edinburgh Univ. Press, Edinburgh, U.K., 1969.

[40] P. J. Hilton and S. Wylie, *Homology Theory.* Cambridge Univ. Press, Cambridge, U.K., 1960.

[41] J. F. P. Hudson, *Piecewise Linear Topology.* Benjamin, New York, 1969.

[42] L. Janos and A. Rosenfeld, "Digital connectedness, an algebraic approach," *Pattern Recognition Letters*, vol. 1, pp. 135–139, 1983.

[43] E. Khalimsky, "Pattern analysis of N-dimensional digital images," in *Proceedings of the IEEE International Conference on Systems, Man and Cybernetics*, pp. 1559–1562, 1986.

[44] E. Khalimsky, "Topological structures in computer science," *J. Appl. Math. Simulation*, vol. 1, pp. 25–40, 1987.

[45] E. Khalimsky, "Motion, deformation and homotopy in finite spaces," in *Proceedings of the IEEE International Conference on Syatems, Man and Cybernetics,* 87CH2503-1, pp. 227–234, 1987.

[46] E. Khalimsky, "Finite, primitive and Euclidean spaces," *J. Appl. Math. Simulation*, vol. 1, pp. 177–196, 1988.

[47] E. Khalimsky, R. D. Kopperman, and P. R. Meyer, "Computer graphics and connected topologies on finite ordered sets," *Topology and its Application*, vol. 36, pp. 1–17, 1990.

[48] C. E. Kim and A. Rosenfeld, "Convex digital solids," Tech. Rep. TR-929, Computer Vision Laboratory, University of Maryland, College Park, USA, 1980.

[49] R. Klette, "The m-dimensional grid point space," *Comput. Vision Graphics Image Process.*, vol. 30, pp. 1–12, 1985.

[50] T. Y. Kong, *Digital Topology with Applications to Image Processing.* Doctoral dissertation, University of Oxford, 1986.

[51] T. Y. Kong and A. Rosenfeld, "Digital Topology: Introduction and Survey," *Comput. Vision Graphics Image Process*, vol. 48, pp. 357–393, 1989.

[52] T. Y. Kong and A. W. Roscoe, "Continuous analogs of axiomatized digital pictures," *Comput. Vision Graphics Image Process.*, vol. 29, pp. 60–86, 1985.

[53] T. Y. Kong, A. W. Roscoe, and A. Rosenfeld, "Concepts of digital topology," *Topology and its Applications*, vol. 46, pp. 219–262, 1992.

[54] T. Y. Kong, "A digital fundamental group," *Comput. Graphics*, vol. 13, pp. 159–166, 1989.

[55] T. Y. Kong and A. W. Roscoe, "A theory of binary digital pictures," *Comput. Vision Graphics Image Process.*, vol. 32, pp. 221–243, 1985.

[56] T. Y. Kong and A. W. Roscoe, "Characterizations of simply-connected finite polyhedra in 3-space," *Bull. London Math. Soc.*, vol. 17, pp. 575–578, 1985.

[57] T. Y. Kong and E. Khalimsky, "Polyhedral analogs of locally finite topological spaces," in *General Topology and Applications: Proceedings of the 1988 Northeast Conference*, (R. M. Shortt, ed.), pp. 153–164, Marcel Dekkar, New York, 1990.

[58] T. Y. Kong, R. D. Kopperman, and P. R. Meyer, "A topological approach to digital topology," *Amer. Math. Monthly*, vol. 98, pp. 901–917, 1991.

[59] T. Y. Kong, R. Litherland, and A. Rosenfeld, "Problems in the topology of binary digital images," in *Open Problems in Topology*, (J. van Mill and G. M. Reed, eds.), pp. 376–385, North-Holland, Amsterdam, 1990.

[60] T. Y. Kong, "On the problem of determining whether a parallel reduction operator for n-dimensional binary images always preserves topology," in *Proceedings of the SPIE Conference on Vision Geometry*, Boston, MA, 1993.

[61] T. Y. Kong and A. Rosenfeld, "Digital topology: a comparison of the graph based and topological approaches," in *Topology and Category Theory in Compute Science* (G. M. Reed, A. W. Roscoe and R. F. Wachter, Eds.), pp. 273–289, Oxford University Press, Oxford, 1991.

[62] R. D. Kopperman, P. R. Meyer, and R. G. Wilson, "A Jordan surface theorem for three-dimensional digital spaces," *Discrete Comput. Geom.*, vol. 6, pp. 155–161, 1991.

[63] V. A. Kovalevsky, "Finite topology as applied to image analysis," *Comput. Vision, Graphics Image Process.*, vol. 46, pp. 141–161, 1989.

[64] V. A. Kovalevsky, "Discrete topology and contour definition," *Pattern Recognition Letters*, vol. 2, pp. 281–288, 1984.

[65] C. N. Lee and A. Rosenfeld, "Simple connectivity is not locally computable for connected 3D images," *Comput. Vision, Graphics Image Process.*, vol. 51, pp. 87–95, 1990.

[66] C. N. Lee and A. Rosenfeld, "Computing the Euler number of a 3D image," *Proceedings, First International Conference on Computer Vision*, pp. 567–571, 1987.

[67] S. Levialdi, "On shrinking binary patterns," *Commun. ACM*, vol. 15, pp. 7–10, 1972.

[68] H. K. Liu, "Two- and three-dimensional boundary detection," *Comput. Graphics Image Process.*, vol. 6, pp. 123–134, 1977.

[69] S. Lobregt, P. W. Verbeek, and F. C. A. Groen, "Three-dimensional skeletonization: principle and algorithm," *IEEE Trans. Pattern Anal. Mach. Intell.*, vol. PAMI-2, pp. 75–77, 1980.

[70] C. M. Ma, "On topology preservation in 3D thinning," *CVGIP: Image Understanding*, vol. 59, pp. 328–339, 1994.

[71] C. M. Ma, "Topology preservation on 3D images," in *Proceedings of the SPIE Conference on Vision Geometry*, Boston, MA, 1993.

[72] D. D. Majumder, "The Indian KBCS/FGCS programme and some applications of pattern recognition and computer vision," *IE(I) Journal-CP*, vol. 74, November, 1993.

[73] G. Malandain, G. Bertrand, and N. Ayache, "Topological segmentation of discrete surfaces," *International Journal of Comp. Vision*, vol. 10, pp. 183–197, 1993.

[74] G. Malandain and G. Bertrand, "Fast characterization of 3D simple points," in *11th Intern. Conf. Patt. Recog.*, pp. 232–235, The Huge, 1992.

[75] C. R. F. Maunder, *Algebraic Topology.* Cambridge Univ. Press, Cambridge, 1980.

[76] D. G. Morgenthaler, "Three-dimensional simple points: serial erosion, parallel thinning and skeletonization," Tech. Rep. TR-1005, Computer Vision Laboratory, University of Maryland, 1981.

[77] D. G. Morgenthaler and A. Rosenfeld, "Surfaces in three-dimensional digital images," *Inform. and Control*, vol. 51, pp. 227–247, 1981.

[78] D. G. Morgenthaler, "Three-dimensional digital topology: the genus," Tech. Rep. TR-980, Computer Vision Laboratory, University of Maryland, 1980.

[79] J. Mukherjee, P. P. Das, and B. N. Chatterjee, "Thinning of 3-D images using the Safe Point Thinning Algorithm (SPTA)," *Pattern Recognition Letters*, vol. 10, pp. 167–173, 1989.

[80] J. Mukherjee, P. P. Das, and B. N. Chatterjee, "On connectivity issues of ESPTA," *Pattern Recognition Letters*, vol. 11, pp. 643–648, 1990.

[81] J. Mukherjee, B. N. Chatterjee, and P. P. Das, "Segmentation of three dimensional surfaces," *Pattern Recognition Letters*, vol. 11, pp. 215–223, 1990.

[82] J. Mylopoulos and T. Pavlidis, "On topological properties of quantized spaces I: the notion of dimension," *J. Assoc. Comput. Mach.*, vol. 18, pp. 239–246, 1971.

[83] J. Mylopoulos and T. Pavlidis, "On topological properties of quantized spaces II: connectivity and order of connectivity," *J. Assoc. Comput. Mach.*, vol. 18, pp. 247–254, 1971.

[84] N. J. Naccache and R. Shingal, "SPTA: a proposed algorithm for thinning binary patterns," *IEEE Trans. Systems Man Cybernet.*, vol. SMC-14, pp. 409–418, 1984.

[85] A. Nakamura and K. Aizawa, "On the recognition of properties of three-dimensional pictures," *IEEE Trans. Pattern Anal. Mach. Intell.*, vol. PAMI-7, pp. 708–713, 1985.

[86] C. M. Park and A. Rosenfeld, "Connectivity and genus in three dimensions," Tech. Rep. TR-156, Computer Science Center, University of Maryland, 1971.

[87] T. Pavlidis, *Algorithms for Graphics and Image Processing.* Computer Science, Rockville, MD, 1982.

[88] K. Preston Jr., M. J. B. Duff, S. Levialdi, P. E. Norgren, and J. I. Toriwaki, "Basics of cellular logic with some applications in medial image processing," *Proc. IEEE*, vol. 67, pp. 826–856, 1979.

[89] K. Preston Jr., "Multi-dimensional logical transforms," *IEEE Trans. Pattern Anal. Mach. Intell.*, vol. PAMI-5, pp. 539–554, 1983.

[90] K. Preston Jr., "The crossing number of a three-dimensional dodecamino," *J. Combin. Inform. Sys. Sci.*, vol. 5, pp. 281–286, 1980.

[91] G. M. Reed and A. Rosenfeld, "Recognition of surfaces in three-dimensional digital images," *Inform. and Control*, vol. 53, pp. 108–120, 1982.

[92] G. M. Reed, "On the characterization of simple closed surfaces in three-dimensional digital images," *Comput. Vision Graphics Image Process.*, vol. 25, pp. 226–235, 1984.

[93] C. Ronse and P. A. Devijver, *Connected Components in Binary Images: The Detection Problem.* Wiley, New York, 1984.

[94] C. Ronse, "Minimal test patterns for connectivity preservation in parellel thinning algorithm for binary images," *Discrete Appl. Math.*, vol. 21, pp. 67–79, 1988.

[95] A. Rosenfeld, "Connectivity in digital pictures," *J. Assoc. Comput. Mach.*, vol. 17, pp. 146–160, 1970.

[96] A. Rosenfeld, "Three dimensional digital topology," *Inform. and Control*, vol. 50, pp. 119–127, 1981.

[97] A. Rosenfeld, "A characterization of parallel thinning algorithms," *Inform. and Control*, vol. 29, pp. 286–291, 1975.

[98] A. Rosenfeld, "Fuzzy digital topology," *Inform. and Control*, vol. 40, pp. 76–87, 1979.

[99] A. Rosenfeld, "Adjacency in digital pictures," *Inform. and Control*, vol. 26, pp. 24–33, 1974.

[100] A. Rosenfeld, "A converse to the Jordan curve theorem for digital curves," *Inform. and Control*, vol. 29, pp. 292–293, 1975.

[101] A. Rosenfeld, *Picture Languages*, ch. 2. Academic Press, New York, 1979.

[102] A. Rosenfeld, "Digital topology," *Amer. Math. Monthly*, vol. 86, pp. 621–630, 1979.

[103] A. Rosenfeld, "On connectivity properties of grayscale pictures," *Pattern Recognit.*, vol. 16, pp. 47–50, 1983.

[104] A. Rosenfeld, "Continuous functions on digital pictures," *Pattern Recognit. Lett.*, vol. 4, pp. 117–184, 1986.

[105] A. Rosenfeld and A. C. Kak, *Digital Picture Processing*, ch. 11. Vol. 2, Academic Press, New York, 2 ed., 1982.

[106] A. Rosenfeld and R. A. Melter, "Digital geometry," *Math. Intelligencer*, vol. 2, pp. 69–72, 1989.

[107] A. Rosenfeld and J. L. Pfaltz, "Sequential operations in digital picture processing," *J. Assoc. Comput. Mach.*, vol. 13, pp. 471–494, 1966.

[108] A. Rosenfeld and D. G. Morgenthaler, "Some properties of digital curves and surfaces," Tech. Rep. TR-942, Computer Vision Laboratory, University of Maryland, College Park, USA, 1980.

[109] A. Rosenfeld, "Arcs and curves in digital pictures," *J. Assoc. Comput. Mach.*, vol. 20, pp. 81–87, 1973.

[110] J. O'Rourke and N. Badler, "Decomposition of three dimensional objects into spheres," *IEEE Trans. on Pattern Anal. Mach. Intell.*, vol. PAMI 1, pp. 295–305, 1979.

[111] P. K. Saha, B. Chanda, and D. D. Majumder, "Principles and algorithms for 2D and 3D shrinking," Tech. Rep. TR/KBCS/2/91, N.C.K.B.C.S. Library, Indian Statistical Institute, Calcutta, India, 1991.

[112] P. K. Saha, B. Chanda, and D. D. Majumder, "A single scan boundary removal thinning algorithm for 2-D binary object," *Pattern Recognition Letters*, vol. 14, pp. 173–179, 1993.

[113] P. K. Saha, B. B. Chaudhuri, B. Chanda, and D. D. Majumder, "Topology preservation in 3D digital space," *Pattern Recognition*, vol. 27, no. 2, pp. 295–300, 1994.

[114] P. K. Saha and B. B. Chaudhuri, "Detection of 3-D simple points for topology preserving transformations with application to thinning," *IEEE Trans. on Pattern Anal. Mach. Intell.*, vol. 16, no. 10, pp. 1028–1032, 1994.

[115] P. K. Saha and B. B. Chaudhuri, "3D digital topology under binary transformation with applications," *Computer Vision Image Understanding*, vol. 63, no. 3, pp. 418–429, 1996.

[116] P. K. Saha and B. B. Chaudhuri, "A new approach to computing the Euler characteristic," *Pattern Recognition*, vol. 28, no. 12, pp. 1955–1963, 1995.

[117] P. K. Saha, B. B. Chaudhuri, and D. D. Majumder, "A new shape preserving parallel thinning algorithm for 3D digital images," *Pattern Recognition*, (accepted for publication ~~revised version submitted~~).

[118] P. K. Saha and B. B. Chaudhuri, "Simple point computation and 3-D thinning with parallel implementation," Tech. Rep. TR/KBCS/1/93, N.C.K.B.C.S. Library, Indian Statistical Institute, Calcutta, India, 1993.

[119] P. K. Saha and B. B. Chaudhuri, "Concepts of minimal seperation and maximal pocket in 3D digital space," *3rd International Conference on Advances in Pattern Recognition and Digital Techniques,* Calcutta, India, pp. 99–106, 28-31 December, 1994.

[120] H. Samet and M. Tamminen, "An improved approach to connected component labelling of images," in *Proceedings, Conference on Comput. Vision and Patt. Recog.* IEEE Publ. 86CH2290-5, pp. 312–318, 1986.

[121] I. Sobel, "Neighborhood coding of binary images for fast contour following and general binary array processing," *Comput. Graphics Image Process.*, vol. 8, pp. 127–135, 1978.

[122] S. N. Srihari, J. K. Udupa, and M. Yau, "Understanding the bin of parts," in *Proceedings, International Conference on Cybernetics and Society*, pp. 44–49, Denver, Colorado, 1979.

[123] S. N. Srihari, "Representation of three-dimensional digital images," *ACM Comput. Surveys*, vol. 13, pp. 400–424, 1981.

[124] R. Stefanelli and A. Rosenfeld, "Some parallel thinning algorithms for digital pictures," *J. Assoc. Comput. Mach.*, vol. 18, pp. 255–264, 1971.

[125] L. N. Stout, "Two discrete forms of the Jordan curve theorem," *Amer. Math. Monthly*, vol. 95, pp. 332–336, 1988.

[126] S. Suzuki and K. Abe, "Topological structural analysis of digitized binary images by border following," *Comput. Vision Graphics Image Process.*, vol. 30, pp. 32–46, 1985.

[127] H. Tamura, "A comparison of line-thinning algorithms from a digital geometry viewpoint," in *Proceedings, 4th International Joint Conference on Pattern Recognition*, pp. 715–719, Kyoto, Japan, 1978.

[128] J. I. Toriwaki, S. Yokoi, T. Yonekura, and T. Fukumura, "Topological properties and topology-preserving transformation of a three-dimensional binary picture," in *Proceedings, 6th International Conference on Pattern Recognition*, pp. 414–419, 1982.

[129] G. Tourlakis and J. Mylopoulos, "Some results on computational topology," *J. Assoc. Comput. Mach*, vol. 20, pp. 439–455, 1973.

[130] Y. F. Tsao and K. S. Fu, "A parallel thinning algorithm for 3D pictures," *Comput. Graphics Image Process.*, vol. 17, pp. 315–331, 1981.

[131] Y. F. Tsao and K. S. Fu, "A 3D parallel skeletonwise thinning algorithm," in *Proceedings, IEEE PRIP Conference*, pp. 678–683, 1982.

[132] Y. F. Tsao and K. S. Fu, "A general scheme for constructing skeleton models," *Information Science*, vol. 27, pp. 53–87, 1982.

[133] L. W. Tucker, "Labelling connected components on a massively parallel tree machine," in *Proceedings, Conference on Comput. Vision and Patt. Recog.*, pp. 124–129, IEEE Publ. 86CH2290-5, 1986.

[134] J. K. Udupa, S. N. Srihari, and G. T. Herman, "Boundary detection in multidimensions," *IEEE Trans. on Pattern Anal. Mach. Intell.*, vol. PAMI-4, pp. 41–50, 1982.

[135] J. K. Udupa and V. G. Ajjanagadde, "Boundary and object labelling in three-dimensional images," *Comput. Vision Graph. Image Process.*, vol. 51, pp. 355–369, 1990.

[136] J. K. Udupa, "Applications of digital topology in medical three-dimensional imaging," *Topology and its Applications*, vol. 46, pp. 181–197, 1992.

[137] S. H. Unger, "Pattern detection and recognition," *Proc. IRE*, pp. 1737–1752, Oct. 1959.

[138] P. W. Verbeek, F. C. A. Vrooman, and B. J. H. Verwer, "Speeding up 3-D binary image processing for robot vision," *SPIE Vol. 595, Computer Vision for Robots, Cannes*, pp. 233–238, 2-6 Dec. 1985.

[139] K. Voss, "Images, objects, and surfaces in Z^n," *International Journal of Pattern Recognition and Artificial Intelligence*, vol. 5, pp. 797–808, 1991.